Low-energy photoionization of guanine quadruplexes

Evangelos Balanikas

Thèse de doctorat

NNT : 2021UPASF031

université PARIS-SACLAY

Low-energy photoionization of guanine quadruplexes

Thèse de doctorat de l'université Paris-Saclay

École doctorale n°571 : sciences chimiques : molécules, matériaux, instrumentation et biosystèmes (2MIB)
Spécialité de doctorat: Chimie
Unité de recherche : Université Paris-Saclay, CEA, CNRS, LIDYL, 91191, Gif-sur-Yvette, France
Référent : Faculté des sciences d'Orsay

Thèse présentée et soutenue à Saclay, le 08/09/2021, par

Evangelos BALANIKAS

Composition du Jury

Isabelle LAMPRE Professeure, Université Paris Saclay, France	Présidente du Jury
Pascale CHANGENET-BARRET Chargée de Recherche (HDR), CNRS, France	Rapporteure & Examinatrice
Virginie LHIAUBET-VALLET Chargée de Recherche, Institute of Chemical Technology, Valencia, Spain	Rapporteure & Examinatrice
Anton GRANZHAN Chargé de Recherche (HDR), CNRS, France	Examinateur
Elise DUMONT Professeure, Ecole Normale de Lyon, France	Examinatrice
Jean-Luc RAVANAT Cadre Scientifique CEA (E6-HDR), France	Examinateur
Dimitra MARKOVITSI Directrice de Recherche Emérite, CNRS, France	Directrice de thèse
Gérard BALDACCHINO Cadre Scientifique CEA (E6-HDR), France	Co-Directeur de thèse
Roberto IMPROTA Senior Researcher, CNR, Naples, Italy	Membre invité

In memory of my best friend Niko who left from this world just before this work starts, being a big motivation to pursue my dreams

To my family members and Jenny for their endless support and happy memories all this past years

Acknowledgments

I would like to express my sincerest gratitude to my supervisor and thesis director, Dr. Dimitra MARKOVITSI for her invaluable guidance, continuous discussions and support through this journey, as well as my co-supervisor Gerard BALDACCHINO, for his patience and support. Without their instructions, knowledge and comments these three years, this work wouldn't have been the same. Big thanks also goes to Dr. Roberto IMPROTA coordinator of the LightDyNAmics project for all his support and remarks, as well as for his hospitality, welcoming me in his lab and giving me valuable knowledge about the theoretical calculations.

I would like to thank my reporters: Dr. Pascale CHANGENET-BARRET and Dr. Virginie LHIAUBET for their reports, essential remarks and questions. Also the examiners: Professeure Isabelle LAMPRE, Dr. Anton GRANZHAN, Professeure Elise DUMONT and Dr. Jean-Luc RAVANAT for reading this manuscript and their insightful questions. Furthermore, I would like to thank our collaborators: Dr. Akos BANYASZ, for creating the experimental set-up and taking the time to show me how it works, as well as giving solutions and troubleshooting. Dr. Lara FERNANDEZ-MARTINEZ, for her contribution with tones of theoretical calculations supporting this work, Dr. Peter PODBEVŠEK for his contribution with NMR measurements and Dr. Thierry DOUKI for his remarks on the final lesions.

A special thanks to Dr. Thomas GUSTAVSSON for all his critical remarks during the preparation for the presentation. The other members of DICO lab, current and former, Elsa, Carolina, Behnaz, Stephane, Caroline, Sandrine, for all the discussions and assistance in the administrative duties, kindness and support, especially during the lunch breaks, even if I skipped them from time to time.

Finally, I would like to thank the grand under the frame of the European Network "LightDyNAmics" (European Union's Horizon 2020 Research and

Innovation Programme under the Marie Sklodowska-Curie grant agreement No 765266), which gave the opportunity for this work to be well accomplished.

Résumé en français

La thèse décrit l'ionisation des quadruplexes de guanines (G-Quadruplexes) en solution aqueuse par absorption directe de photons ayant une énergie inférieure au potentiel d'ionisation de chacun des groupes les composant. Les G-Quadruplexes sont impliqués dans de nombreuses fonctions biologiques et sont étudiés pour des applications en nanotechnologie. Leur photo-ionisation génère des électrons et des radicaux de guanine (G) connus pour provoquer des dommages de l'ADN ; ce phénomène pourrait être également mis à profit pour le développement des biocapteurs basés sur la photoconductivité et la photodissociation de l'eau.

L'objectif de la thèse était de (i) quantifier les électrons et les radicaux G générés, (ii) suivre leur évolution, (iii) comparer leur comportement avec celui des doubles et simples brins et (iv) déterminer les facteurs qui affectent la photo-ionisation ainsi que la dynamique réactionnelle des radicaux. 16 systèmes modèles et l'ADN génomique ont été étudiés en utilisant la spectroscopie d'absorption nanoseconde avec excitation laser à 266 nm.

Un résultat important de ce travail est que a photo-ionisation à basse énergie dépend fortement de la structure secondaire de l'ADN. Elle n'est pas observée pour les mono-nucléosides/mono-nucléotides. Les rendements quantiques d'ionisation ϕ déterminés pour des doubles et simples brins sont $(1.5\pm0.5) \times10^{-3}$, alors que ceux des G-Quadruplexes varient entre 3.5×10^{-3} et 15×10^{-3}. Un tel comportement est en contraste flagrant avec ce qui est décrit dans la littérature pour l'ionisation de l'ADN à hautes énergies et montre qu'un mécanisme différent est sous-jacent.

Comme les G-Quadruplexes présentent un important polymorphisme structural, l'effet de différents paramètres sur le ϕ ont été testés. La variation du nombre des brins d'ADN ou de tétrades qui composent les G-Quadruplexes ainsi que leur topologie (parallèle/antiparallèle) ne semblent pas jouer de rôle important. Par contre, ϕ est très influencé par le type de cations métalliques situés dans leur cavité centrale (Na^+/K^+) ainsi que par la nature (adénine/thymine) et la position (3' et 5') des groupes périphériques. Sur la base de ces résultats, un

mécanisme de photo-ionisation indirecte a été proposé : une petite partie des états à transfert de charge formés pendant la relaxation électronique subit une séparation des charges ; ensuite l'éjection de l'électron s'effectue à partir de la base chargée négativement.

A 30 ns, ce qui correspond à notre résolution temporelle, les électrons éjectés ont été hydratés. Pour tous les systèmes modèles, ceux-ci disparaissent avec la même constante de temps de 0.5 µs, en réagissant avec le tampon phosphate. Ce déclin est plus rapide dans le cas de l'ADN génomique, indiquant des réactions complémentaires avec ce long système moléculaire.

Les radicaux observés sont ceux de la guanine. Nous avons identifié et quantifiés ces radicaux en comparant leur spectre d'absorption avec ceux de trois types de radicaux monomériques décrits dans la littérature : le radical cation $(G^{+})\bullet$ et deux radicaux déprotonés $(G\text{-}H1)\bullet$ and $(G\text{-}H2)\bullet$. Les spectres des radicaux cations des G-Quadruplexes ont été également obtenus par leur photo-ionisation à pH 3, où la déprotonation est limitée.

Pour tous les systèmes étudiés, la concentration de l'ensemble des radicaux à 3 µs a été trouvée égale à celle des électrons éjectés. La demi-vie de cette concentration est de quelques millisecondes. Elle est deux fois plus élevée pour des doubles brins que pour de simples brins qui les composent. Nous avons interprété cette observation par leur plus grande rigidité par rapport aux simples brins, dans lesquels les conformations réactives peuvent être atteintes plus rapidement.

Dans les simples et doubles brin, les radicaux cations se déprotonent en formant des radicaux $(G\text{-}H1)\bullet$, alors que dans des G-Quadruplexes leur déprotonation conduit à $(G\text{-}H2)\bullet$. Cela s'explique par le fait que les protons H1 sont engagés des liaisons hydrogène de type Hoogsteen. Néanmoins, pour plusieurs G-Quadruplexes une tautomérisation $(G\text{-}H2)\bullet \rightarrow (G\text{-}H1)\bullet$ a été observée par la suite, éventuellement corrélée avec une ouverture de ces liaisons.

La dynamique de déprotonation $(G^{+})\bullet \rightarrow (G\text{-}H1)\bullet$ dans l'ADN génomique a été déterminée pour la première fois. Elle peut être approximée par une fonction mono-exponentielle avec une constante de temps de 300 ns. Une dynamique de réaction bien plus complexe, qui s'étend d'au moins 30 ns à plus de 50 µs a été

observée pour la déprotonation $(G^{+})\bullet \rightarrow (G\text{-}H2)\bullet$ dans les G-Quadruplexes. Nous avons attribué ce comportement « multi-échelle » à leur structure anisotrope, l'exposition à l'eau (vers lequel le proton est transféré) étant plus important pour les tétrades extérieures.

*

La thèse a été effectuée dans le cadre du réseau européen "LightDyNAmics" (European Union's Horizon 2020 Research and Innovation Programme under the Marie Sklodowska-Curie grant agreement No 765266).

Abstract

The thesis describes the ionization of guanine quadruplexes (G-Quadruplexes) in aqueous solution by direct absorption of photons with an energy below the ionization potential of their components. G-Quadruplexes are involved in many biological functions and are being studied for applications in nanotechnology. Their photoionization generates electrons and guanine (G) radicals known to cause DNA damage; this phenomenon could also be used for the development of biosensors based on photoconductivity and photo-dissociation of water.

The aim of the thesis was to (i) quantify the electrons and G-radicals generated, (ii) monitor their evolution, (iii) compare their behavior with that of double and single strands and (iv) determine the factors affecting photoionization and the reaction dynamics of the radicals. 16 model systems as well as genomic DNA were studied using nanosecond absorption spectroscopy with laser excitation at 266 nm.

An important result of the work is that low-energy photoionization is strongly dependent on the secondary structure of the DNA. It is not observed for mononucleosides/mononucleotides. The ionization quantum yields ϕ determined for double and single strands are $(1.5\pm0.5)\times10^{-3}$, while those for G-quadruplexes vary between 3.5×10^{-3} and 15×10^{-3}. Such behavior is in sharp contrast to what is described in the literature for DNA ionization at high energies and shows that a different mechanism is operative.

As G-quadruplexes exhibit significant structural polymorphism, the effect of various structural parameters on ϕ was tested. Variation in the number of DNA strands or tetrads that make up G-Quadruplexes as well as their topology (parallel/antiparallel) do not seem to play an important role. On the other hand, ϕ is highly influenced by the type of metal cations in their central cavity (Na^+/K^+) as well as by the nature (adenine/thymine) and position (3' of 5') of the peripheral groups. Based on these results, an indirect photoionization mechanism was proposed: a small part of the charge transfer states formed during electronic

relaxation undergoes charge separation; then electron ejection takes place from the negatively charged base.

At 30 ns, which corresponds to our time resolution, the ejected electrons are hydrated. For all model systems, these disappear with the same time constant of 0.5 μs, reacting with the phosphate buffer. This decay is faster in the case of genomic DNA, indicating complementary reactions with this long molecular system.

The radicals observed are those of guanine. We identified and quantified these radicals by comparing their absorption spectra with those of three types of monomeric radicals described in the literature: the cation radical $(G^{+})\bullet$ and two deprotonated radicals (G-H1)• and (G-H2)•. Spectra of the cation radicals of G-Quadruplexes were also obtained by their photoionization at pH 3, where deprotonation is limited.

For all systems studied, the concentration of the ensemble of radicals at 3 μs was found to be equal to that of ejected hydrated electrons. The half-life of this concentration is a few milliseconds. It is twice as high for double strands as for the single strands that compose them. We interpreted this observation by their greater rigidity compared to single strands, in which the reactive conformations can be reached more quickly.

In single and double strands the cation radicals deprotonate to (G-H1)• radicals, whereas in G-Quadruplexes their deprotonation leads to (G-H2)•. This can be explained by the fact that the H1 protons are engaged in Hoogsteen-type hydrogen bonds. Nevertheless, for several G-Quadruplexes a (G-H2)• → (G-H1)• tautomerization was subsequently observed, possibly correlated with an opening of these bonds.

The dynamics of $(G^{+})\bullet$ → (G-H1)• deprotonation in genomic DNA was determined for the first time. It can be approximated by a mono-exponential function with a time constant of 300 ns. A much more complex reaction dynamics, which is spanning from at least 30 ns to more than 50 μs, was observed for $(G^{+})\bullet$ → (G-H2)• deprotonation in G-Quadruplexes. We attributed this 'multiscale' behavior to their anisotropic structure, with the exposure to water (to which the proton is transferred) being more important for the outer tetrads.

*

The PhD thesis was performed in the frame of the European Network "LightDyNAmics" (European Union's Horizon 2020 Research and Innovation Programme under the Marie Sklodowska-Curie grant agreement No 765266).

Table of contents

Prologue 15

References 20

Chapter 1 General considerations and state of the art 23

1.1 Telomeres and G-Quadruplexes 24

1.2 G-Quadruplex structures 25

1.3 DNA photoionization 28

1.4 Guanine radicals 31

1.4.1 Monomeric guanine radicals 33

1.4.2 Guanine radicals in single and double strands 35

1.4.3 Guanine radicals in G-Quadruplexes 37

1.5 References Chapter 1 39

Chapter 2 Materials and methods 45

2.1 Sample preparation 46

2.2 Steady-state spectroscopy 48

2.2.1 Absorption spectra and melting curves 48

2.2.2 Circular dichroism 50

2.3 Laser Flash photolysis 52

2.3.1 General concept 52

2.3.2 Description of the setup used 53

2.4 Determination of absorbed photons 55

2.5 References Chapter 2 58

Chapter 3 Photo-ejected electrons 61

3.1 Ejected electrons 62

3.1.1 Quantification and dynamics of hydrated electrons 62

3.1.2 Determination of one-photon ionization quantum yields 64

3.2 Factors affecting low-energy photoionization 67

3.3 Low-energy photoionization mechanism 69

3.4 References Chapter 3 74

Chapter 4 Guanine radical spectra and dynamics 79

4.1 General considerations and spectral features 80

4.2 Survival probability of the radical population 82

4.3 Radicals in DNA duplexes 85

4.3.1 Radical spectra 85
4.3.2 Radical dynamics 86
4.4 Radicals in G-Quadruplexes 88
4.4.1 Spectra of radical cations at **pH 3** 88
4.4.2 Spectral evolution at pH 7 91
4.4.3 Deprotonation dynamics 94
4.4.4 Detection of unknown reaction products 100
4.5. Reaction schemes in DNA multimers 105
4.6 Final DNA damage after low energy photoionization 107
4.7 Chapter 4 references 110
Chapter 5 Conclusions 114

Prologue

The objective of the PhD work described in this manuscript was to characterize the primary processes underlying oxidative damage induced by absorption of low-energy UV radiation directly by guanine quadruplexes (G-Quadruplexes): (i) quantify the ejected electrons, (ii) follow the evolution of the resulting radical cations (electron holes), (iii) compare their behavior with duplexes and single strands and (iv) obtain information about the factors that affect both the photoionization process and the radical decay dynamics.

During the past few decades, the interest of various scientific communities in G-Quadruplexes, which are four-stranded DNA/RNA structures, increased continuously. G-Quadruplexes have been detected in vivo[1] and their involvement in important biological processes (DNA repair, cell-apoptosis, cell division)[2-4] are being extensively studied. They may be formed through the entire genome, and especially in the ends of the chromosomes, the telomeres. Their possible implication in cancer cell proliferation made them targets for the development of new anticancer therapies.[5,6] G-Quadruplexes are also promising for applications in the field of nanotechnology,[7] exploiting, for example, their 'molecular wire' behavior,[8,9] based on the transport of electron holes.[10-12]

G-Quadruplexes are known to be prone to oxidative damage,[2,13] which is correlated with carcinogenesis and aging.[3] Oxidative damage can be induced through redox reactions between DNA and other chemical species or direct electron ejection under the effect of radiation. Beyond the biological consequences of oxidative damage in G-Quadruplexes, photo-generation of electron holes could be useful for the development of bio-sensors based on photoconductivity.

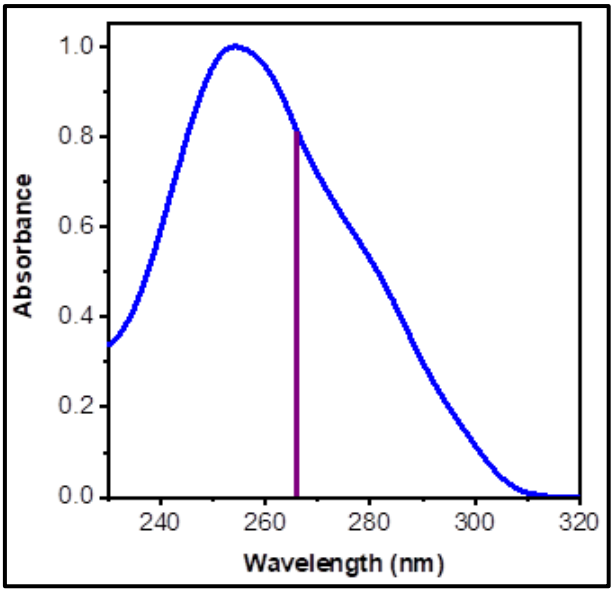

Figure 1. *Steady state absorption spectrum of the* ***G****-Quadruplexes* ***OXY/K*** $^{+}$ *(blue). The vertical violet line corresponds to the laser excitation wavelength (266 nm).*

The main method used in this study was nanosecond transient absorption spectroscopy (laser flash photolysis), probing the time domain between 30 ns and 200 ms following the excitation flash. Experiments were performed under low-energy excitation (266 nm, Figure 1). The term "low-energy" is used in comparison to the ionization potential of the various components of nucleic acids, which, in principle, preclude vertical electron photo-detachment upon irradiation around the absorption maximum. It is good to stress here that, although nanosecond flash photolysis has been a laboratory tool for over half a century now, specific protocols had been developed in the host laboratory for these studies. The reason is that such experiments require detection of very weak signals (absorbance ~10^{-4}) arising from DNA systems undergoing damage during the measurement. The support to the experimental results will come through various theoretical calculations performed by our collaborators. From the European project, Dr. Roberto Improta from the *Istituto di Biostrutture e Bioimmagini in Napoli* and Dr. Peter Podbevšek *Slovenian NMR Center, National Institute of Chemistry in Ljubljana. O*utside the European project, Dr. Lara Martinez-Fernandez from the *Departamento de*

Química, Facultad de Ciencias and Institute for Advanced Research in Chemistry (IADCHEM), Universidad Autónoma de Madrid.

Table 1. *The DNA structures studied during the thesis.*

	Sequence	Abbreviation	Structure
1	TAGGG(TTAGGG)$_3$TT	TEL25Na$^+$	Monomolecular Antiparallel G-Quadruplex
2	GGG(TTAGGG)$_3$	TEL21/K$^+$	Monomolecular Hybrid G-Quadruplex
3	TGGGGT	(TG$_4$T)$_4$/Na$^+$	Tetramolecular Parallel G-Quadruplexes
4		(TG$_4$T)$_4$/K$^+$	
5	TGGGG	(TG$_4$)$_4$/K$^+$	
6	GGGGT	(G$_4$T)$_4$/K$^+$	
7	AGGGGA	(AG$_4$A)$_4$	
8	AGGGG	(AG$_4$)$_4$/K$^+$	
9	GGGGA	(G$_4$A)$_4$/K$^+$	
10	TAGGGGAT	(TAG$_4$AT)$_4$	
11	AGGGGGA	(AG$_5$A)$_4$/K$^+$	
12	GGGGTTTTGGGG	OXY/K$^+$	Bimolecular Antiparallel G-Quadruplexes
13		OXY/Na$^+$	
14	calf thymus DNA	CT-DNA	Duplexes
15			
16	30 base-pairs	S1•S2	
17	**	S1	Single Strands
18	30 bases	S2	
19	TG	TG	
20	GT	GT	

* *The studies on (TG$_4$T)$_4$/Na$^+$ and (TG$_4$T)$_4$/K$^+$ were started by Dr. A. Banyasz and Dr. B. Behmand and completed by me.*

** ***S1:*** *5'-CGTACTCTTTGGTGGGTCGGTTCTTTCTAT-3'* ***S2:*** *3'-GCATGAGAAACCACCCAGCCAAGAAAGATA-5'*

At the beginning of my work, the generation of guanine radicals via low-energy photoionization of only one G-Quadruplex structure had been published by the host laboratory.[14] I studied the photoionization and the radical dynamics for 13 different G-Quadruplexes. For comparison, I also studied the behavior of four single strands and two duplexes, including genomic DNA.

Part of the results were published in the following articles, which are also included at the end of the manuscript with links to the open access version:

(1) Banyasz, A.; **Balanikas,** E.; Martinez-Fernandez, L.; Baldacchino, G.; Douki, T.; Improta, R.; Markovitsi, D., Radicals generated in tetramolecular guanine quadruplexes by photo-ionization: spectral and dynamical features. *J. Phys. Chem. B* 2019**,** *123*, 4950-4957.

(2) **Balanikas**, E.; Banyasz, A.; Baldacchino, G.; Markovitsi, D. Populations and Dynamics of Guanine Radicals in DNA strands: Direct versus Indirect Generation. Molecules 2019, 24, 2347.

(3) Behmand, B.; **Balanikas**, E.; Martinez-Fernandez, L.; Improta, R.; Banyasz, A.; Baldacchino, G.; Markovitsi, D., Potassium Ions Enhance Guanine Radical Generation upon Absorption of Low-Energy Photons by **G**-Quadruplexes and Modify Their Reactivity. J. Phys. Chem. Lett. 2020, 11, 1305−1309.

(4) **Balanikas**, E.; Banyasz, A.; Baldacchino, G.; Markovitsi, D. Guanine Radicals Generated in Telomeric **G**-Quadruplexes by Direct Absorption of Low-Energy UV Photons: Effect of Potassium Ions. Molecules 2020, 25, 2094.

(5) **Balanikas, E**.; Banyasz, A.; Douki, T.; Baldacchino, G.; Markovitsi, D. Guanine Radicals Induced in DNA by Low-Energy Photoionization. Accounts of Chemical Research 2020.

(6) **Balanikas, E**.; Martinez-Fernandez, L.; Improta, R.; Podbevšek, P.; Baldacchino, G.; Markovitsi, D. The Structural Duality of Nucleobases in Guanine Quadruplexes Controls Their Low-Energy Photoionization. J. Phy. Chem. Lett. 2021, 12, 8309-8313

(7) Balanikas, E.; Banyasz, A.; Baldacchino, G.; Markovitsi.D, Deprotonation dynamics of guanine radical cations, *manuscript under revision 2021*

Book chapter: **Balanikas, E**.; Markovitsi, D. DNA photoionization: from high to low energies . In "DNA photodamage: from light absorption to cellular responses and skin cancer". Eds. Douki, T. Improta, R. Publisher: Royal Chemical Society. *In press*

In addition to the work described in this manuscript and carried out by nanosecond transient absorption spectroscopy, during my thesis, I received training in other techniques. (i) Time-resolved fluorescence using two detection techniques, upconversion and time-correlated single photon counting, supervised by Dr. Thomas Gustavsson at the host laboratory. (ii) Quantum chemistry calculations at the Istituto di Biostrutture e Bioimmagini (Naples, for one month), under the supervision of Dr. Roberto Improta; thus, I was initiated in the time-dependent differential functional theory (TD-DFT). (iii) A two months stay is also planned (June-July 2021) at Politecnico di Milano, supervised by Pr. Giulio Cerullo where I will be trained in femtosecond transient absorption spectroscopy.

The manuscript is organized as follows. Chapter 1 presents some general considerations on G-Quadruplexes, DNA photoionization and the spectral and dynamical properties of guanine radicals. Chapter 2 describes the methodology followed in the work. Chapter 3 focuses on electron ejection and the photoionization mechanism while Chapter 4 deals with guanine radicals. Finally, the most important outcomes of the study are summarized in the Conclusion.

References

(1) Lipps, H. J.; Rhodes, D. G-quadruplex structures: in vivo evidence and function. *Trends in Cell Biology* **2009**, *19*, 414-422.

(2) Fouquerel, E.; Lormand, J.; Bose, A.; Lee, H. T.; Kim, G. S.; Li, J. F.; Sobol, R. W.; Freudenthal, B. D.; Myong, S.; Opresko, P. L. Oxidative guanine base damage regulates human telomerase activity. *Nat. Struct. Mol. Biol.* **2016**, *23*, 1092-1100.

(3) Blackburn, E. H.; Epel, E. S.; Lin, J. Human telomere biology: A contributory and interactive factor in aging, disease risks, and protection. *Science* **2015**, *350*, 1193-1198.

(4) Biffi, G.; Tannahill, D.; McCafferty, J.; Balasubramanian, S. Quantitative visualization of DNA G-quadruplex structures in human cells. *Nature Chem.* **2013**, *5*, 182-186.

(5) Ruden, M.; Puri, N. Novel anticancer therapeutics targeting telomerase. *Cancer Treatment Rev.* **2013**, *39*, 444-456.

(6) Martinez, P.; Blasco, M. A. Telomere-driven diseases and telomere-targeting therapies. *J. Cell Biol.* **2017**, *216*, 875-887.

(7) Mergny, J. L.; Sen, D. DNA quadruple helices in nanotechnology. *Chem. Rev.* **2019**, *119*, 6290-6325.

(8) Livshits, G. I.; Stern, A.; Rotem, D.; Borovok, N.; Eidelshtein, G.; Migliore, A.; Penzo, E.; Wind, S. J.; Di Felice, R.; Skourtis, S. S.; Carlos Cuevas, J.; Gurevich, L.; Kotlyar, A. B.; Porath, D. Long-range charge transport in single G-quadruplex DNA molecules. *Nature Nanotech.* **2014**, *9*, 1040-1046.

(9) Sha, R. J.; Xiang, L. M.; Liu, C. R.; Balaeff, A.; Zhang, Y. Q.; Zhang, P.; Li, Y. Q.; Beratan, D. N.; Tao, N. J.; Seeman, N. C. Charge splitters and charge transport junctions based on guanine quadruplexes. *Nature Nanotech.* **2018**, *13*, 316-+.

(10) Genereux, J. C.; Barton, J. K. Mechanisms for DNA Charge Transport. *Chem. Rev.* **2010**, *110*, 1642-1662.

(11) Thazhathveetil, A. K.; Harris, M. A.; Young, R. M.; Wasielewski, M. R.; Lewis, F. D. Efficient Charge Transport via DNA G-Quadruplexes. *J. Am. Chem. Soc.* **2017**, *139*, 1730-1733.

(12) Choi, J.; Park, J.; Tanaka, A.; Park, M. J.; Jang, Y. J.; Fujitsuka, M.; Kim, S. K.; Majima, T. Hole Trapping of G-Quartets in a G-Quadruplex. *Angew. Chem. Int. Ed.* **2013**, *52*, 1134-1138.

(13) Petersen, S.; Saretzki, G.; Zglinicki, T. v. Preferential Accumulation of Single-Stranded Regions in Telomeres of Human Fibroblasts. *Experimental Cell Research* **1998**, *239*, 152-160.

(14) Banyasz, A.; Martinez-Fernandez, L.; Balty, C.; Perron, M.; Douki, T.; Improta, R.; Markovitsi, D. Absorption of Low-Energy UV Radiation by Human Telomere G-Quadruplexes Generates Long-Lived Guanine Radical Cations. *J. Am. Chem. Soc.* **2017**, *139*, 10561-10568.

Chapter 1

General considerations and state of the art

In this chapter, I introduce the G-quadruplexes, their biological relevance and their structure. I also present what is reported in the literature about DNA photoionization. Then, I focus on guanine radicals. I describe the time-resolved approaches used so far for their study, their spectral properties and what is known about their evolution as a function of the secondary DNA structure. I also point out some discrepancies that appeared in the literature.

1.1 Telomeres and G-Quadruplexes

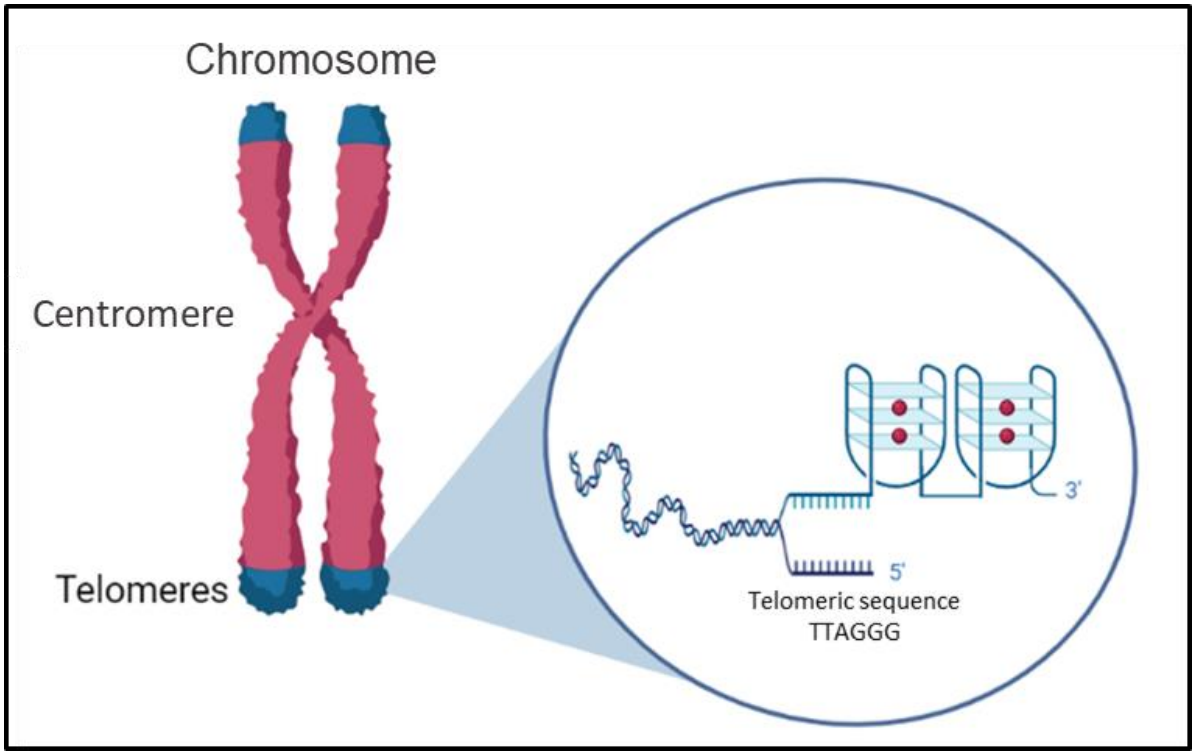

Figure 1. *Schematic illustration of the formation of* ***G****-Quadruplexes on the telomeres of the chromosome; the figure was created with BioRender.com*

The vast majority of genomic DNA is normally maintained as a Watson–Crick duplex, in which G–C pairing prevents formation of G-Quadruplexes[1]. However, guanines within a G-rich region have the potential to form four-stranded structures, which will be discussed in detail in section 1.2. Eukaryotic cells contain many G-rich regions capable of forming quadruplexes in DNA, with telomeres to be the most favorable.[1]

Telomeres are highly regulated and dynamic DNA/protein complexes at chromosome ends.[1,2] They protect the genomic DNA through various mechanisms and are essential for genome stability, cell proliferation and human health. Dysfunctional critically short telomeres may trigger cell senescence or apoptosis,

which in turn lead to G-related degenerative pathologies and loss of regenerative capacity.[2]

Telomeres shorten progressively with cell division, owing to the end replication problem. To compensate for this shortening, a protein called telomerase lengthens telomeres by adding GGTTAG repeats.[3] In humans, telomeres consist of approximately 1,600 TTAGGG duplex repeats and terminate in a single-strand overhang;[4] these and other repeats are known to give rise to G-Quadruplexes. In humans and model systems (i.e. different cell types of human and mammalian), telomeric DNA is often particularly susceptible to damage but abnormalities may occur genome-wide.[5-7] G-Quadruplexes in telomeric DNA were shown to be more prone to oxidative damage reactions than the general genome.[8]

1.2 G-Quadruplex structures

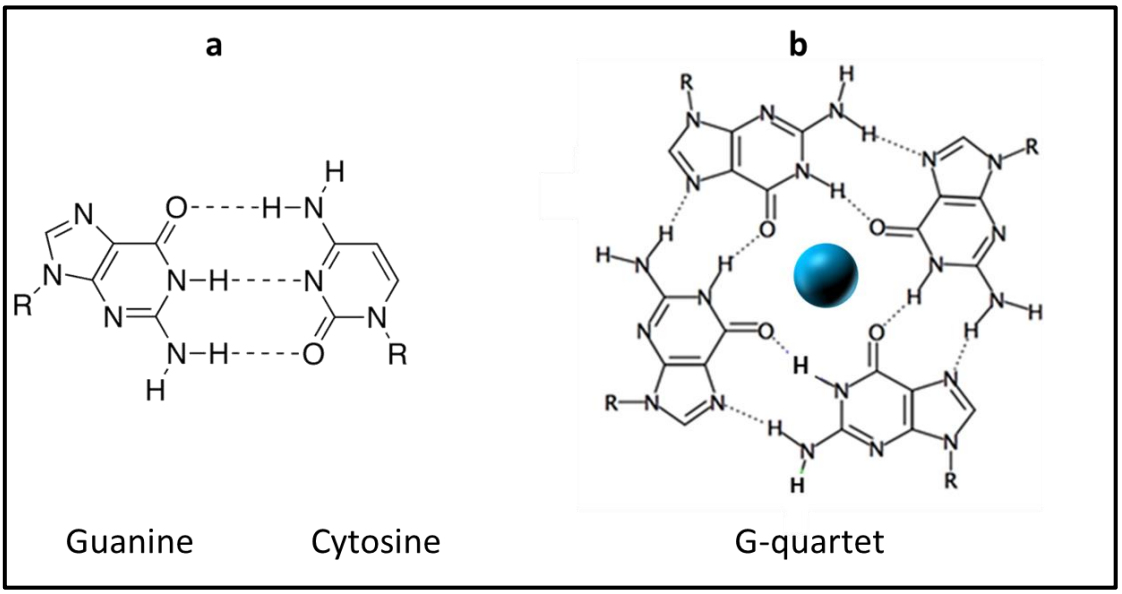

Figure 2. *Schematic illustration of* ***a)*** *a guanine cytosine base-pair and* ***b)*** *the* ***G****-tetrad; the blue sphere in the central cavity represents a cation.*

The DNA double helices are constructed by four major DNA bases: adenine, thymine, cytosine and guanine (**G**); guanines are paired with cytosines via three Watson–Crick hydrogen bonds (Figure 2a). However, under certain conditions, **G**s have the ability to self-associate and form tetrads (also called **G**-quartets).[9,10] These are square planar arrays, in which each **G** is connected to two others, via Hoogsteen bonds (Figure 2b). The vertical stacking of **G**-quartets gives rise to **G**-Quadruplex structures.[10] **G**-Quadruplexes may be formed by lipophilic guanosine analogues in non-polar solvents[11,12] or by guanine rich DNA or RNA strands in aqueous solution.[9,13,14]

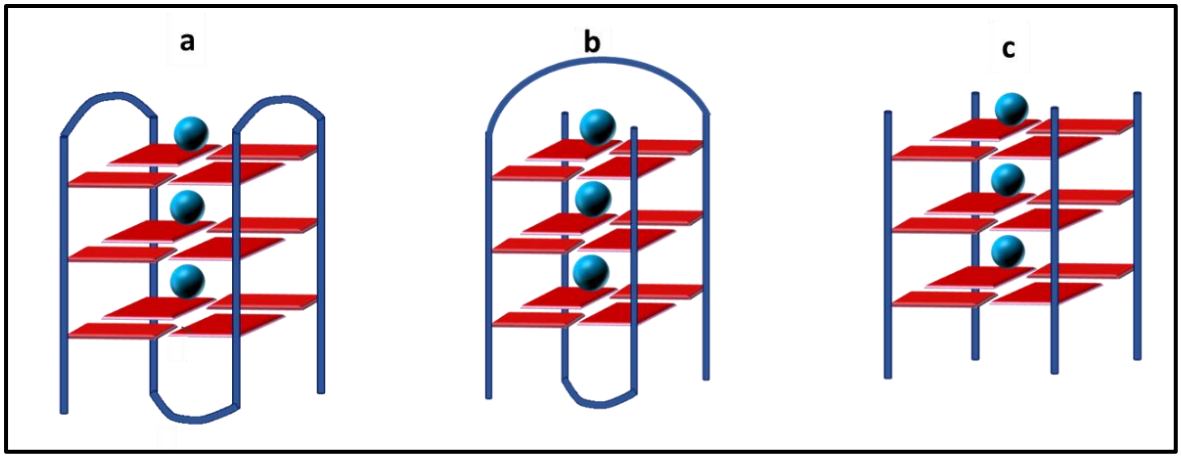

Figure 3. *Schematic illustration of the **G**-Quadruplexes studied during this work **a)** monomolecular, formed by folding of a single strand, **b)** bimolecular, formed by association of two single strands and **c)** tetramolecular, formed by association of four single strands; blue spheres represent metal ions (Na^+ or K^+) located in the central cavity.*

The formation of **G**-Quadruplexes requires the presence of cations (blue spheres in Figures 2 and 3), especially those of alkali metals (such as K^+, Na^+); non-metallic cations, like the NH_4^+, have also been used in order to stabilize **G**-Quadruplex structures.[9,10,14] These cations are located in the central cavity of the **G**-Quadruplex.

G-Quadruplexes present an important polymorphism.[9,10] Depending on the number of strands the quadruplexes may be, for example:

a) Monomolecular, formed by folding of one single strand, such as those containing the human telomere repeat (Figure 3a)

b) Bimolecular, formed by association of two strands. A well-studied example is the sequence $G_4T_4G_4$ from the telomeres of Oxytricha nova (Figure 3b)

c) Tetramolecular, with four separate strands associating together, such as TGGGGT (Figure 3c).

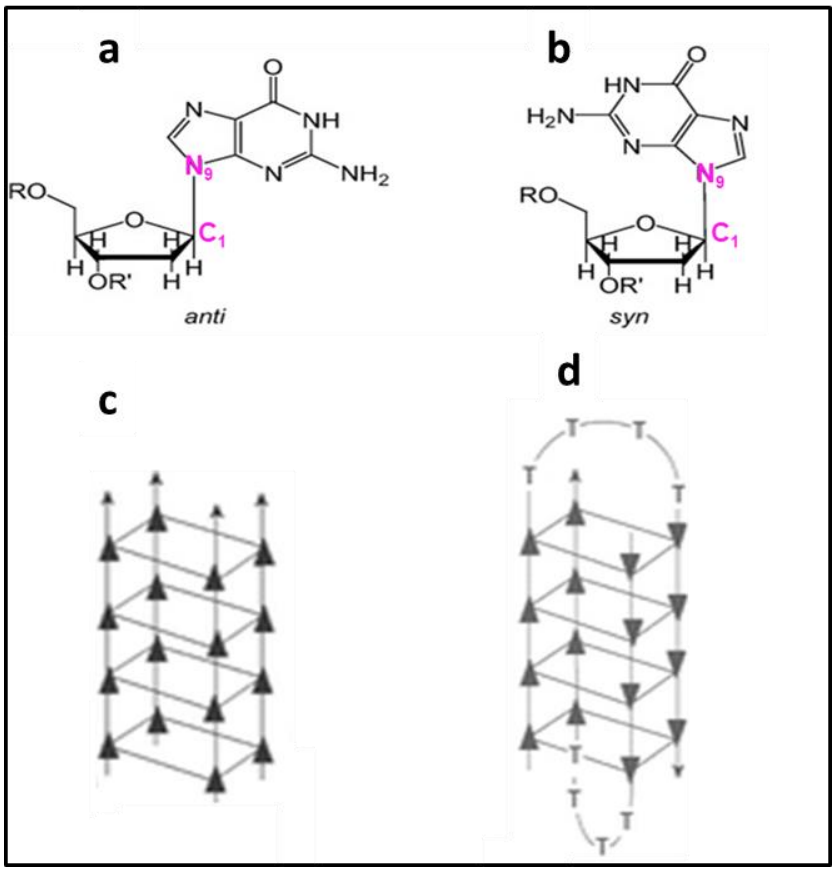

Figure 4. *Schematic illustration of* ***a)*** *guanine with anti glycosidic bond angle,* ***b)*** *a guanine with syn glycosidic bond angle,* ***c)*** *a tetramolecular* ***G****-Quadruplex ((TGGGT)$_4$) formed by guanines with anti glycosidic bonds only (parallel structure),[15]* ***d)*** *a bimolecular* ***G****-Quadruplex ((****G****GGGTTTTGGGG)$_4$) formed by guanines with syn and anti glycosidic conformation along each strand (antiparallel structure).[15] The glycosidic bond is the one between the N9 and the C1 (in magenta) of the sugar moiety.*

In the case of monomolecular and bimolecular G-quadruplexes, the formed loops can be diagonal, lateral (also termed edgewise) or chain-reversal (also named propeller), depending on the number of G-quartets, the loop length, sequence and sometimes on the nature of the alkali metal ion.[10,16] Chain-reversal loops connect two strands in the same parallel orientation, whereas diagonal and lateral loops connect chains in opposing, antiparallel orientations.[9,10] There are also cases of G-quadruplexes forming hybrid forms in equilibrium such as the human telomeric sequence in presence of K^+ ions.[17,18]

The arrangement of guanines may be also parallel or antiparallel in respect to the glycosidic bond formed in the backbone of the guanines (*anti* guanines, *syn* guanines; Figures 4a and b). The parallel quadruplexes have all Gs stacked with only *anti*-glycosidic bond angles (Figure 4c). In antiparallel quadruplexes Gs are stacked with alternating *syn-anti* or *anti-syn* glycosidic bond angles[14,15,19] (Figure 4d).

1.3 DNA photoionization

Absorption of UV radiation by DNA may lead to electron ejection, provided that the photon energy is sufficiently high in respect to the ionization potential Experimental ionization potentials (IP_{exp}) of DNA/RNA components in aqueous environment were reported recently,[20,21] through joint experimental and theoretical studies.[21-23] IP_{exp} were determined by recording the photoelectron spectra of the various DNA components in liquid jet, between 6 and 10 eV, and were derived from the band peaks. Theoretical calculations were performed by TD-DFT method and employing the polarizable continuum model to account the aqueous solvent. These theoretical studies showed that the IP_{exp} correspond to the so-called Vertical Ionization Potential (VIP), meaning that electron detachment takes place mainly prior to relaxation of the excited molecule (Table 1). Computations also found that base-pairing and base-stacking have only a weak effect on VIPs in line with experimental finding that the photoelectron spectrum

obtained for herring sperm DNA resembles that of an equimolar of the four constitutive mononucleotides. [24]

***Table 1**. Experimental Ionization Potentials (IP_{exp}) and computed lower Vertical Ionization Potentials (VIP) in eV; determined for DNA/RNA components in water by photoelectron spectroscopy and quantum chemistry calculations, respectively[21].*

	ribose	deoxyribose	dT	TMP	Cyt	CMP	Ado	$dAMP^-$	Guo	$dGMP^-$
IP_{exp}	9.4	9.4	-	8.1	8.1	-	7.6	7.7	7.3	-
VIP	9.2	9.1	7.9	7.8	7.8	7.8	7.7	7.7	7.4	7.1

DNA photoionization in solution is still observable at energies somewhat lower than the values in Table 1, where flash photolysis measurements are possible. More precisely, three decades ago, the groups of Steenken, O'Neill and Frölinde, had studied this effect on DNA in aqueous solution, using excitation at 193 nm (6.4 eV).[25-30] One-photon ionization quantum yields (Φ_1) determined by this method are presented in Table 2.

***Table 2**. One-photon ionization quantum yields (Φ_1 x10^3) determined at 193 nm (6.42 eV) in aqueous solution.*

dT	dC	dA	dG/dGMP	CT-DNA[a]	$H_2PO_4^-/HPO_4^{2-}$	H_2O
55[25]	17[25]	24[25]	73/70[25]	36[31]/58[29]	330/520[25]	13[32]

a) duplex calf thymus DNA in water[31] and $NaClO_4$ aqueous solution[29]

As found by photoelectron spectroscopy, the ϕ_1 determined for duplex genomic DNA corresponds roughly to the average of the ϕ_1 values found for its monomeric constituents, suggesting that the same direct photoionization mechanism is operative.

On 2005, Marguet and Markovitsi reported that excitation at 266 nm (4.7 eV) of DNA single and double strands containing adenine bases induces one-photon ionization with quantum yields of the order of 10^{-3}.[33] This result, obtained also by nanosecond flash photolysis, was quite unexpected because the excitation wavelength is 3 eV lower that the adenosine VIP. These findings were confirmed ten years later, after upgrading of the experimental setup by Dr A. Banyasz. A series of various DNA systems were studied with better precision.[34-36] The ϕ_1 values reported in a series of papers are gathered in Table 3.

***Table 3**. One-photon ionization quantum yields at 266 nm of various DNA systems reported by the host laboratory before the beginning of my thesis.*

DNA Oligomer	Type	ϕ_1 x 10^{-3}
5'-GGG(TTAGGG)$_3$-3'/Na^+	Monomolecular G-Quadruplex	4.5 ± 0.6[36]
$(AT)_{10}(AT)_{10}$	Double strand	1.1 ± 0.1[33]
$(A)_{20}(T)_{20}$	Double strand	1.4 ± 0.1[33]
$(GC)_5(GC)_5$	Double strand	1.2 ± 0.2[37]
$(A)_{20}$	Single strand	1.1 ± 0.1[33]
$(T)_{20}$	Single strand	<0.5[33]
TTAGGG	Single strand	<0.5[36]

Two important conclusions were drawn from these studies:

1. Low-energy photoionization is not detectable for mono-nucleotides or single strands with poor base stacking (ϕ_1 <0.3x10^{-4}).[36]
2. The ϕ_1 value determined for the only G-Quadruplex examined, TEL21/Na^+, was about four times higher than that found for duplexes.

In parallel with the solution studies, gas phase experiments using electrospray mass spectrometry and laser irradiation, also at 266 nm, observed electron photo-detachment from DNA $[6\text{-mer}]^{-3}$ strands.[38]

Remark: In this section, I refer exclusively to one-photon ionization. However, I note that several groups studied biphotonic or two photo-ionization of DNA. In general, two-photon ionization can occur in two ways: (i) two photons are absorbed simultaneously by the studied molecules[39,40] or (ii) one photon excites electronically the chromophore and, then, a second photon is absorbed by an excited state (usually long-lived).[41] For example, this process had already described for excitation at 248 nm (4.9 eV) but one-photon ionization at this wavelengths was precluded.[42]

1.4 Guanine radicals

Three different time-resolved approaches were used so far to study guanine radicals at room temperature by recording their absorption spectra on the UV-visible spectral domain. Below it is briefly explained how these methods work.

a) Electron beam induced indirect oxidation

This technique is a multi-step process,[43,44] starting from the interaction between an electron beam and the aqueous solvent in which DNA is dissolved. It starts with ionization of the water giving rise to hydrated electrons e_{hydr}^-. Usually tert-butyl alcohol is added in the solution in order to scavenge the $OH^{\bullet}$ radicals, which are also formed during the radiolysis of the water,[45] thus avoiding their reaction with DNA. The produced hydrated electrons e_{hydr}^- react with an appropriate solute molecule to create a strong oxidant. A typical system used to

this purpose is peroxodisulfate $S_2O_8^{2-}$ whose reaction with hydrated electrons gives rise to sulfate radical anions $SO_4^{\bullet -}$ (eq.1)

$$e_{hydr}^- + S_2O_8^{2-} \rightarrow SO_4^{2-} + SO_4^{\bullet -} \quad \text{(eq. 1)}$$

The $SO_4^{\bullet -}$ anions interact in their turn with the guanines and create the guanine radical cations ($(G^{\bullet})^+$) through electron abstraction (equation 2).

$$SO_4^{\bullet -} + G \rightarrow SO_4^{2-} + (G^{\bullet})^+ \quad \text{(eq. 2)}$$

We remark that this method involves many steps and requires diffusion of the intermediate species for each reaction to occur.

b) Photosensitized oxidation

This method, based on nanosecond flash photolysis, is similar to the method a) but contains only two steps. Production of the oxidant, such as $SO_4^{\bullet -}$, is achieved by means of a laser pulse, whose wavelength varies, according to the study, between 300 nm and 360 nm.[46,47]

$$h\nu + S_2O_8^{2-} \rightarrow 2SO_4^{\bullet -} \quad \text{(eq. 3)}$$

c) Photoionization

This approach is also based on nanosecond flash photolysis: radical cations are formed following electron ejection without addition of oxidants. Older studies, used 193 nm excitation,[25,48] while the most recent ones, carried out in the host laboratory, used 266 nm excitation.[35-37,49]

$$h\nu_{266} + G \rightarrow (G^{\bullet})^+ + e^- \quad \text{(eq.4)}$$

We note that while low-energy excitation (266 nm) ionizes only DNA while high energy experiments (193 nm) ionize also the aqueous solvent and buffer

ingredients (Table 3), potentially leading to secondary reactions. As explained previously, monomeric radicals cannot be produced by low-energy ionization.

Equations 2 and 4 describe generation of an electron hole on guanine but similar reactions may take place on other bases. However, numerous investigations have revealed that the electron holes formed by electron loss in DNA can migrate through the duplexes[50-55] or G-Quadruplexes.[50,55,56] Eventually, they are trapped by guanine sites because guanine has the lowest oxidation potential among all nucleobases.[57]

1.4.1 Monomeric guanine radicals

The absorption spectra of G radicals corresponding to monomeric guanine derivatives (dG, dGMP, 1-methylG…), were determined by Candeias and Steenken, using the methods a) and c) described in the previous section. Experiments performed for various pH values and associated with conductivity measurements, showed that the pKa value of the G radical cation is 3.9 for the dG and 4.7 for the methyl-guanosine.[25,44] Consequently, at neutral pH, G radical cations are unstable and tend to lose a proton. The spectra of radical cations and deprotonated radicals of dG (Figure 5a) are very similar. They are characterized by three peaks of decreasing intensity at 300-310 nm, 390 nm and 510 nm. The only differences between the spectra of the two radicals is that deprotonation shifts the UV band slightly to longer wavelengths and induces a weak red tail extended between 590 and 750 nm.[25,44]

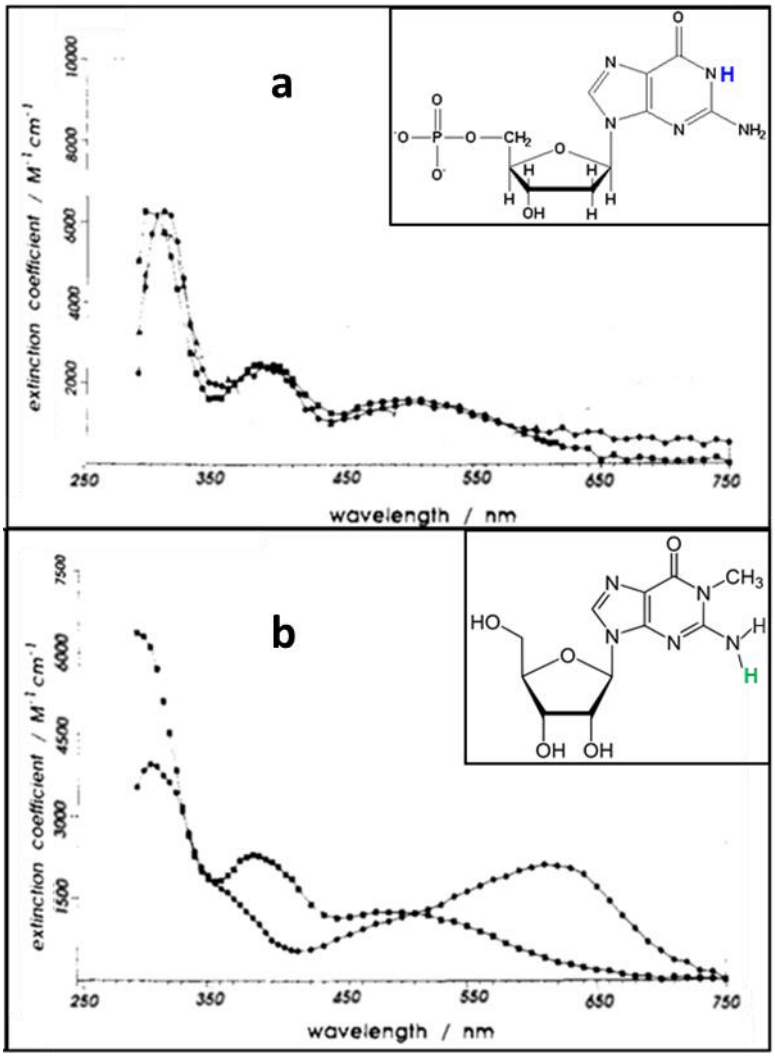

Figure 5. a*) Absorption spectra recorded at 10 µs after reaction of $SO_4^{\bullet-}$ with deoxyguanosine at pH 3.1 (points with 0 intensity between 650 and 750 nm) and pH 6.6 (weak tail between 600 and 700nm).* ***b****) Absorption spectra recorded at 100µs after reaction of $Br_2^{\bullet-}$ with 1-methylguanosine at pH 3.0 (points with 0 intensity between 600 and 700 nm) and pH 7 (intense band between 600 and 700 nm). Reprinted with permission from {Candeias, L. P.; Steenken, S. Stucture and acid-base properties of one-electron-oxidized deoxyguanosine, guanosine, and 1-methylguanosine. J. Am. Chem. Soc. 1989, 111, 1094-1099}. Copyright 1989, American Chemical Society*[44]

By comparing the results obtained for dG and 1-methylG, Candeias and Steenken concluded that for the former compound deprotonation takes place at position 1 (blue proton in the inset of Figure 5a) leading to the deprotonated radical $(G\text{-}H1)^{\bullet}$.[44] When this position is blocked by a methyl group, the proton at

position 2 (green proton in the inset of Figure 5b) is lost. In this case, the deprotonated radical **(G-H2)•** is formed; its spectrum, is characterized by an intense band around 630nm[44] (Figure 5b inset). A better quality spectrum of **(G-H2)•** was reported later by Chatgilialoglu et al. by using pulse radiolysis to study 8-bromo-1-methylguanine.[3]

The deprotonation dynamics of monomeric **(G+)•** was determined by Kobayashi using pulse radiolysis[43,58] (approach a). He exploited the fact that, in contrast to **(G+)•** , **(G-H1)•** radicals absorb at 625 nm. Thus, by recording the absorption rise at this wavelength (Figure 6), he reported a deprotonation rate constant of 1.8×10^7 s^{-1}. [58]

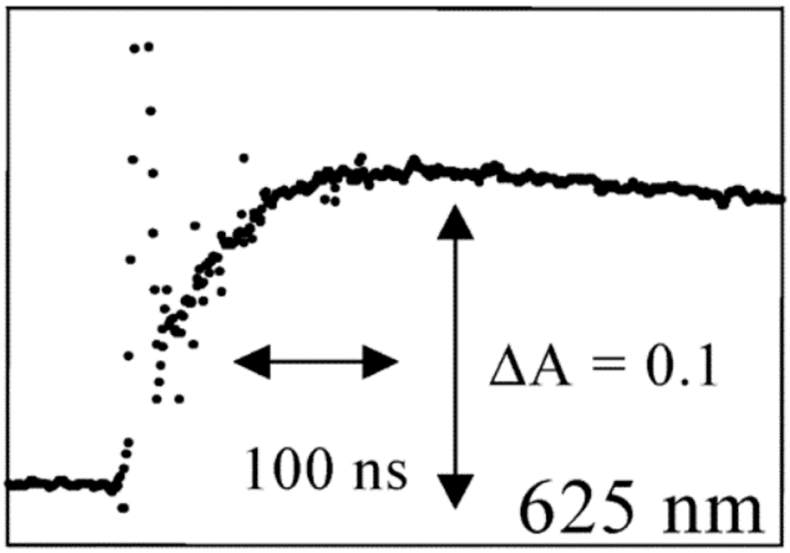

Figure 6. *Absorbance changes at 625 nm after pulse radiolysis of deoxyguanosine, in the presence of ammonium persulfate and tert-butyl alcohol at pH 7.0.*[43]

1.4.2 Guanine radicals in single and double strands

The absorption spectra of **G** radicals in single and double-stranded DNA were reported to be qualitatively similar to those of monomeric d**G**.[46]

Deprotonation in these systems takes place also at the position 1 of **G** (Figure 5a). However, Steenken discussed a specificity of the deprotonation process within duplexes.[25,26,44] In this case, the H1 proton may be transferred either to the cytosine (X) or to the bulk water (Y) (Figure 7a).[37]

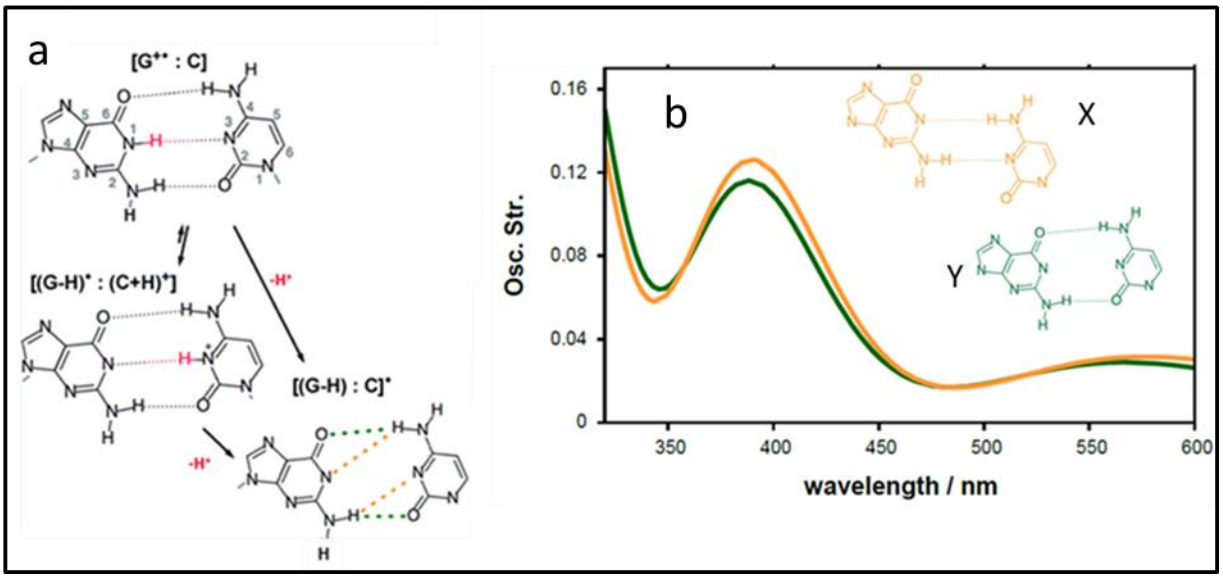

Figure 7. a) *Deprotonation of the guanine cation in a guanine–cytosine Watson–Crick pair; The H1 proton (red) may be transferred to either the cytosine creating an intermediate [(**G**-H)•: (C+H)+] which then gives [(**G**-H) : C]• or the proton is transferred to the bulk water leading to directly to [(**G**-H) : C]•. The orange dashes indicate possible rearrangement of the hydrogen bonds.* ***b)*** *Absorption spectra computed for the guanine deprotonated radical [(**G**-H) : C]• in the G:C Watson Crick pair formed by the mononucleotides dGMP and dCMP (Figure Y) and in the species resulting from rearrangement of two hydrogen bonds (Figure X).*[37]

Using the same approach as for monomeric cations (method a), Kobayashi reported that deprotonation is slowed down within duplexes. Fitting the rise at 625 nm obtained for model duplexes with two-exponential functions, he determined two rate constants of (1.3×10^7 s^{-1}) and (3.0×10^6 s^{-1}). [43]

The dynamics of deprotonated radicals was studied by two different groups. They were both based on flash photolysis experiments. On the one hand,

Shafirovich and co-workers used $SO_4^{\bullet-}$ radical to oxidize DNA, [46] and on the other, the host laboratory used low-energy photoionization.[37] Important discrepancies appeared in the results reported by the two groups. On the one hand, Shafirovich and co-workers reported that deprotonated radicals survive for hundreds of ms[46] in duplexes and even longer in single strands. On the other, the host laboratory showed that they decay in duplexes within 20 ms[37]

1.4.3 Guanine radicals in G-Quadruplexes

Two publications dealing with G radicals in G-quadruplexes had been published very recently. The first one, by Su and coll., published on 2015,[47] was performed by flash photolysis using $SO_4^{\bullet-}$ as oxidant (approach b). The second, published on 2017, was made by the host laboratory using low-energy photoionization.[36]

Su and coll. examined four G-quadruplexes formed in the presence of K^+ ions. They drew two important conclusions. Firstly, they found that $(G^+)^\bullet$ deprotonation in G-quadruplexes is clearly slower compared to that in monomers and duplexes.[47] The reported rate constants range from $2x10^{-5}$ to $14x10^{-5}$ s^{-1}, corresponding to lifetimes from 0.7 μs to 6 μs.[47] Secondly, they discovered that deprotonation of $(G^+)^\bullet$ gives rise to $(G\text{-}H2)^\bullet$ radicals because the hydrogen in position 1 is blocked by hydrogen bonding (Figure 8).[47]

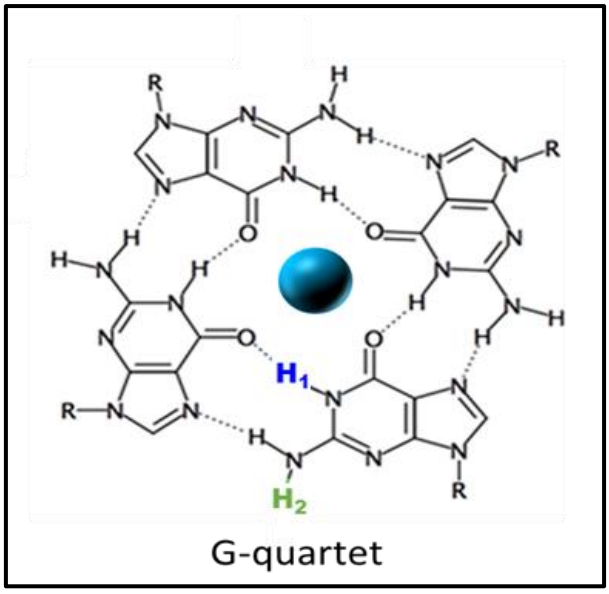

Figure 8. *Schematic illustration of the* ***G****-tetrad showing the deprotonation position which may lead either to* ***(G-H2)•*** *(green proton) or to* ***(G-H1)•*** *(blue proton); the blue sphere in the central cavity represents a metal cation.*

Both conclusions were confirmed by the second study, dealing exclusively with telomeric G-Quadruplexes formed in the presence of Na^+ ions (TEL21/Na^+).[36] However, in this case, radical cations were found to deprotonate more slowly compared to what was reported in the previous study, decaying completely within 2 ms.[36] In addition, Banyasz et al. detected for the first time a tautomerization of deprotonated radicals: $(G\text{-}H2)^{\bullet} \rightarrow (G\text{-}H1)^{\bullet}$ in TEL21/Na^+, which is probably a occurs through base pair opening on the position one of the guanine in the G-tetrad (Figure 8) and takes place on the ms time-scale. They also showed that $(G\text{-}H1)^{\bullet}$ radicals survive in the examined telomeric G-quadruplexes for at least 200 ms. [36]

1.5 References Chapter 1

(1) Quadruplexes and the Biology of G-Rich Genomic Regions. In *Quadruplex Nucleic Acids*; Neidle, S., Balasubramanian, S., Eds.; The Royal Society of Chemistry, 2006; pp 228-252.

(2) Fouquerel, E.; Lormand, J.; Bose, A.; Lee, H. T.; Kim, G. S.; Li, J. F.; Sobol, R. W.; Freudenthal, B. D.; Myong, S.; Opresko, P. L. Oxidative guanine base damage regulates human telomerase activity. *Nat. Struct. Mol. Biol.* **2016**, *23*, 1092-1100.

(3) Greider, C. W.; Blackburn, E. H. A telomeric sequence in the RNA of Tetrahymena telomerase required for telomere repeat synthesis. *Nature* **1989**, *337*, 331-337.

(4) Hockemeyer, D.; Collins, K. Control of telomerase action at human telomeres. *Nat Struct Mol Biol* **2015**, *22*, 848-852.

(5) Palm, W.; Lange, T. d. How Shelterin Protects Mammalian Telomeres. *Annual Review of Genetics* **2008**, *42*, 301-334.

(6) Blackburn, E. H.; Greider, C. W.; Szostak, J. W. Telomeres and telomerase: the path from maize, Tetrahymena and yeast to human cancer and aging. *Nat. Med.* **2006**, *12*, 1133-1138.

(7) Armanios, M.; Blackburn, E. H. The telomere syndromes. *Nat Rev Genet* **2012**, *13*, 693-704.

(8) Blackburn, E. H.; Epel, E. S.; Lin, J. Human telomere biology: A contributory and interactive factor in aging, disease risks, and protection. *Science* **2015**, *350*, 1193-1198.

(9) Structural Diversity of G-Quadruplex Scaffolds. In *Quadruplex Nucleic Acids*; Neidle, S., Balasubramanian, S., Eds.; The Royal Society of Chemistry, 2006; pp 81-99.

(10) Neidle, S. The structures of quadruplex nucleic acids and their drug complexes. *Curr. Opin. Struct. Biol.* **2009**, *19*, 239-250.

(11) Forman, S. L.; Fettinger, J. C.; Pieraccini, S.; Gottareli, G.; Davis, J. T. Toward artificial ion channels: A lipophilic G-quadruplex. *J. Am. Chem. Soc.* **2000**, *122*, 4060-4067.

(12) Mezzina, E.; Mariani, P.; Itri, R.; Masiero, S.; Pieraccini, S.; Spada, G. P.; Spinozzi, F.; Davis, J. T.; Gottarelli, G. The self-assembly of a lipophilic guanosine nucleoside into polymeric columnar aggregates: The nucleoside structure contains sufficient information to drive the process towards a strikingly regular polymer. *Chem. Europ. J.* **2001**, *7*, 388-395.

(13) Burge, S.; Parkinson, G. N.; Hazel, P.; Todd, A. K.; Neidle, S. Quadruplex DNA: sequence, topology and structure. *Nucl. Ac. Res.* **2006**, *34*, 5402-5415.

(14) Fundamentals of Quadruplex Structures. In *Quadruplex Nucleic Acids*; Neidle, S., Balasubramanian, S., Eds.; *R. Soc. Chem.*, 2006; pp 1-30.

(15) Masiero, S.; Trotta, R.; Pieraccini, S.; De Tito, S.; Perone, R.; Randazzo, A.; Spada, G. P. A non-empirical chromophoric interpretation of CD spectra of DNA G-quadruplex structures. *Org. Biomol. Chem.* **2010**, *8*, 2683-2692.

(16) Balasubramanian, S.; Neidle, S.: *Quadruplex DNA structures*; *RCS* Publishing, 2006.

(17) Phan, A. T.; Kuryavyi, V.; Luu, K. N.; Patel, D. J. Structure of two intramolecular G-quadruplexes formed by natural human telomere sequences in K+ solution. *Nucl. Ac. Res.* **2007**, *35*, 6517-6525.

(18) Dai, J. X.; Carver, M.; Punchihewa, C.; Jones, R. A.; Yang, D. Z. Structure of the Hybrid-2 type intramolecular human telomeric G-quadruplex in K+ solution: insights into structure polymorphism of the human telomeric sequence. *Nucl. Ac. Res.* **2007**, *35*, 4927-4940.

(19) Martínez-Fernández, L.; Banyasz, A.; Markovitsi, D.; Improta, R. Topology Controls the Electronic Absorption and Delocalization of Electron Holes in Guanine Quadruplexes. *Chemistry – A European Journal* **2018**, *24*, 15185-15189.

(20) Slavicek, P.; Winter, B.; Faubel, M.; Bradforth, S. E.; Jungwirth, P. Ionization Energies of Aqueous Nucleic Acids: Photoelectron Spectroscopy of Pyrimidine Nucleosides and ab Initio Calculations. *J. Am. Chem. Soc.* **2009**, *131*, 6460-6467.

(21) Schroeder, C. A.; Pluharova, E.; Seidel, R.; Schroeder, W. P.; Faubel, M.; Slavicek, P.; Winter, B.; Jungwirth, P.; Bradforth, S. E. Oxidation Half-Reaction of Aqueous Nucleosides and Nucleotides via Photoelectron Spectroscopy Augmented by ab Initio Calculations. *J. Am. Chem. Soc.* **2015**, *137*, 201-209.

(22) Pluharova, E.; Jungwirth, P.; Bradforth, S. E.; Slavicek, P. Ionization of Purine Tautomers in Nucleobases, Nucleosides, and Nucleotides: From the Gas Phase to the Aqueous Environment. *J Phys Chem B* **2011**, *115*, 1294-1305.

(23) Pluharova, E.; Slavicek, P.; Jungwirth, P. Modeling Photoionization of Aqueous DNA and Its Components. *Acc. Chem. Res.* **2015**, *48*, 1209-1217.

(24) Pluharova, E.; Schroeder, C.; Seidel, R.; Bradforth, S. E.; Winter, B.; Faubel, M.; Slavicek, P.; Jungwirth, P. Unexpectedly Small Effect of the DNA Environment on Vertical Ionization Energies of Aqueous Nucleobases. *J. Phys. Chem. Lett.* **2013**, *4*, 3766-3769.

(25) Candeias, L. P.; Steenken, S. Ionization of purine nucleosides and nucleotides and their components by 193-nm laser photolysis in aqueous solution: model studies for oxidative damage of DNA. *J. Am. Chem. Soc.* **1992**, *114*, 699-704.

(26) Candeias, L. P.; O'Neill, P.; Jones, G. D. D.; Steenken, S. Ionization of polynucleotides and DNA in aqueous solution by 193 nm pulsed laser light: identification of base derived radicals. *Int. J. Radiat. Biol.* **1992**, *61*, 15-20.

(27) Bothe, E.; Gorner, H.; Opitz, J.; Schulte-Frohlinde, D.; Siddiqi, A.; Wala, M. Single- and double-strand break formation in double-stranded dna upon nanosecond laser-induced photoionization. *Photochem. Photobiol.* **1990**, *52*, 949-959.

(28) Opitz, J.; Schulte-Frohlinde, D. Laser-induced photoionization and single-strand break formation for polynucleotides and single-stranded DNA in aqueous solution: model studies for the direct effect of high energy radiation on DNA. *J. Photochem. Photobiol.* **1987**, *39*, 145-163.

(29) Melvin, T.; Plumb, M. A.; Botchway, S. W.; Oneill, P.; Parker, A. W. 193 nm light induces single-strand breakage of DNA predominantly at guanine. *Photochem. Photobiol.* **1995**, *61*, 584-591.

(30) O'Neill, P.; Parker, A. W.; Plumb, M. A.; Siebbeles, L. D. A. Guanine modifications following ionization of DNA occurs predominantly via intra- and not interstrand charge migration: An experimental and theoretical study. *J. Phys. Chem. B* **2001**, *105*, 5283-5290.

(31) Candeias, L. P.; Oneill, P.; Jones, G. D. D.; Steenken, S. Iionization of polynucleotides and DNA in aqueous solution by 193 nm pulsed laser light - identification of base-derived radicals. *Int. J. Radiat. Biol.* **1992**, *61*, 15-20.

(32) Bartels, D. M.; Crowell, R. A. Photoionization yield vs energy in H2O and D2O. *J. Phys. Chem. A* **2000**, *104*, 3349-3355.

(33) Marguet, S.; Markovitsi, D.; Talbot, F. One and two photon ionization of DNA single and double helices studied by laser flash photolysis at 266 nm. *J. Phys. Chem. B* **2006**, *110*, 11037-11039.

(34) Banyasz, A.; Gustavsson, T.; Onidas, D.; Changenet-Barret, P.; Markovitsi, D.; Importa, R. Multi-pathway excited state relaxation of adenine oligomers in aqueous solution: A Joint Theoretical and Experimental Study. *Chem. Eur. J.* **2013**, *19*, 3762-3774

(35) Banyasz, A.; Ketola, T.; Martinez-Fernandez, L.; Improta, R.; Markovitsi, D. Adenine radicals generated in alternating AT duplexes by direct absorption of low-energy UV radiation. *Faraday Disc.* **2018**, *207*, 181-197.

(36) Banyasz, A.; Martinez-Fernandez, L.; Balty, C.; Perron, M.; Douki, T.; Improta, R.; Markovitsi, D. Absorption of Low-Energy UV Radiation by Human Telomere G-Quadruplexes Generates Long-Lived Guanine Radical Cations. *J. Am. Chem. Soc.* **2017**, *139*, 10561-10568.

(37) Banyasz, A.; Martínez-Fernández, L.; Improta, R.; Ketola, T.-M.; Balty, C.; Markovitsi, D. Radicals generated in alternating guanine–cytosine duplexes by direct absorption of low-energy UV radiation. *Phys. Chem. Chem. Phys.* **2018**, *20*, 21381-21389.

(38) Gabelica, V.; Rosu, F.; De Pauw, E.; Antoine, R.; Tabarin, T.; Broyer, M.; Dugourd, P. Electron photodetachment dissociation of DNA anions with covalently or noncovalently bound chromophores. *J. Am. Soc. Mass Spectrom.* **2007**, *18*, 1990-2000.

(39) Galasso, V. Ab initio study of multiphoton absorption properties of formaldehyde, acetaldehyde, and acetone. *J. Chem. Phys* **1990**, *92*, 2495-2504.

(40) Tsuchida, A.; Sakai, W.; Nakano, M.; Yamamoto, M. Electron capture of dopants in two-photonic ionization in a poly(methyl methacrylate) solid. *J. Phys. Chem.* **1992**, *96*, 8855-8858.

(41) Cadet, J.; Wagner, J. R.; Angelov, D. Biphotonic ionization of DNA: from model studies to cell. *Photochem. Photobiol.* **2019**, *95*, 59-72.

(42) Malone, M. E.; Cullis, P. M.; Symons, M. C. R.; Parker, A. W. Biphotonic Photoionization of cytosine and its derivatives with UV radiation at 248 nm: an epr study in low-temperature perchlorate glasses. *J. Phys. Chem.* **1995**, *99*, 9299-9308.

(43) Kobayashi, K.; Tagawa, S. Direct observation of guanine radical cation deprotonation in duplex DNA using pulse radiolysis. *J. Am. Chem. Soc.* **2003**, *125*, 10213-10218.

(44) Candeias, L. P.; Steenken, S. Stucture and acid-base properties of one-electron-oxidized deoxyguanosine, guanosine, and 1-methylguanosine. *J. Am. Chem. Soc.* **1989**, *111*, 1094-1099.

(45) Le Caër, S. Water radiolysis: influence of oxide surfaces on h2 production under ionizing radiation. *Water* **2011**, *3*, 235-253.

(46) Rokhlenko, Y.; Cadet, J.; Geacintov, N. E.; Shafirovich, V. Mechanistic aspects of hydration of guanine radical cations in DNA. *J. Am. Chem. Soc.* **2014**, *136*, 5956-5962.

(47) Wu, L.; Liu, K.; Jie, J.; Song, D.; Su, H. Direct observation of guanine radical cation deprotonation in G-Quadruplex DNA. *J. Am. Chem. Soc.* **2015**, *137*, 259-266.

(48) Melvin, T.; Cunniffe, S.; Papworth, D.; Roldan-Arjona, T.; Oneill, P. Irradiation of DNA with 193 nm light yields formamidopyrimidine-DNA glycosylase (Fpg) protein-sensitive lesions. *Photochem. Photobiol.* **1997**, *65*, 660-665.

(49) Banyasz, A.; Ketola, T.; Muñoz-Losa, A.; Rishi, S.; Adhikary, A.; Sevilla, M. D.; Martinez-Fernandez, L.; Improrta, R.; Markovitsi, D. UV-induced adenine radicals induced in dna A-tracts: Spectral and Dynamical Characterization *J. Phys. Chem. Lett.* **2016**, *7*, 3949-3953.

(50) Kawai, K.; Majima, T. Hole transfer kinetics of DNA. *Acc. Chem. Res.* **2013**, *46*, 2616-2625.

(51) Lewis, F. D.; Young, R. M.; Wasielewski, M. R. Tracking photoinduced charge separation in DNA: from Start to Finish. *Acc. Chem. Res.* **2018**, *51*, 1746-1754.

(52) Angelov, D.; Spassky, A.; Berger, M.; Cadet, J. High-intensity UV laser photolysis of DNA and purine 2'-deoxyribonucleosides: Formation of 8-oxopurine damage and oligonucleotide strand cleavage as revealed by HPLC and gel electrophoresis studies. *J. Am. Chem. Soc.* **1997**, *119*, 11373-11380.

(53) Meggers, E.; Michel-Beyerle, M. E.; Giese, B. Sequence dependent long range hole transport in DNA. *J. Am. Chem. Soc.* **1998**, *120*, 12950-12955.

(54) Saito, I.; Nakamura, T.; Nakatani, K.; Yoshioka, Y.; Yamaguchi, K.; Sugiyama, H. Mapping of the hot spots for DNA damage by one-electron oxidation: Efficacy of GG doublets and GGG triplets as a trap in long-range hole migration. *J. Am. Chem. Soc.* **1998**, *120*, 12686-12687.

(55) Genereux, J. C.; Barton, J. K. Mechanisms for DNA charge transport. *Chem. Rev.* **2010**, *110*, 1642-1662.

(56) Choi, J.; Park, J.; Tanaka, A.; Park, M. J.; Jang, Y. J.; Fujitsuka, M.; Kim, S. K.; Majima, T. Hole trapping of G-Quartets in a G-Quadruplex. *Angew. Chem. Int. Ed.* **2013**, *52*, 1134-1138.

(57) Palecek, E.; Bartosik, M. Electrochemistry of Nucleic Acids. *Chem. Rev.* **2012**, *112*, 3427-3481.

(58) Kobayashi, K.; Yamagami, R.; Tagawa, S. Effect of base sequence and deprotonation of guanine cation radical in DNA. *J. Phys. Chem. B* **2008**, *112*, 10752-10757.

Chapter 2

Materials and methods

This chapter presents the main methods and protocols followed to carry out the work of the thesis. I provide details about the materials used, the preparation and handling of the various DNA systems, as well as the methods applied for their characterization (melting curves, steady-state and circular dichroism spectroscopy). Finally, I focus on the nanosecond flash photolysis technique. I present the general principle of its functioning and details concerning the precise experimental setup with which my measurements were performed.

2.1 Sample preparation

Oligonucleotides were purchased from Eurogentec Europe, purified by reversed phase HPLC and tested by MALDI-TOF. The aqueous solutions were prepared by using phosphate buffers which were composed by an equimolar mixture of NaH_2PO_4/Na_2HPO_4 or KH_2PO_4/K_2HPO_4 in concentrations 0.15 or 0.015 mol·L^{-1} each, depending on the experiment. All the solutions were prepared using ultra-pure water, delivered by a MILLIPORE (Milli-Q Integral) system. For most of the experiments, the pH of the buffer, measured by a HANNA Instrument Apparatus (pH 210), was adjusted to 7 by addition of a concentrated NaOH/KOH (1 mol L^{-1}) solution. The purity of the buffer ingredients was 99.99%.

A stock concentrated solution, prepared by dissolving the oligomer powder in 2-4 mL, was heated to 96°C in an Eppendorf dry bath for 5 minutes, so that the DNA strands dissociate. Then, the solution was cooled (cooling time: 1 h) to the melting point of the corresponding system, reported in the literature, where the temperature was maintained for 10 min. Subsequently, the solution was cooled all the way to 4°C for 2 h, where it is incubated for 1-3 days. This procedure is called DNA annealing.

In some G-quadruplexes forming sequences, heating the solution to 96°C does not completely dissociate the DNA strands.[1] This problem appeared in particular with the Oxytricha sequences (see prologue Table 1; 12 and 13). In this case, prior to the annealing, I carried out a pre-treatment,[2] allowing the DNA strands to dissociate by breaking hydrogen bonds. In practice, I added in the stock solution a few drops KOH/NaOH (1 mol L^{-1}) and adjusted the pH to 12. After stirring for a few seconds and observing complete dissolution, I neutralized the pH with a solution of phosphoric acid (H_3PO_4; 1 mol L^{-1}) and then started the annealing.

For transient absorption measurements, an appropriate quantity of the stock solution was diluted so that their absorbance at 266 nm to be 2.4 ± 0.2 over 1 cm. The latter solution was either stored at -20°C or used directly for the

experiments. If the solutions were frozen, prior to the experiment, they were heated to 50°C, so that to destroy higher aggregates possibly formed at high concentration[3] and then cooled slowly to room temperature.

The calf thymus DNA, purified using a Chelex ion-exchange resin and subsequent extensive dialysis, was provided by Dr. T. Douki (CEA Grenoble) as a saturated aqueous solution. In this case, a phosphate buffer more concentrated than usually was prepared so that after dilution to reach a concentration of 0.015 mol L^{-1} or 0.15.

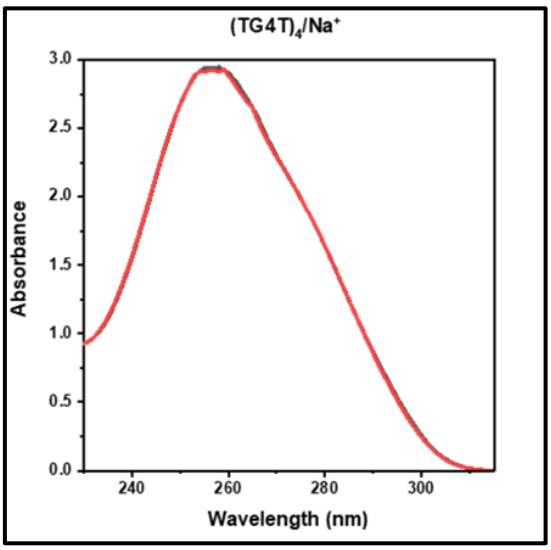

***Figure 1**. Steady state absorption spectra of $(TG_4T)_4/Na^+$ in pH 3 (black) and pH= 7 (red).*

For experiments at pH 3 (see Chapter 4. Section 4.4.1), where deprotonation of guanine radical cations is precluded,[4] I used two protocols. A DNA solution in the normal phosphate buffer (pH 7) was prepared and its absorption spectrum was recorded. Subsequently, a few drops (typically 2 µL) of concentrated hydrochloric acid (HCl 1 mol L^{-1}) were slowly added to the solution which was well stirred; the procedure was repeated until reaching pH 3. Then the absorption spectrum was recorded again and compared to that obtained for pH 7 (Figure 1). The absence of spectral modification shows that protonation does not occur prior to photoionization. In the second approach, I replaced HCl by phosphoric acid (H_3PO_4

; 1 mol L^{-1}). As a matter of fact, Cl^- ions have a well-known absorption peaking at 330 nm[5] and also a weak absorption at 266 nm (Figure 1 in reference 5); this could possibly lead to the creation of chlorine radicals, which are very reactive versus DNA.[6]

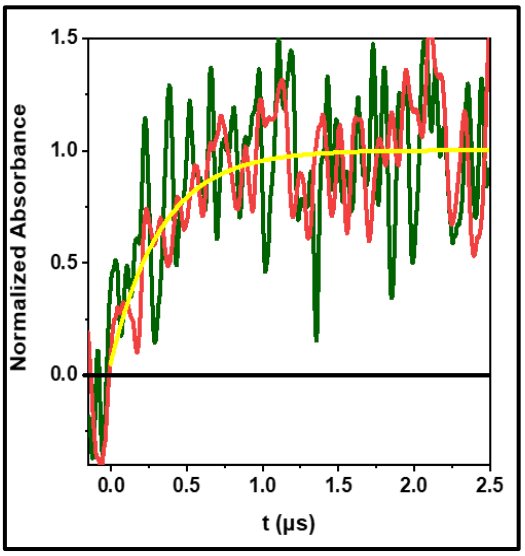

***Figure 2**. Normalized transient absorption signals recorded for CT-DNA at 720 nm; (red) N_2O saturated solution; (green) $NaNO_3$ solution; the yellow line corresponds to the fit with a mono-exponential function.*

For the study of radicals on short times (≤ 2μs) I used electron scavengers so that to eliminate the much stronger absorbance of hydrated electrons (Chapter 3). To this end, I saturated the DNA solution in the usual phosphate buffer by the N_2O gas.[7] Alternatively, I dissolved DNA in an aqueous solution containing $NaNO_3$ with the same ionic strength as the phosphate buffer. Both scavengers gave the same results (Figure 2).

2.2 Steady-state spectroscopy

2.2.1 Absorption spectra and melting curves

It is well-known that formation of duplex DNA induces a decrease in the absorbance around 260 nm (hypochromism; 17% in Figure 3a). Such a

hypochromism is also observed at 260 nm for G-quadruplexes but it is weaker compared to duplexes (13% in Figure 5b)[2,8] (Figure 3b). **G**-quadruplexes exhibit, in addition, a hyperchromism around 295 nm (21% in Figure 3a).[8] These spectral changes are due to the existence of electronic coupling among the bases (see for example ref. 9).

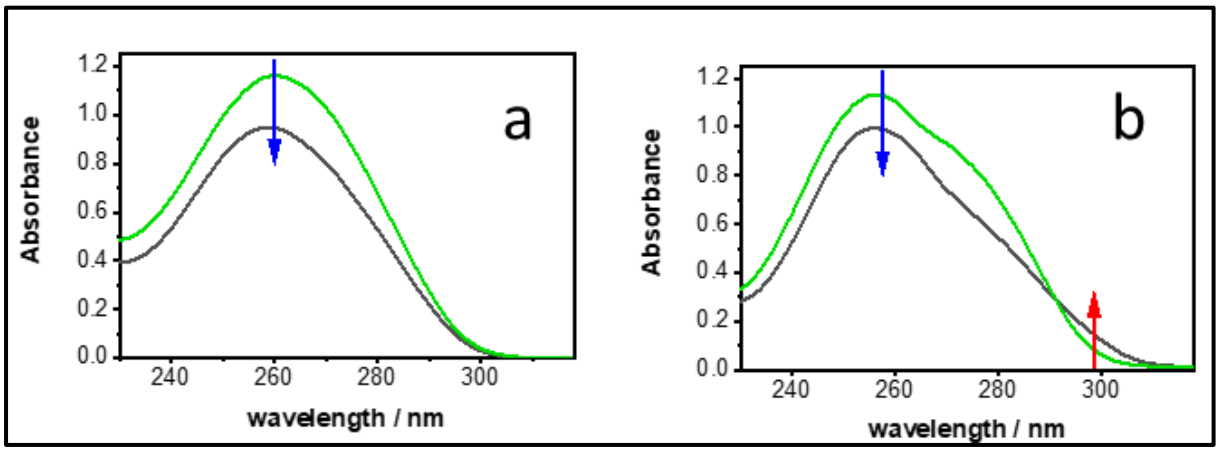

***Figure 3. a**) Steady-state absorption spectra recorded at 23°C (black) and 96°C (green) for the S1•S2 duplex (a) and OXY/Na^+ **G**-quadruplex (**b**). Blue and red arrows show, respectively, the hypochromism and the hyperchromism.*

The widely used melting curves to characterize duplexes and **G**-quadruplexes are based precisely on the above mentioned properties of hypochromism and hyperchromism, respectively. Examples are shown in Figure 4. They were obtained automatically by recording absorption spectra of the sample every 4°C upon increasing the temperature from 16°C and 96°C; the whole procedure lasts for 160 minutes. The melting curve allows the determination of the melting temperature of the system, which is 76 °C and 60 °C, respectively, for the duplex and the G-quadruplex in Figure 4.

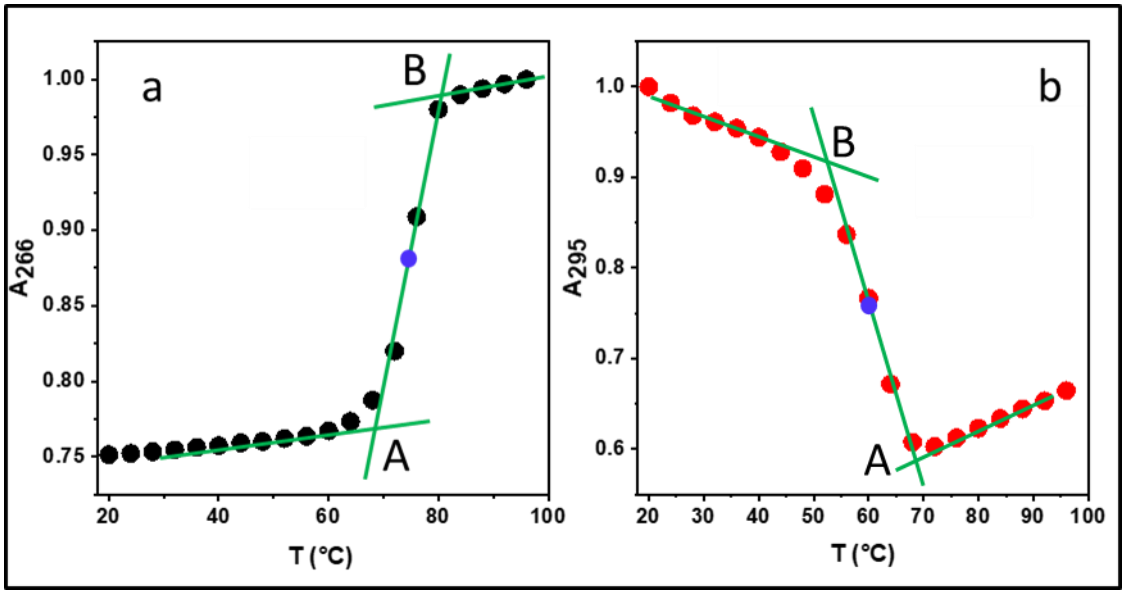

***Figure 4**. Melting curves (circles) recorded for **a) S1•S2** duplex at 266 nm and **b)** $(TG_4T)_4/Na^+$ at 295 nm.; The middle-points (blue) of the segments AB give the melting temperature..*

2.2.1 Circular dichroism

Steady-state circular dichroism (CD) spectroscopy is also widely used to characterize the three-dimensional secondary structure of G-Quadruplexes by measuring the difference in absorbance of right- and left-circularly polarized light.[9,11,12] It should be noted, however, that in most studies, the interpretation of CD spectra is empirical and is done by comparison with CD spectra of previously identified G-Quadruplex structures. It has been observed that the shape of the CD spectra depends significantly on the topology of the G-Quadruplexes [10] (Figure 5 a and b). Recently, these spectral modifications started to be rationalized in the frame of the exciton theory, considering the dipolar coupling between electronic transitions. The latter depends substantially on the relative position of the different bases and determines the intensity and position of the CD bands.[10,13] During the past few years CD spectra were also reconstructed by quantum chemistry methods.[14]

The CD spectra of the tetramolecular G-quadruplexes studied in my thesis were recorded by Dr. Peter Podbevšek at *Slovenian NMR Center, National*

Institute of Chemistry in Ljubljana. All of them exhibit the characteristic feature of parallel structures: a positive peak around 260 nm and two negative peaks at 240 nm and 290 nm.[10] Several examples are shown in Figure 5c.

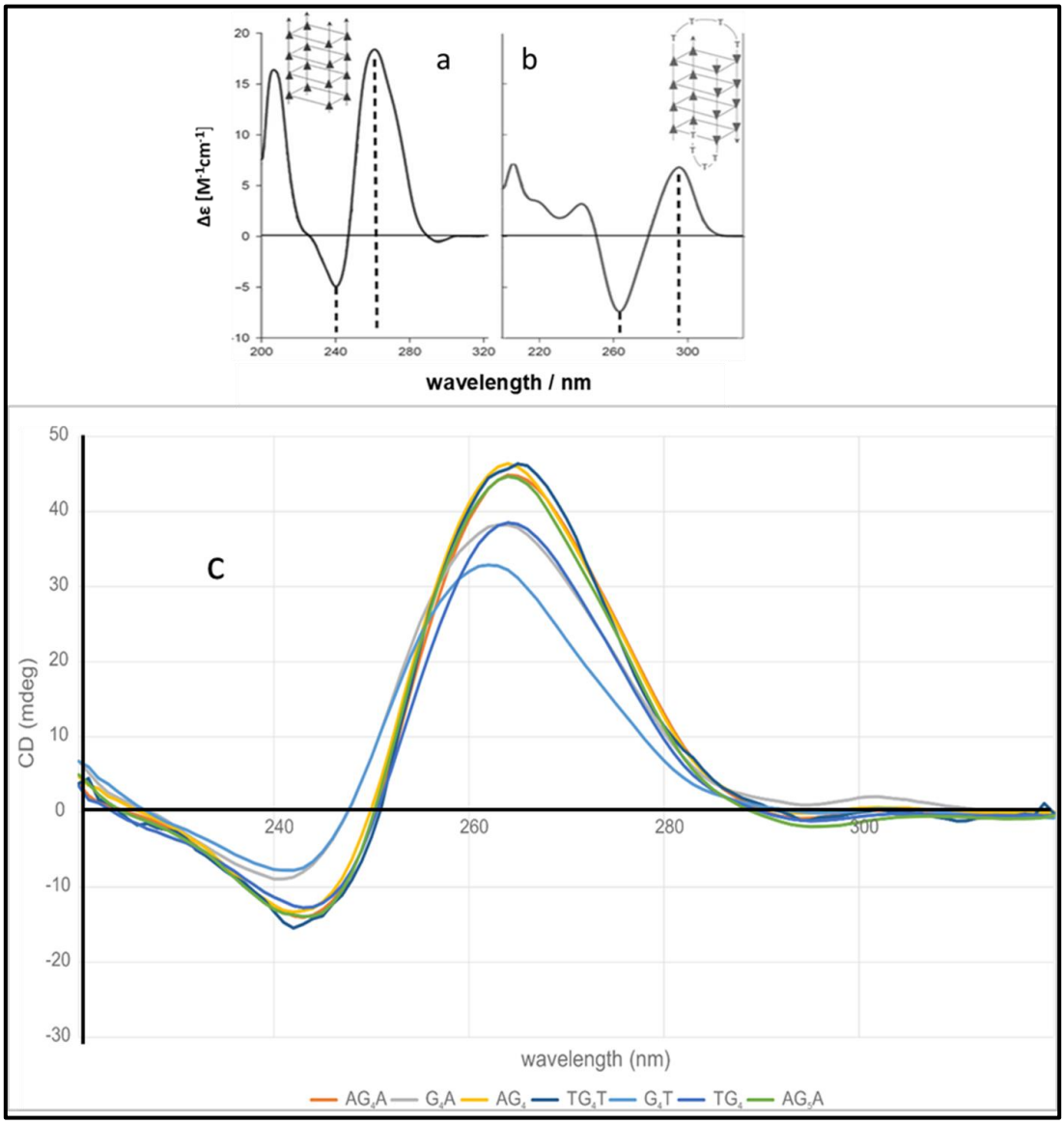

Figure 5. *Model CD spectra of parallel* ***a****) and antiparallel* ***b****) G-Quadruplexes.*[10] ***c****) CD spectra of* $(AG_4A)_4/K^+$ *(orange),* $(G_4A)_4/K$ *(grey),* $(AG_4)_4/K$ *(yellow),* $(AG_5A)_4/K^+$ *(green),* $(TG_4T)_4/K$ *(dark blue)* $(G_4T)_4/K$ *(light blue) and* $(TG_4)_4/K$ *(blue).*

2.3 Laser Flash photolysis

2.3.1 General concept

Flash photolysis is an essential technique[15] allowing the recording of dynamics of unstable transient states and transient chemical species. It consists in exciting a material by an intense pulse of light. The pulse populates higher energy electronic levels compared to the ground state which subsequently may give rise to chemical reactions.[15] This is presented schematically in Figure 6. Then the generated excited states or transient species (X) are characterized by their absorption spectrum which is obtained using a continuous light source. As X is unstable, its decay and, consequently, its absorbance decreases providing information about the reaction dynamics.

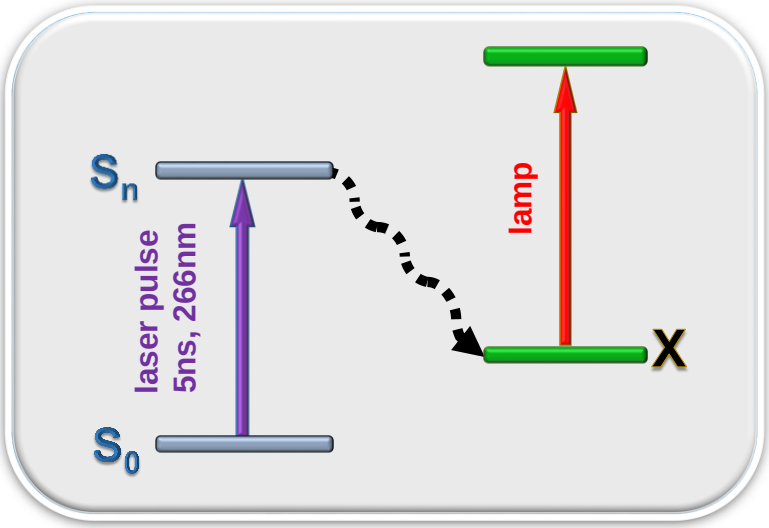

***Figure 6**. Schematic representation of the principle underlying flash photolysis measurements; after excitation of the sample at 266 nm from the ground state S_0 towards a singlet excited state S_n, a transient species X is formed. The absorption of X is probed using the light of a continuous light source (lamp)*

2.3.2 Description of the setup used

The excitation source is the fourth harmonic (266 nm) of a Nd:YAG laser (Spectra-Physics, Quanta Ray); the pulse duration is 5 ns. The excited area at the surface of the sample is 0.6 × 1.0 cm^2 (Figure 7a). The analyzing beam, orthogonal to the exciting beam, is provided by a 150 W Xe-arc lamp (OSRAM XBO). The optical path through the sample is 1 cm, while laterally it is limited to 0.1 cm in order to use the most homogeneous part of the light. The probed volume is located in the very first 0.1 cm (Figure 7b) part of the cell along the propagation of the exciting laser beam and delimited by four dedicated slits (Figure 7c). The transmitted light is then dispersed in a Jobin-Yvon SPEX 270M monochromator. Fast shutters are placed in the path of both laser and lamp beams; thus, the excitation rate is decreased from 10 Hz to 0.2 Hz.

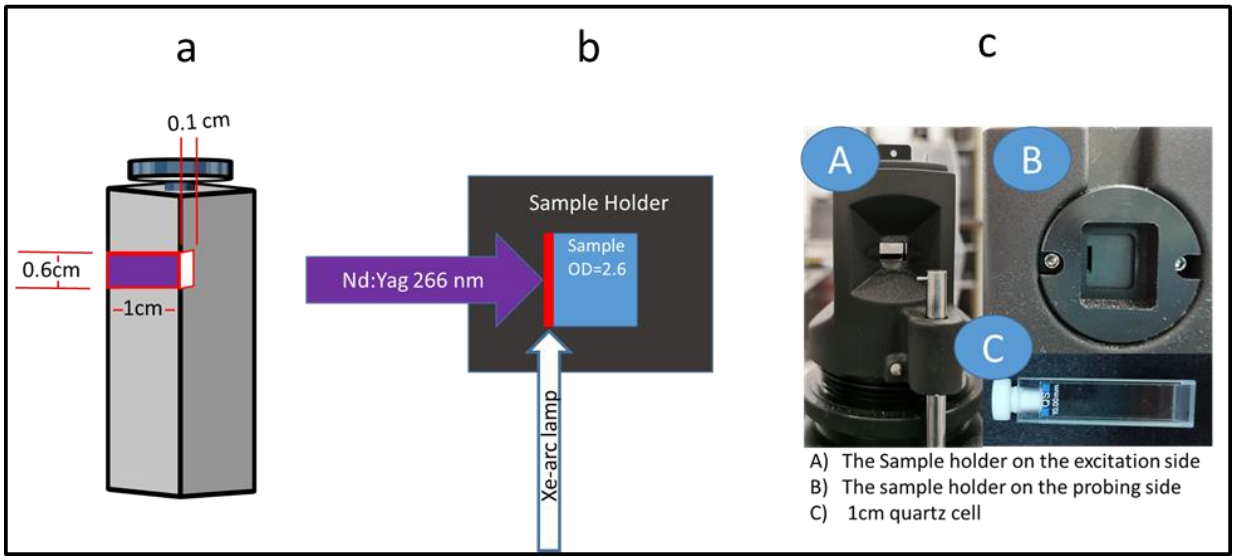

***Figure 7. a**) Schematic representation of the sample volume probed during the measurements. **b**) Optical path-lengths of the exciting and probing beams through the sample holder. **c**) Photos of the (A) excitation side and (B) probing side of the sample holder, as well as the 1cm x 1cm quartz cell used for the experiment (C).*

The selected wavelength intensity is finally detected by a Hamamatsu R928 photomultiplier and recorded by a Lecroy Waverunner oscilloscope (8054, 1 GHz bandwidth). The signals recorded by the oscilloscope are transformed from voltage to intensity (eq.1). During the measurement, the software collects three different variables: the lamp intensity, which is the initial intensity (I_0), the intensity of noise (I_N), which is the intensity recorded when both the laser and the lamp shutters are closed, and the intensity after excitation of the sample I(t). Then these intensities are transformed to absorbance (eq. 2) automatically through the labview software, which, in the end, provides the transient absorbance as a function of time.

$$I = \frac{V}{R} \qquad \text{(eq.1)}$$

$\boldsymbol{I}$: *intensity* $\boldsymbol{V}$: *Voltage measured by the osciloscope*
$\boldsymbol{R}$: *the resistance used for the measurement*

$$A = -log_{10}\frac{I(t)-I_N}{I_0-I_N} \qquad \text{(eq.2)}$$

For measurements on the sub-μs scale, the Xe-arc lamp can be intensified via an electric discharge (ARC LAMP PULSER Applied photophysics). This discharge is needed, because the measurements are limited by the 50 Ω-resistance in the oscilloscope input, which is necessary for using the highest bandwith of the oscilloscope. Under these conditions, the time-resolution is estimated to be 30 ns. Transient absorption spectra are recorded using a wavelength-by-wavelength approach.

At each wavelength, a series of three successive signals, resulting from 20-50 laser shots each, were recorded; if judged to be reproducible they were averaged to reduce the signal-to-noise ratio. During the measurement 2-3 mL of the studied solution were contained in a 1 cm x 1 cm quartz cell and stirred mildly while the temperature was maintained at 23 °C. To summarize, the acquisition chain is illustrated in Figure 8.

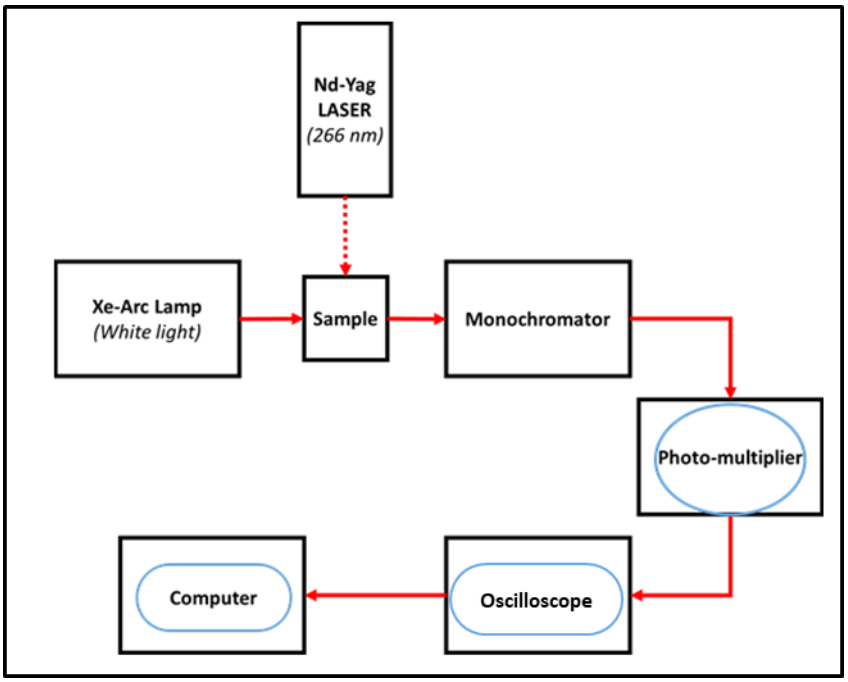

Figure 8. *Schematic illustration of the flash photolysis set-up used in this study.*

2.4 Determination of absorbed photons

The number of absorbed photons, required for the determination of quantum yields, was derived from the energy absorbed by the probed volume of solution (0.06 cm^3). The latter was determined from the energy of the incident pulse, measured by a NIST-traceable pyroelectric sensor (OPHIR NOVA2, PE25) and the absorbance of the sample; potential variations during a measurement were monitored by detecting a fraction of the exciting beam shot-by-shot using a second pyroelectric sensor. Alternatively, the absorbed energy was obtained by subtracting the energy transmitted by the sample from the incident one, using as a blank a cell containing only the aqueous solvent. In addition, the absorbance of the naphthalene triplet state, whose quantum yield in cyclohexane is 0.75, [16] served as cross-check.

The absorbed pulse energy was converted into the concentration of absorbed photons via the formula

$$[hv_{absorbed}] = \frac{E_{inc} \cdot \lambda \cdot \left(1 - 10^{-0.1 \cdot A_{266}}\right)}{N_a \cdot V_p \cdot h \cdot c} \qquad \text{(eq.5)}$$

$\boldsymbol{E_{inc}}$: *incident energy* $\boldsymbol{\lambda}$: *wavelength* $\boldsymbol{A_{266}}$: *steady state absorbance at* 266*nm*

$\boldsymbol{V_p}$: *probed volume* $\boldsymbol{h}$: *plank constant* $\boldsymbol{c}$: *speed of light* $\boldsymbol{N_a}$; *Avogadro consta*

For measurements with naphthalene, solutions in cyclohexane I used solutions with an absorbance of 0.4 ± 0.1 at 266 nm over 1 cm. Special precautions were needed. The quartz spectroscopic cells should be water free, because water contamination alters the final results. The solution was sealed well and placed into a water bath where it was saturated with argon while the temperature was maintained at 8 ± 1 °C to hinder fast evaporation of cyclohexane (freezing point at 6°C). After saturation (about 15-20 minutes), the absorbance of the solution was measured again. Then the decay of the triplet state was recorded at 415 nm (Figure 9) and fitted with a mono-exponential function $A_0 + A_1\exp(t/\tau_1)$. Subsequently, by using the A_1 value and the molar absorption coefficient ε_{415} = 24500 mol^{-1} L cm^{-1},[16] I determined the concentration of the formed triplet state. This concentration, divided by the concentration of absorbed photons in the probed volume of the solution (0.6 cm^3) provided the quantum yield. As expected from the literature, it was found to be 0.75 ± 0.04. [16]

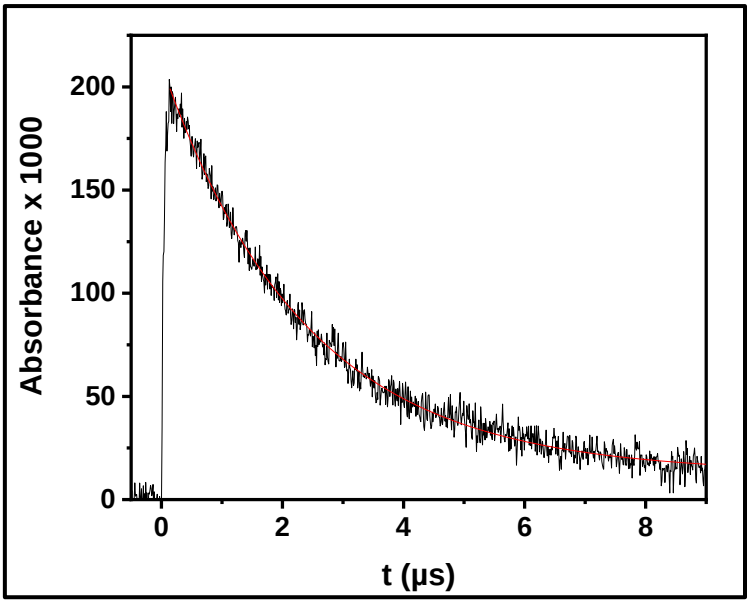

Figure 9. *Transient absorption decay recorded for an argon saturated solution of naphthalene in cyclohexane at 415 nm (black) with incident energy of 3.15 mJ; absorbance at 266 nm: 0.42; the red line correspond to the fit with a single exponential function:* $A_0 + A_1 exp(t/\tau_1)$

2.5 References Chapter 2

(1) Mergny, J.-L.; De Cian, A.; Ghelab, A.; Saccà, B.; Lacroix, L. Kinetics of tetramolecular quadruplexes. *Nucl. Ac. Res.* **2005**, *33*, 81-94.

(2) Hua, Y.; Changenet-Barret, P.; Gustavsson, T.; Markovitsi, D. The effect of size on the optical properties of guanine nanostructures: a femtosecond to nanosecond study. *Phys. Chem. Chem. Phys.* **2013**, *15*, 7396-7402.

(3) Abu-Ghazalah, R. M.; Rutledge, S.; Lau, L. W. Y.; Dubins, D. N.; Macgregor, R. B., Jr.; Helmy, A. S. Concentration-dependent structural transitions of human telomeric DNA sequences. *Biochem.* **2012**, *51*, 7357-7366.

(4) Candeias, L. P.; Steenken, S. Stucture and acid-base properties of one-electron-oxidized deoxyguanosine, guanosine, and 1-methylguanosine. *J. Am. Chem. Soc.* **1989**, *111*, 1094-1099.

(5) Maric, D.; Burrows, J. P.; Meller, R.; Moortgat, G. K. A study of the UV—visible absorption spectrum of molecular chlorine. *J. Photochem. Photobiol. A,* **1993**, *70*, 205-214.

(6) Jie, J.; Liu, K.; Wu, L.; Zhao, H.; Song, D.; Su, H. Capturing the radical ion-pair intermediate in DNA guanine oxidation. *Science Advances* **2017**, *3*, e1700171.

(7) von Sonntag, C.: *Free-radical-induced DNA damage and its repair* Springer-Verlag: Berlin-Heildelberg, 2006.

(8) Mergny, J. L.; Phan, A. T.; Lacroix, L. Following G-quartet formation by UV-spectroscopy. *Febs Letters* **1998**, *435*, 74-78.

(9) Martinez-Fernandez, L.; Changenet, P.; Banyasz, A.; Gustavsson, T.; Markovitsi, D.; Improta, I. A Comprehensive study of guanine excited state relaxation and photoreactivity in G-Quadruplexes. *J. Phys. Chem. Lett.* **2019**, *10*, 6873-6877.

(10) Masiero, S.; Trotta, R.; Pieraccini, S.; De Tito, S.; Perone, R.; Randazzo, A.; Spada, G. P. A non-empirical chromophoric interpretation of CD spectra of DNA G-quadruplex structures. *Organic & Biomolecular Chemistry* **2010**, *8*, 2683-2692.

(11) Randazzo, A.; Spada, G. P.; Webba da Silva, M. Circular dichroism of quadruplex strucures. *Top. Curr. Chem.* **2013**, *330*, 67–86.

(12) Del Villar-Guerra, R.; Trent, J. O.; Chaires, J. B. G-Quadruplex secondary structure obtained from Circular Dichroism Spectroscopy. *Angew. Chem. Int. Ed.* **2018**, *57*, 7171-7175.

(13) Karsisiotis, A. I.; Hessari, N. M.; Novellino, E.; Spada, G. P.; Randazzo, A.; da Silva, M. W. Topological characterization of nucleic acid G-Quadruplexes by UV absorption and circular dichroism. *Angew. Chem. Int. Ed.* **2011**, *50*, 10645-10648.

(14) Martínez-Fernández, L.; Esposito, L.; Improta, R. Studying the excited electronic states of guanine rich DNA quadruplexes by quantum mechanical methods: main achievements and perspectives. *Photochem. Photobiol. Sci.* **2020**, *19*, 436-444.

(15) Porter, G. Flash Photolysis and Spectroscopy. A New Method for the Study of Free Radical Reactions. *Proceedings of the Royal Society of London. Series A, Mathematical and Physical Sciences* **1950**, *200*, 284-300.

(16) Amand, B.; Bensasson, R. Determination of triplet quantum yields by laser flash absorption spectroscopy. *Chemical Physics Letters* **1975**, *34*, 44-48.

Chapter 3

Photo-ejected electrons

This chapter is dedicated to the characterization of ejected electrons which are quantified by observing their hydrated form. After presenting their reaction dynamics, I explain how one-photon ionization quantum yields (Φ_1) are determined. I show the Φ_1 values obtained for single-, double- and four-stranded DNA as well as the factors affecting them. I focus in particular on G-Quadruplexes for which I examine the role of their topology, the number of tetrads composing them, the type of the metal cations in their central cavity and the type and position of the ending groups. Finally, I discuss how these results can be explained by an indirect photoionization mechanism.

3.1 Ejected electrons

3.1.1 Quantification and dynamics of hydrated electrons

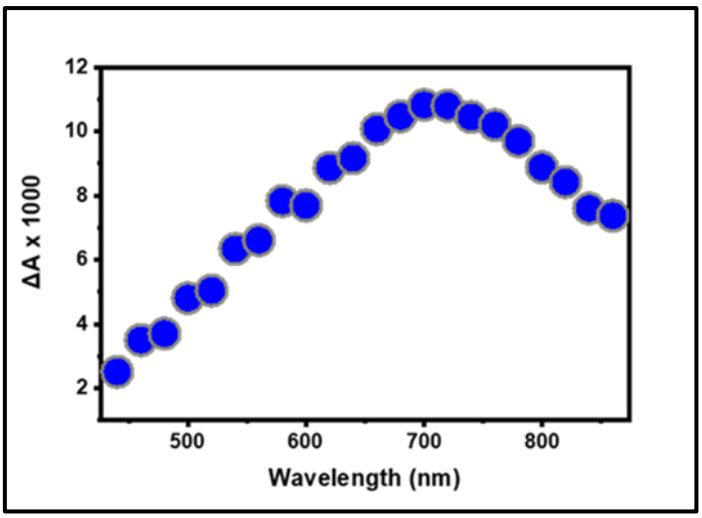

Figure 1. *Transient absorption spectrum recorded at 30 ns for CT-DNA with incident excitation intensity of 2.0×10^{6} $W\cdot cm^{-2}$.*

Electrons ejected in aqueous solutions are known to get hydrated within a few ps.[1] The absorption spectrum of hydrated electrons (e_{hyd}^-) is characterized by a large band peaking at 720 nm.[2] Figure 1 shows the transient absorption spectrum recorded for CT-DNA at 30 ns after excitation pulse. It exhibits indeed such an absorption band. Note that all the results on hydrated electrons were obtained for argon saturated solutions because O_2 reacts very rapidly with them.

In the case of small DNA structures, their decay can be described with a mono-exponential function: $A_1 + A_0 \times \exp(-t/\tau)$ at (Figure 2), where A_0 corresponds to the hydrated electron absorption and the A_1 is constant proportional to a small concentration of deprotonated radicals (G-H) and a correction to the base line after due to the ARC LAMP PULSER; for the usual buffer concentration (0.15 $mol\cdot L^{-1}$ MH_2PO_4 / 0.15 $mol\cdot L^{-1}$ M_2HPO_4 where M is either K^+ or Na^+) the $\tau = 0.5\pm0.1\mu s$. In principle, e_{hyd}^- may disappear reacting with $H_2PO_4^-$ or the H^+ ions.[3,4]

$[e^-_{hyd}] + [H^+] \rightarrow [H^\bullet]$ k=1.1 x 10^7 dm^3 mol^{-1} s^{-1}, [5] (eq.1)

$[e^-_{hyd}] + [H_2PO_4^-] \rightarrow [H^\bullet] + [HPO_4^{2-}]$ k=2.3x 10^{10} dm^3 mol^{-1} s^{-1},[6] (eq.2)

Given the above rate constants, the high concentration of $H_2PO_4^-$ (0.15 mol L^{-1}) and the pH of the solvent (7), it appears that the major reaction path corresponds to Eq. 2. In addition, upon changing the buffer concentration the e_{hydr}^- decays are modified (Figure 3a). Although the involved reaction is a second order one, in fact, we deal with pseudo-mono-molecular reaction because the concentration of $[e^-_{hyd}]_0$ (1x10^{-6} mol L^{-1}) is several orders of magnitude lower than that of $[H_2PO_4^-]$. From the A_0 value derived from the fit and the ε value of e_{hyd}^- (19700 $mol^{-1}Lcm^{-1}$ at 720 nm, taken from reference 2 at a given wavelength, we deduce the initial concentration of hydrated ejected electrons $[e^-_{hyd}]_0$ (eq.3).

$$[e^-_{hyd}]_0 = \frac{A_0}{\varepsilon \cdot \ell} \qquad \text{(eq.3)}$$

$\ell = 1cm, \varepsilon$: *molar absorption coefficient at coresponding wavelength*

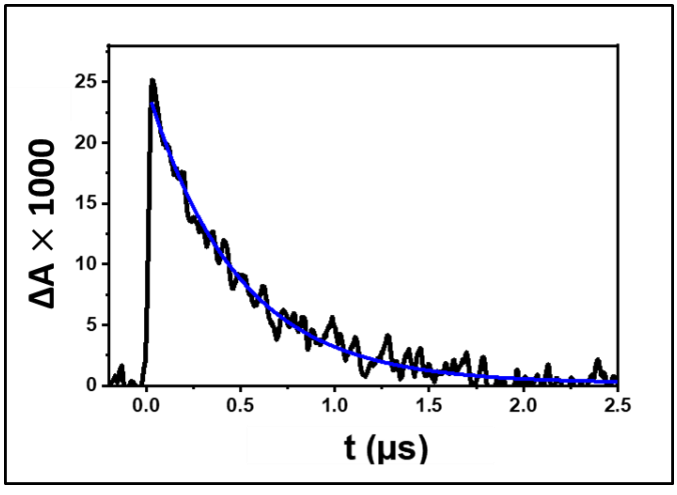

Figure 2. *Transient absorption signal recorded at 700 nm for OXY/K^+ solutions (black). The blue line corresponds to fit with the model function $A_1+A_0 exp(-t/\tau)$ with τ= 0.5 μs.*

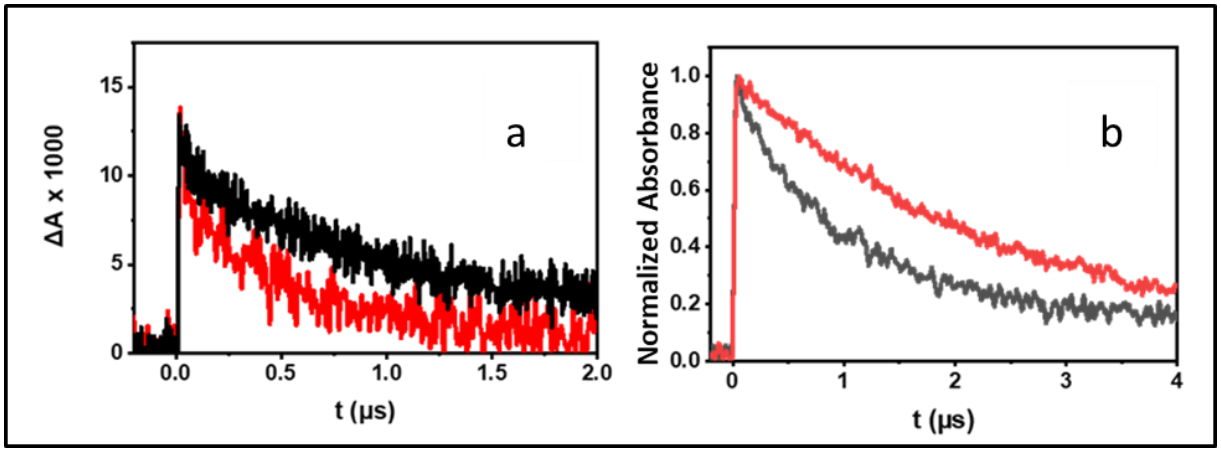

Figure 3. *Transient absorption decays recorded at 700 nm for* ***a)*** *CT-DNA in dilute buffer (0.015 mol·L^{-1} NaH_2PO_4 / 0.015 mol·L^{-1} Na_2HPO_4) (black) and concentrated buffer (0.15 mol·L^{-1} NaH_2PO_4 / 0.15 mol·L^{-1} Na_2HPO_4) (red).* ***b)*** *CT-DNA (black) and the short duplex S1•S2 (red) in diluted buffer (0.015 mol·L^{-1} NaH_2PO_4 / 0.015 mol·L^{-1} Na_2HPO_4.*

The decays of e_{hyd}^- issued from CT-DNA are significantly faster compared to those of smaller systems, such as the S1•S2 model duplex (Figure 3b). Moreover, they cannot be fitted with single exponential functions, revealing the existence of additional reaction paths, involving DNA.[7] Such reactions could be favored by the flexibility of the very long duplex,[8,9] increasing locally the encounter probability between nucleic acid components and e_{hyd}^- produced by the same helix. For that reason, in order to determine the initial electron concentration in the case of the CT-DNA, I fitted the decays with two exponential function $y = A_1 \exp(-x/t_1) + A_2 \exp(-x/t_2) + y_0$ and extracted the initial electron concentration from the value of the fitted line at 30 ns.

3.1.2 Determination of one-photon ionization quantum yields

The determination of the one-photon ionization quantum yield begins with the construction of the ionization curve (Figure 4). To achieve this, one varies the incident excitation energy, typically in the range 0.5 – 6 mJ, and records the transient absorption decays of the hydrated electrons at selective energies. Then,

one determines for each decay the initial electron concentration $[e_{hyd}^-]_0$. Subsequently, one plots $[e_{hyd}^-]_0/[hv]$ versus [hv], where the [hv] is the concentration of the absorbed photons within the irradiation volume (see Chapter 2.4.3). Figure 4 presents the ionization curve obtained for the tetramolecular G-Quadruplex $(AG_4A)_4/K^+$. The fit of the experimental points with a linear function (eq.4), provides the quantum yield for one-photon ionization Φ_1. The Φ_1 is derived from the intercept of the fitted line on the vertical axis (arrow in Figure 4), while the contribution of two-photon ionization is given by the slope α (angle between the dashed line and the fit) of the curve.

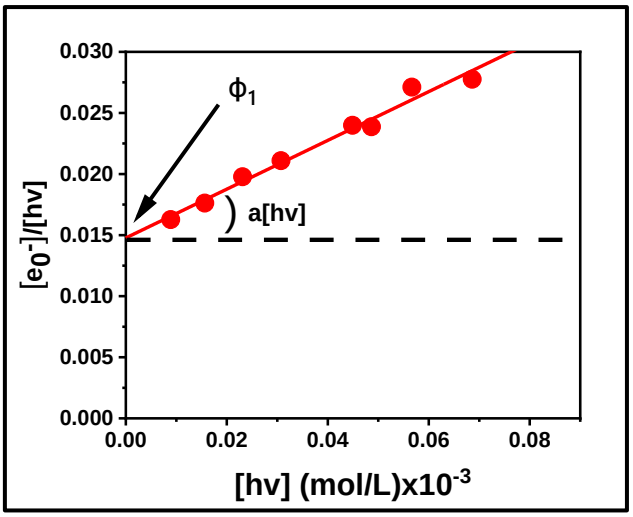

***Figure 4**. Ionization curve of the G-Quadruplex $(AG_4A)_4/K^+$ (red circles). The red line corresponds to the fit with a linear function $[e_{hyd}^-]_0/[hv]= a[hv]+ \Phi_1$; [hv] and $[e_{hyd}^-]_0$ denote, respectively, the concentration of absorbed photons per laser pulse and the initial concentration of hydrated electrons. The arrow shows the intercept of the fitted line with the y-axis, which gives the Φ_1.*

$$[e_{hyd}^-]_0/[hv] = \Phi_1 + \alpha[hv] \qquad \text{(eq.4)}$$

It must be noted that despite using low excitation intensities ($I_{inc}<2.0\times10^6$ Wcm^{-2}, corresponding to excitation energies $E_{inc}<6mJ$), the two-photon ionization,

resulting from the absorption of a second photon by long-lived electronic excited states, cannot be completely prevented.

While the experimental points obtained for incident excitation intensity I_{inc} lower 2.0×10^{6} Wcm^{-2}, can be fitted with a linear model function (eq.3) this is not true for higher intensities. Upon further increasing the excitation intensity, the ionization curve loses its linearity and exhibits a plateau. This is shown in Figure 5a in the case of CT-DNA. The change in the regime appears at intensities where the number of absorbed photons is about four times lower than the number of bases. For comparison with literature studies, where high intensities were used to provoke DNA ionization,[10-12] the concentration of absorbed photons [hv] has been replaced in Figure 5b by the incident excitation intensity I_{inc}. This saturation effect explains why older studies did not detect one-photon ionization.

The detailed characterization of this phenomenon is out of the scope of the present study. It was mentioned in order to underline that the effects described here can be hindered when high excitation intensities are used. Such intensities were used in previous studies to describe one photon oxidation with energies higher than which exceeds the saturation band.[10-12]

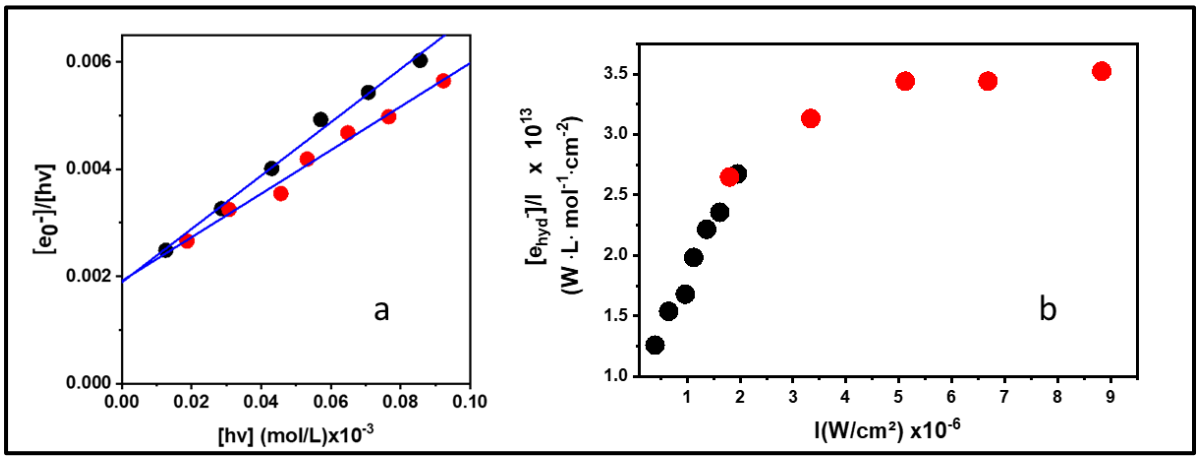

***Figure 5**. Effect of the incident excitation intensity I_{inc} on the yield of hydrated electrons observed for CT-DNA in phosphate buffer (0.015 mol·L^{-1} NaH_2PO_4 / 0.015·mol L^{-1} Na_2HPO_4). Black and red points correspond to experiments performed on different days. Laser pulse energy range: **a**) 0.5 - 6mJ; **b**) 5.5 - 26mJ.*

3.2 Factors affecting low-energy photoionization

One of the aims of this study was to understand the factors involved in low-energy photoionization and propose a possible mechanism. To achieve such objective, I studied the effect of various structural parameters of DNA on ϕ_1.

In Tables 1-3, are gathered the ϕ_1 values determined for the single-, double- and four-stranded systems. Results obtained prior to this study are included. In agreement with previous studies, which reported that the ϕ_1 of single strands characterized by poor base stacking ($(T)_{20}$ and TTAGG) is lower than 3×10^{-4},[13,14] I did not detect low-energy ionization for dinucleotides (Table 1). In contrast, for the longer strand S1 I found the same ϕ_1 value $(1.1 \pm 0.3) \times10^{-3}$ as that reported previously for the single stand $(A)_{20}$, known to adopt a helical structure.[15] In the case of duplexes (Table 2), one found that the ϕ_1 values of S1•S2 and CT-DNA are somewhat higher $(2.0 \pm 0.2) \times10^{-3}$ than those previously determined for the model duplexes $(AT)_{10}$•$(AT)_{10}$ and $(GC)_5$•$(GC)_5$ and $(A)_{20}$•$(T)_{20}$ (1.1 ± 0.1, 1.2 ± 0.2 and 1.4 ± 0.1 respectively) $\times10^{-3}$.[16-19] Finally, the ϕ_1 values of all the G-Quadruplexes are higher than those of duplexes, reaching 15×10^{-3}. In addition they exhibit more important variations (factor 4.2) compared to duplexes (factor 2.0).

Table 1. *Quantum yields ($\phi_1\times10^3$) of one-photon ionization at 266 nm determined for single strands; in blue, the values reported previously are shown.*

Sequence	Abbreviation	Buffer Ions	Quantum Yield
Adenine Single Strand	$(A)_{20}$	Na^+	1.1 ± 0.1[15]
Thymine Single Strand	$(T)_{20}$		<0.5[15]
TTAGGG	TTAGGG		<0.5[14]
S1	S1		1.1 ± 0.3
TG	TG	K^+	<<0.5
GT	GT		<<0.5

Table 2. *Quantum yields ($\phi_1 \times 10^3$) of one-photon ionization at 266 nm determined for duplexes; in blue are shown the values reported previously.*

Sequence	Abbreviation	Buffer Ions	Quantum Yield
Alternating AT	$(AT)_{10}\bullet(AT)_{10}$	Na^+	1.1 ± 0.1[15]
Homopolymeric AT	$(A)_{20}\bullet(T)_{20}$	Na^+	1.4 ± 0.1[15]
Alternating GC	$(GC)_5\bullet(GC)_5$	Na^+	1.2 ± 0.2[18]
Genomic DNA	CT-DNA	Na^+	2.0 ± 0.2[22]
		K^+	1.9 ± 0.1[22]
		Water	1.6 ± 0.3
5'-CGTACTCTTTGGTGGGTCGGTTCTTTCTAT-3' 3'-GCATGAGAAACCACCCAGCCAAGAAAGATA-5'	S1•S2	Na^+	2.1 ± 0.4[2]

Table 3. *Quantum yields ($\phi_1 \times 10^3$) of one-photon ionization at 266 nm G-Quadruplexes; in blue is shown the value reported previously.*

Molecularity	Sequence	Abbreviation	Quantum Yield
Mono-molecular G-Quadruplex	*GGG(TTAGGG)$_3$*	TEL21/Na^+	4.5 ± 0.6[14]
	TAGGG(TTAGGG)$_3$TT	TEL25/Na^+	5.2 ± 0.3[2]
		TEL21/K^+	9.4 ± 0.1[23]
Bi-molecular G-Quadruplex	GGGGTTTTGGGG	OXY/Na^+	6.0 ± 0.2[22]
		OXY/K^+	7.9 ± 0.1[22]
Tetra-molecular G-Quadruplex	TGGGGT	$(TG4T)_4/Na^+$	3.5 ± 0.5[19]
		$(TG4T)_4/K^+$	8.1 ± 0.5[20]
	TGGGG	$(TG4)_4/K^+$	4.7 ± 0.7
	GGGGT	$(G4T)_4/K^+$	8.8 ± 0.2
	AGGGGA	$(AG4A)_4/K^+$	14.8 ± 0.5
	AGGGG	$(AG4)_4/K^+$	9.9 ± 0.4
	GGGGA	$(G4A)_4/K^+$	12.6 ± 0.1
	TAGGGGAT	$(TAG4AT)_4/K^+$	7.0 ± 0.5
	AGGGGGA	$(AG5A)_4/K^+$	14.4 ± 0.1

3.3 Low-energy photoionization mechanism

The first results on low-energy photoionization of DNA obtained prior to that study (in blue in Tables 1-3) indicated the importance of secondary structure. Due to this observation and the knowledge that the VIP of bases are not affected by base-pairing and base-stacking (Table 1 in Chapter 1) an indirect mechanism, potentially involving excited charge transfer states had been evoked.[19] However, a direct mechanism could not be ruled out. On the one hand, the high ϕ_1 value found for TEL21/Na^+ could be due to the existence of guanine stacks which were absent from the duplexes studied previously (Table 2). In addition, the VIP values may present an important dispersion in secondary structures; thus, the VIP values of a small number sites may be much lower than the peak values determined by photoelectron spectroscopy.[20]

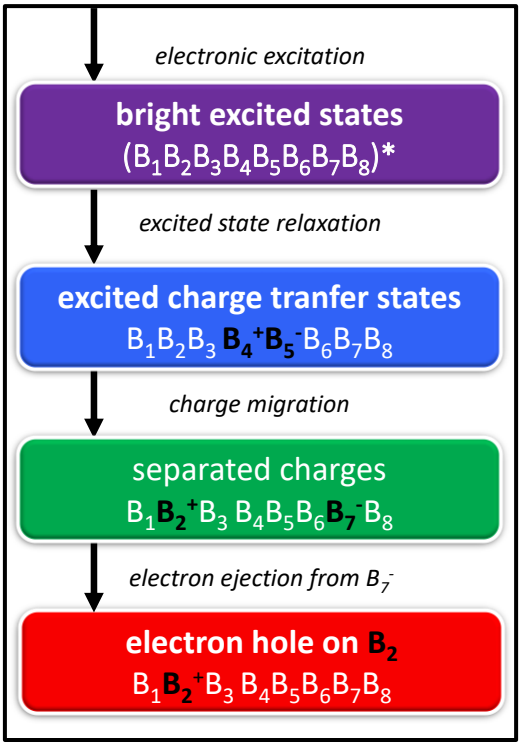

***Figure 6**. A proposed indirect photoionization mechanism: successive steps potentially leading to electron ejection after UV excitation. B_i designate stacked nucleobases.*

The results obtained during my thesis brought additional arguments in favor of an indirect mechanism. Potential successive steps are schematically depicted in Figure 6. (i) Photon absorption populates excited states. (ii) Very rapidly, an important part of the excited state population evolves toward excited charge transfer states, in which negative and positive charges are located on adjacent stacked nucleobases. Population of excited charge transfer states both in duplexes[21-24] and G-quadruplexes,[25-28] is well documented. (iii) A small part of the excited charge transfer states undergoes charge separation. The occurrence of charge separation along DNA strands has also been reported.[29] Guanine repeats characterized by lower oxidation potential[30] may behave as traps for electron holes (iv) As the VIP of "anionic" nucleobases is lower than that of "neutral" ones,[31] electron ejection may take place from the negatively charged moiety, leaving an electron hole at some other part of the system.

Below is discussed how the ensemble of the ϕ_1 values are explained by the indirect mechanism shown in Figure 6. I first focus on G-Quadruplexes for which I examined the effect of several structural parameters on ϕ_1: number of tetrads, topology, metal cations located in the central cavity of the guanine core, as well as the nature and the position of ending groups. Then I comment the findings on single and double strands.

The highest ϕ_1 in G-Quadruplexes could be due to more efficient trapping of the positive charge within stacked guanine tetrads; in this way, charge separation becomes more efficient, by increasing the probability of electron ejection from a base located outside the guanine core.

From the studies performed so far, it appears that the number of tetrads composing the G-quadruplex core alone does not play a key role on their capacity to photo-eject an electron. For example, the ϕ_1 of $(TG_4T)_4/K^+$ with four tetrads ($8.1x10^{-3}$) is lower than that of TEL21/K^+, characterized by three tetrads ($9.4x10^{-3}$). This comparison is even clearer for the tetramolecular G-quadruplexes $(AG_4A)_4/K^+$ and $(AG_5A)_4/K^+$ in which guanines have the same parallel arrangement (see Chapter 2, Figure 5): addition of an extra tetrad does not modify

$\boldsymbol{\phi}_1$. In table 3, it is also clear that topology plays a rather minor role: OXY/K^+ and $(TG4T)_4/K^+$ have similar $\boldsymbol{\phi}_1$ although their guanines adopt, respectively, parallel and antiparallel orientations in respect to the glycosidic bonds. Yet the $\boldsymbol{\phi}_1$ of OXY/Na^+ (6.0×10^{-3}) is significantly higher than that of $(TG4T)_4/Na^+$ (3.5×10^{-3}), which is the lowest value among all the studied G-quadruplexes. This could be due to the fact that its dissociation constant to single strands is relatively high.[32]

For all the studied sequences, the type of metal cations in the buffer in which G-quadruplexes are formed and studied play an important role: the $\boldsymbol{\phi}_1$ values found for K^+ are significantly higher compared to Na^+. In the case of $(TG4T)_4/K^+$, I tested that the photoionization is not affected upon diluting the buffer by a factor 10. In addition, I have not found this cation effect for CT-DNA (Table 2). Therefore, it was concluded that the cations located in the central cavity of G-Quadruplexes are responsible for the observed differences in $\boldsymbol{\phi}_1$. Theoretical calculations on stacked tetrads with parallel and antiparallel arrangement showed that the presence in the central cavity of small and more mobile Na^+ cations compared to K^+, favor the stabilization of excited charge transfer states between stacked guanines.[33,34] This stabilization is accompanied by a decrease in the distance between two guanines. Such a geometrical distortion of the stacking should make the charge migration step less favorable, explaining the lower $\boldsymbol{\phi}_1$ values.

The ending groups of tetramolecular G-quadruplexes having the same guanine core (four tetrads with parallel arrangement of guanines) have a striking effect on $\boldsymbol{\phi}_1$. Changing the thymines with adenines or with 5'-TA/AT-3' (Figure 7b) induces, respectively, an 88% increase and 14% decrease in $\boldsymbol{\phi}_1$. Furthermore, their positioning at the 3' ends leads to significantly higher values compared to 5' ends analogs (Figure 7a).

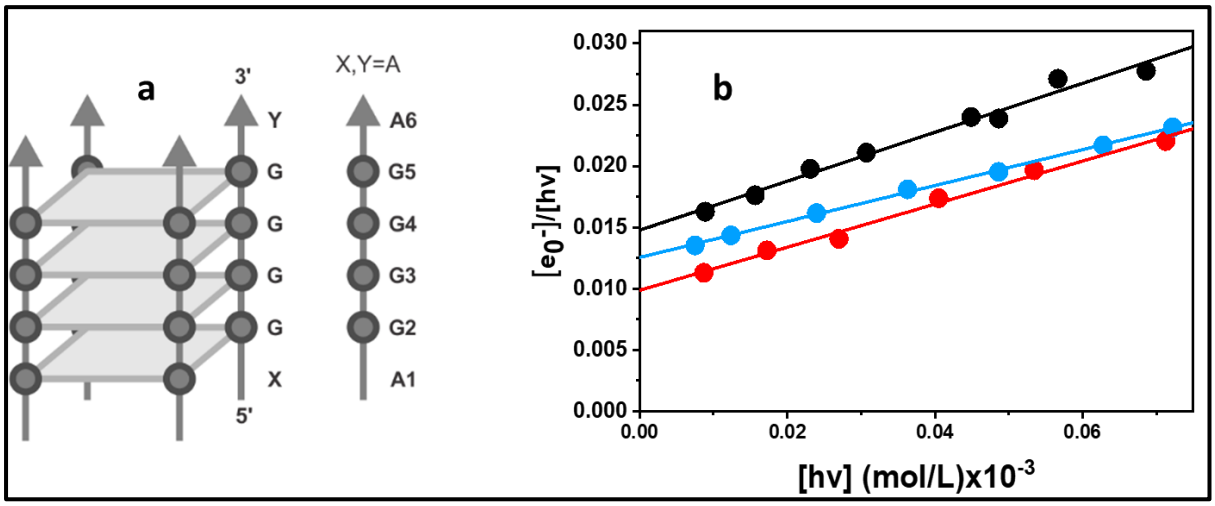

***Figure 7**. **a)** Schematic representation of parallel tetramolecular G-Quadruplexes. **b)** Ionization curves determined for $(AG_4A)_4/K^+$ (black circles), $(AG_4)_4/K^+$ (red circles), $(\mathbf{G}_4A)_4/K^+$ (light blue circles). The lines correspond to fits with linear functions $[e_{hyd}^-]_0/[hv]= a[hv]+ \phi 1$; [hv] and $[e_{hyd}^-]_0$ denote, respectively, the concentration of absorbed photons per laser pulse and the initial concentration of hydrated electrons. .*

Consequently, it appears that the synergy between central core and peripheral groups is an important factor in the low-energy photo-ionization. They could interfere both on the formation of excited charge transfer states and/or in charge separation. The positive charge could be trapped by the guanine core, where it may be delocalized,[35-38] while the negative one is born by an ending group E. This process is tentatively described as:

$$E^-G^+GGGP \rightarrow P^-(GGGG)^+E$$

or

$$EGG\text{-}G^+GP \rightarrow E^-(GGGG)^+E$$

where the radical signs were omitted for simplicity. The formation of excited states between a guanine and an ending group depends on their stacking. We can speculate, that adenines, that are larger than thymines, are better stacked explaining the higher $\mathbf{\Phi}_1$ values. Addition of a thymine to the 3' and 5' part of the

$(AG_4A)_4/K^+$ G-Quadruplex should increase conformational motions in the ending group hindering stacking; thus going from $(AG_4A)_4/K^+$ to $(TAG_4AT)_4/K^+$ reduces $\boldsymbol{\phi}_1$ from 15×10^{-3} to 7×10^{-3}. Regarding the position of the ending groups, quantum chemistry calculations on stacked dinucleotides showed that the excited charge transfer states are more stable towards the 3' end compared to their 5' counterpart,[39-42] in line with the values in Table 3.

Going from the above discussion on tetramolecular G-quadruplexes with parallel arrangement to monomolecular structures with antiparallel arrangement, we also observe a similar effect of the ending groups: when the groups TA at the 5' end and TT at the 3' end are removed from the telomeric sequence $\boldsymbol{\phi_1}$ decreases from 5.2×10^{-3} (TEL21/Na^+) to 4.5×10^{-3} (TEL25/Na^+). The bases in the loops connecting the guanine tetrads in monomolecular and biomolecular G-quadruplexes are expected to play a similar role as the ending groups. For example, quantum chemistry calculations on TEL21/Na^+ showed that charge transfer states may be formed between a thymine in the loop and a guanine in the core.[27]

Duplexes are devoid of the structural diversity characterizing G-quadruplexes. Yet, they do undergo low-energy photoionization albeit with a lower $\boldsymbol{\phi_1}$ (Table 2). In this case, charge separation may be facilitated by conformational motions and base sequence. Thus, repetitive sequences (homopolymeric AT, alternating AT or alternating GC), exhibit quite similar $\boldsymbol{\phi_1}$. But $\boldsymbol{\phi_1}$ increases by *ca.* 40% in random sequences containing GGG steps (S1•S2 and CT-DNA).

3.4 References Chapter 3

(1) Gauduel, Y.; Migus, A.; Chambaret, J. P.; Antonetti, A. Femtosecond reactivity of electron in aqueous solutions. *Rev. Phys. Appl.* **1987**, *22*, 1755-1759.

(2) Torche, F.; Marignier, J.-L. Direct evaluation of the molar absorption coefficient of hydrated electron by the isosbestic point method. *J. Phys. Chem. B* **2016**, *120*, 7201-7206.

(3) Hydrogen Atom and Hydrated Electron. In *Free-radical-induced DNA damage and its repair: a chemical perspective*; Springer Berlin Heidelberg: Berlin, Heidelberg, 2006; pp 77-86.

(4) von Sonntag, C.: *Free-radical-induced DNA damage and its repair* Springer-Verlag: Berlin-Heildelberg, 2006.

(5) Buxton, G. V.; Greenstock, C. L.; Helman, W. P.; Ross, A. B. Critical review of rate constants for reactions of hydrated electrons, hydrogen atoms and hydroxyl radicals (·OH/$O^{\cdot-}$) in aqueous solution. *J. Phys.Chem. Ref. Data* **1988**, *17*, 513-886.

(6) Chen, R.; Avotinsh, Y.; Freeman, G. R. Solvent effects on the reactivity of solvated electrons with ions in isobutanol/water mixed solvents. *Canadian Journal of Chemistry* **1994**, *72*, 1083-1093.

(7) Kumar, A.; Becker, D.; Adhikary, A.; Sevilla, M. D. Reaction of electrons with DNA: radiation damage to radiosensitization. *Int. J.Mol. Sci.* **2019**, *20*.

(8) Peters, J. P.; Maher, L. J., III. DNA curvature and flexibility in vitro and in vivo. *Q. Rev. Bioph.* **2010**, *43*, 23-63.

(9) Tree, D. R.; Muralidhar, A.; Doyle, P. S.; Dorfman, K. D. Is DNA a good model polymer? *Macromolecules* **2013**, *46*, 8369-8382.

(10) Nikogosyan, D. N. Two-quantum photochemistry of nucleic acids: comparison with conventional low-intensity UV photochemistry and radiation chemistry. *Int. J. Radiat. Biol.* **1990**, *57*, 233-299.

(11) Wala, M.; Bothe, E.; Görner, H.; Schulte-Frohlinde, D. Quantum yields for the generation of hydrated electrons and single strand breaks in poly(C),

poly(A) and single-stranded DNA in aqueous solution on 20 ns laser excitation at 248 nm. *J. Photochem. Photobiol. A-Chem.* **1990**, *53*, 87-108.

(12) Douki, T.; Angelov, D.; Cadet, J. UV laser photolysis of DNA: effect of dublex stability on charge-transfer efficiency. *J. Am. Chem. Soc.* **2001**, *123*, 11360-11366.

(13) Banyasz, A.; Martinez-Fernandez, L.; Balty, C.; Perron, M.; Douki, T.; Improta, R.; Markovitsi, D. Absorption of Low-Energy UV radiation by human telomere g-quadruplexes generates long-lived guanine radical cations. *J. Am. Chem. Soc.* **2017**, *139*, 10561-10568.

(14) Marguet, S.; Markovitsi, D.; Talbot, F. One and two photon ionization of DNA single and double helices studied by laser flash photolysis at 266 nm. *J. Phys. Chem. B* **2006**, *110*, 11037-11039.

(15) Crespo-Hernández, C. E.; Kohler, B. Influence of secondary structure on electronic energy relaxation in adenine homopolymers. *J. Phys. Chem. B* **2004**, *108*, 11182-11188.

(16) Banyasz, A.; Ketola, T.; Muñoz-Losa, A.; Rishi, S.; Adhikary, A.; Sevilla, M. D.; Martinez-Fernandez, L.; Improrta, R.; Markovitsi, D. UV-induced adenine radicals induced in DNA A-tracts: Spectral and Dynamical Characterization *J. Phys. Chem. Lett.* **2016**, *7*, 3949-3953.

(17) Banyasz, A.; Ketola, T.; Martinez-Fernandez, L.; Improta, R.; Markovitsi, D. Adenine radicals generated in alternating AT duplexes by direct absorption of low-energy UV radiation. *Faraday Disc.* **2018**, *207*, 181-197.

(18) Balanikas, E.; Banyasz, A.; Baldacchino, G.; Markovitsi, D. Populations and Dynamics of Guanine Radicals in DNA strands: Direct versus Indirect Generation. *Molecules* **2019**, *24*, 2347.

(19) Banyasz, A.; Martinez-Fernandez, L.; Improta, R.; Ketola, T. M.; Balty, C.; Markovitsi, D. Radicals generated in alternating guanine-cytosine duplexes by direct absorption of low-energy UV radiation. *Phys. Chem. Chem. Phys.* **2018**, *20*, 21381-21389.

(20) Schroeder, C. A.; Pluharova, E.; Seidel, R.; Schroeder, W. P.; Faubel, M.; Slavicek, P.; Winter, B.; Jungwirth, P.; Bradforth, S. E. Oxidation half-reaction of aqueous nucleosides and nucleotides via photoelectron spectroscopy augmented by ab initio calculations. *J. Am. Chem. Soc.* **2015**, *137*, 201-209.

(21) Chen, J.; Zhang, Y.; Kohler, B. Excited states in DNA strands investigated by ultrafast laser spectroscopy. *Top. Curr. Chem.* **2015**, *356*, 39-87.

(22) Markovitsi, D. UV-induced DNA Damage: The role of electronic excited states. *Photochem. Photobiol.* **2016**, *92*, 45-51.

(23) Schreier, W. J.; Gilch, P.; Zinth, W. Early events of dna photodamage. *Ann. Rev. Phys. Chem.* **2015**, *66*, 497-519.

(24) Banyasz, A.; Martínez-Fernández, L.; Improta, R.; Ketola, T.-M.; Balty, C.; Markovitsi, D. Radicals generated in alternating guanine–cytosine duplexes by direct absorption of low-energy UV radiation. *Phys. Chem. Chem. Phys.* **2018**, *20*, 21381-21389.

(25) Kwok, W.-M.; Ma, C.; Phillips, D. L. Femtosecond time- and wavelength-resolved fluorescence and absorption study of the excited states of adenosine and an adenine oligomer. *J. Am. Chem. Soc.* **2006**, *128*, 11894-11905

(26) Hua, Y.; Changenet-Barret, P.; Improta, R.; Vayá, I.; Gustavsson, T.; Kotlyar, A. B.; Zikich, D.; Šket, P.; Plavec, J.; Markovitsi, D. Cation effect on the electronic excited states of guanine nanostructures studied by time-resolved fluorescence spectroscopy. *J. Phys. Chem. C* **2012**, *116*, 14682-14689.

(27) Martinez-Fernandez, L.; Changenet, P.; Banyasz, A.; Gustavsson, T.; Markovitsi, D.; Improta, I. A comprehensive study of guanine excited state relaxation and photoreactivity in G-Quadruplexes. *J. Phys. Chem. Lett.* **2019**, *10*, 6873-6877.

(28) Ma, C. S.; Chan, R. C.-T.; Chan, C. T.-L.; Wong, A. K.-W.; Kwok, W.-M. Real-time monitoring excitation dynamics of human telomeric Guanine Quadruplexes: effect of folding topology, metal cation, and confinement by nanocavity water pool. *J. Phys. Chem. Lett.* **2019**, *10*, 7577−7585.

(29) Bucher, D. B.; Pilles, B. M.; Carell, T.; Zinth, W. Charge separation and charge delocalization identified in long-living states of photoexcited DNA. *Proc. Natl. Acad. Sci. USA* **2014**, *111*, 4369-4374.

(30) Palecek, E.; Bartosik, M. Electrochemistry of nucleic acids. *Chem. Rev.* **2012**, *112*, 3427-3481.

(31) Schiedt, J.; Weinkauf, R.; Neumark, D. M.; Schlag, E. W. Anion spectroscopy of uracil, thymine and the amino-oxo and amino-hydroxy tautomers of cytosine and their water clusters. *Chem. Phys.* **1998**, *239*, 511-524.

(32) Hua, Y. Structures auto-assemblées de guanines étudiées par spectroscopie optique résolue en temps. 2013, Thèse de doctorat Chimie physique Paris 11 2013http://www.theses.fr/2013PA112149/document.

(33) Improta, R. Quantum mechanical calculations unveil the structure and properties of the absorbing and emitting excited electronic states of guanine quadruplex. *Chem. Eur. J.* **2014**, *20*, 8106-8115.

(34) Changenet-Barret, P.; Hua, Y.; Gustavsson, T.; Markovitsi, D. Electronic excitations in g-quadruplexes formed by the human telomeric sequence: a time-resolved fluorescence Study. *Photochem. Photobiol.* **2015**, *91*, 759-765.

(35) Capobianco, A.; Caruso, T.; D'Ursi, A. M.; Fusco, S.; Masi, A.; Scrima, M.; Chatgilialoglu, C.; Peluso, A. Delocalized hole domains in guanine-rich DNA oligonucleotides. *J. Phys. Chem. B* **2015**, *119*, 5462-5466.

(36) Sun, W. M.; Varsano, D.; Di Felice, R. Effects of G-Quadruplex topology on electronic transfer integrals. *Nanomaterials* **2016**, *6*.

(37) Martinez-Fernandez, L.; Banyasz, A.; Markovitsi, D.; Improta, I. Topology controls the electronic absorption delocalization of electron hole in guanine quadruplexes. *Chem. Europ. J.* **2018**, *24*, 15185-15189.

(38) Kumar, A.; Adhikary, A.; Sevilla, M. D.; Close, D. M. One-electron oxidation of ds(5 '-GGG-3 ') and ds(5 '-G(8OG)G-3 ') and the nature of hole distribution: a density functional theory (DFT) study. *Phys. Chem. Chem. Phys.* **2020**, *22*, 5078-5089.

(39) Aquino, A. J. A.; Nachtigallova, D.; Hobza, P.; Truhlar, D. G.; Hattig, C.; Lischka, H. The Charge-Transfer States in a stacked nucleobase dimer complex: A Benchmark Study. *J. Comput. Chem.* **2011**, *32*, 1217-1227.

(40) Santoro, F.; Barone, V.; Lami, A.; Improta, R. The excited electronic states of adenine-guanine stacked dimers in aqueous solution: a PCM/TD-DFT study. *Phys. Chem. Chem. Phys.* **2010**, *12*, 4934-4948.

(41) Martinez-Fernandez, L.; Improta, R. Novel adenine/thymine photodimerization channels mapped by PCM/TD-DFT calculations on dApT and TpdA dinucleotides. *Photochem. Photobiol. Sci.* **2017**, *16*, 1277-1283.

(42) Martinez-Fernandez, L.; Improta, R. Sequence dependence on DNA photochemistry: a computational study of photodimerization pathways in TpdC and dCpT dinucleotides. *Photochem. Photobiol. Sci.* **2018**, *17*, 586-591.

Chapter 4

Guanine radicals

In this Chapter, first I explain how the G radicals in the examined systems are identified and quantified by comparing their absorption spectra with those reported in the literature for three types of monomeric radicals: radical cations $(G^{+})^{\bullet}$ and two deprotonated radicals $(G\text{-}H1)^{\bullet}$ and $(G\text{-}H2)^{\bullet}$. Based on this comparison, I examine the survival probability and half-lives of the total radical population as a function of various structural parameters. After discussing the $(G^{+})^{\bullet} \rightarrow (G\text{-}H1)^{\bullet}$ deprotonation in duplexes, completed within 2 μs, I focus on G-Quadruplexes, for which only $(G^{+})^{\bullet} \rightarrow (G\text{-}H2)^{\bullet}$ deprotonation occurs. For some of them, I present the spectra of $(G^{+})^{\bullet}$ determined in pH 3, where deprotonation is hindered. For G-quadruplexes at pH 7, I show that deprotonation is highly anisotropic, spanning from 30 ns to over 50 μs, sometimes being followed by $(G\text{-}H2)^{\bullet} \rightarrow (G\text{-}H1)^{\bullet}$ tautomerization. Finally, I discuss the spectral fingerprints of unknown reaction intermediates and reaction products.

4.1 General considerations

In the previous chapter, I have mentioned that transient absorption experiments on the sub-microsecond timescale, between 30 ns and 2 μs, provide information about the hydrated ejected electrons. Taking this a step further, in this chapter, I will discuss the radicals, mainly observable between 2 μs and hundreds of millisecond.

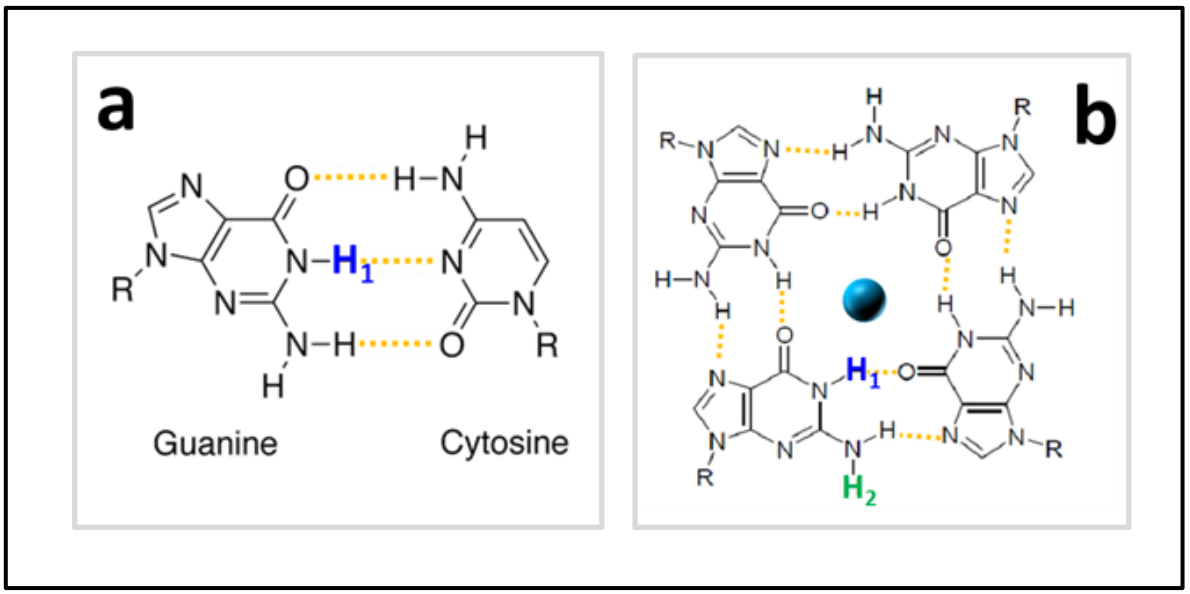

Figure 1. *Schematic representation of a guanine-cytosine pair* ***a****) and* ***b****) a guanine tetrad.* ***(G-H1)•*** *and* ***(G-H2)•*** *radicals correspond, respectively, to transfer of the protons in blue and green toward the aqueous solvent.* Na^+ *or* K^+ *are represented by the blue sphere.*

As already explained in Chapter 1, the guanine radical cations $(G^{+})^{\bullet}$ formed during the ionization process are known to be unstable, because they are stronger acids than the initial nucleobases. Consequently, when they are generated in neutral aqueous solutions they tend to lose a proton[1] (Figure 1) reaching a more stable state. Moreover, the spectra of deprotonated radicals depend on the position from which the proton is lost. In Figure 2a are compared the absorption spectra of the radical cation $(G^{+})^{\bullet}$ and the two deprotonated radicals $(G\text{-}H1)^{\bullet}$ and $(G\text{-}H2)^{\bullet}$,

which are used to identify and quantify the radicals present in the studied systems.

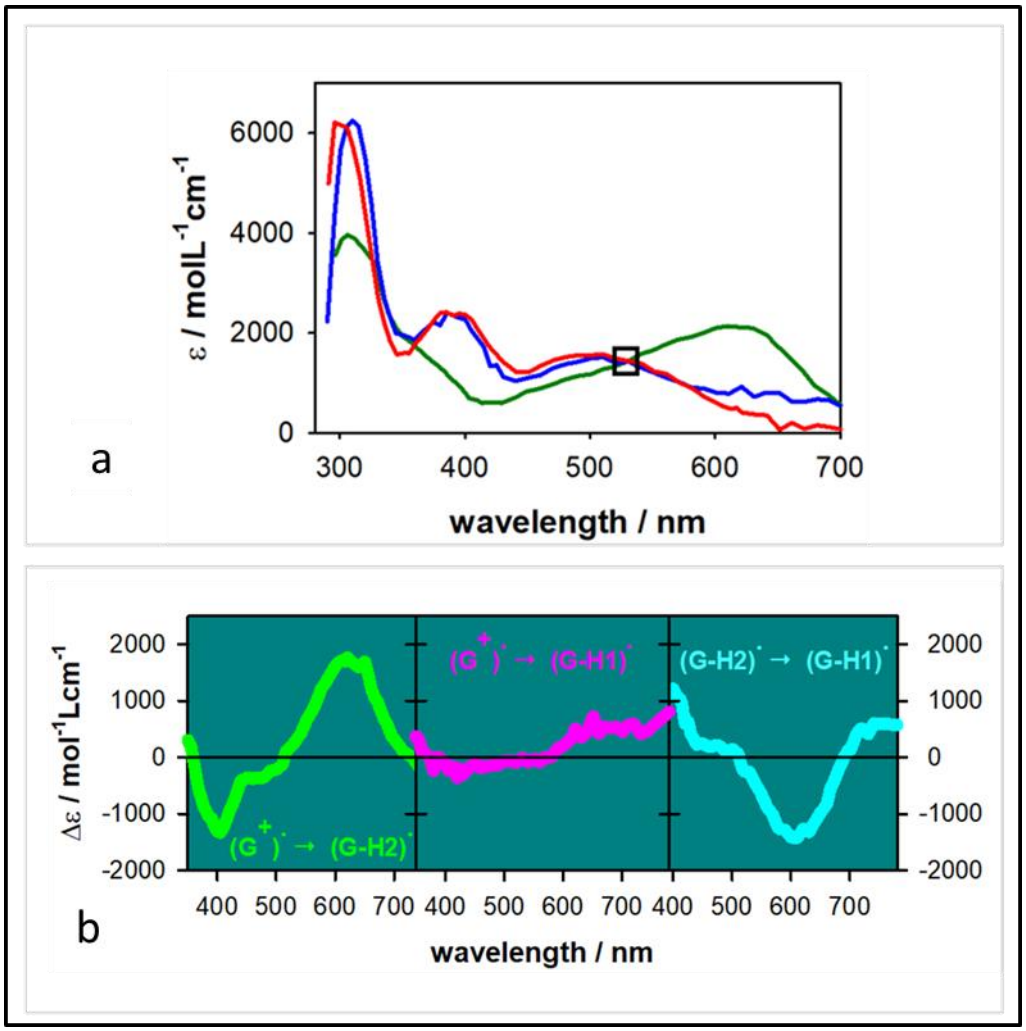

***Figure 2. a**) Absorption spectra of monomeric (**G**$^{+}$)• (red),[2] **(G-H1)•** radical (blue)[2] and **(G-H2)•** (green),[3] resulting, respectively, from loss of the protons in blue and green (Figure 1); the black square indicates an isosbestic point, which is a the spectral region where the ε values of all radicals are similar (Δε<100 mol^{-1}L·cm^{-1}).[4] **b**) Difference spectra corresponding to (**G**$^{+}$)• → **(G-H2)•**, (**G**$^{+}$)• → **(G-H1)•** and **(G-H2)•** → **(G-H1)•** processes. They were determined from the spectra of monomeric guanosine radicals.[2,3] Δε < 0 will be reflected by a decay in the transient absorption signal while Δε> 0 by a rise.*

Figure 2b shows the differential spectra corresponding to pairs of radical spectra, which are useful in order to follow the evolution of one type of radical to

the other. Thus we observe that (i) $(G^{+})^{\bullet} \rightarrow (G\text{-}H2)^{\bullet}$ deprotonation can be better followed around 400 and 620 nm. (ii) The spectra of $(G^{+})^{\bullet}$ and $(G\text{-}H1)^{\bullet}$ are quite similar in the visible domain but can be differentiated in the near infra-red. (iii) $(G\text{-}H2)^{\bullet} \rightarrow (G\text{-}H1)^{\bullet}$ tautomerization can be detected at 720 nm.

Changes in the UV spectral range are not informative because, on the one hand, G-Quadruplexes absorb at longer wavelengths compared to monomeric guanosine,[5] and, on the other, photon absorption by DNA is known to induce formation of photo-dimers;[6] some of them absorb in the UVA region and their dynamics intervenes in the millisecond time-scale.[7,8] As it will be shown in the last section, the fingerprint of reaction products was detected in this spectral region.

4.2 Survival probability of the radical population

By observing the three radical spectra in Figure 2a, we remark the existence of a quasi-isosbestic point around 500-515 nm (black square). Thus, regardless the radical evolution in a given system, the survival probability of the total radical concentration at time t, is $P_t = [R]_t/[R]_0$ (where $[R]_t$ is total radical concentration at given time t and $[R]_0$ initial radical concentration). P_t may be evaluated from the ΔA value at these wavelengths. For a quantitative description, the experimental traces recorded on the microsecond and millisecond time-scale were fitted with bi-exponential functions.

The $[R]_t$ at 3 μs , which is determined from the ΔA at wavelengths between 500 and 515 nm by using an ε value of 1500 $mol^{-1}Lcm^{-1}$, matches the concentration of hydrated ejected electrons, corresponding to the initially created electron holes ($[R]_0=[e_{hyd}^{-}]_0$). Therefore, it can be concluded that, within the precision of our measurements (≤±5%, depending on the system) all the generated radicals are still present at 3 μs. This means that only a very small fraction of the radical population, associated with our experimental error, reacts at earlier times.

Consequently, the survival probability of the total radical population is given by the decays recorded at this quasi-isosbestic point, setting $[R]_t$ at 3 µs equal to 1.

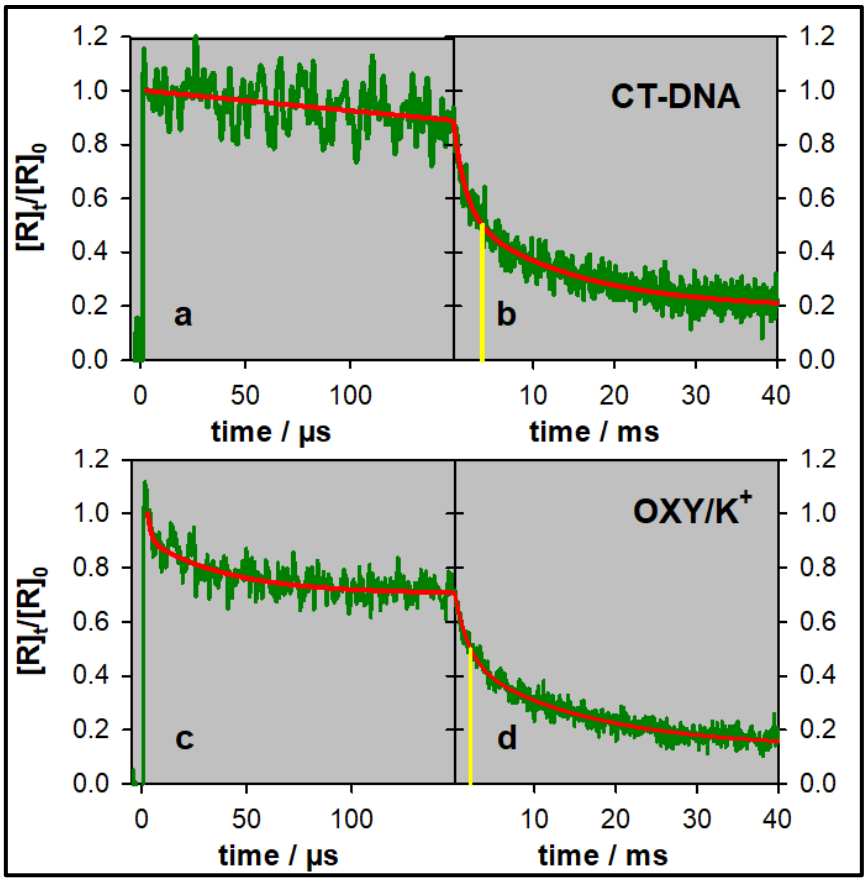

Figure 3. *Survival probability of the total radical population in CT-DNA (**a** and **b**) and OXY/K⁺ (**c** and **d**). Experimental decays (green) recorded at 500 nm (**a** and **b**) and 512 nm (**c** and **d**) are fitted with multi-exponential functions (red). The vertical yellow lines indicate* $\tau_{1/2}$.

In Figure 3, the survival probability of the total radical population in CT-DNA (a and b) and OXY/K⁺ (c and d) are presented. Kinetics are, fitted with bi-exponential functions. The yellow lines indicate the radical half-life $\tau_{1/2}$, which is the time needed for the radical population to be reduced by 50% ($[R]_t/[R]_0 = 0.5$). These times are of a few milliseconds in both duplexes and G-Quadruplexes (Table 1). After collecting the $\tau_{1/2}$ values of the various studied systems, we came up to some important conclusions.

Table 1. *Half-lives (in ms) of the total radical population for the studied DNA duplexes and **G**-Quadruplexes. In bold are presented the values of **G**-Quadruplexes which were studied in both K^+ (blue) and Na^+ (black).*

Abbreviation	Cation	Half-lives (ms)	Secondary structure
S1	Na^+	(2.0± 0.3)	**single strands**
S2	Na^+	(1.7± 0.3)	
S1•S2	Na^+	(4.0 ± 0.2)	**duplexes**
CT-DNA	Na^+	(3.7± 0.2)	
	K^+	(3.6± 0.2)	
TEL21	Na^+	**(6.7 ± 0.5)[5]**	**G-Quadruplexes**
	K^+	**(1.4± 0.1)**	
TEL25	Na^+	(3.5± 0.2)	
OXY	Na^+	**(4.1 ± 0.2)**	
	K^+	**(2.1± 0.2)**	
$(TG_4T)_4$	Na^+	**(6.0 ± 0.5)**	
	K^+	**(3.1± 0.2)**	
$(AG_4A)_4$	K^+	(2.0± 0.1)	

Firstly, we found that the $\tau_{1/2}$ in duplexes, both genomic DNA (CT-DNA) and the model duplex (S1•S2), are similar (around 4 ms). A somewhat shorter value (2.7 ms) was reported previously for guanine radicals in alternating GC duplexes.[9] In the case of the (S1•S2), the $\tau_{1/2}$ is twice as long than those determined for the two parent single strands S1 and S2.[10] A similar increase in $\tau_{1/2}$ upon base-pairing was reported for adenine radicals in A-tracts.[11] This can be explained by the larger conformational motions in single strands, allowing the system to adopt more rapidly reactive configurations, thus increasing the reaction rate.

Secondly, clearly shorter $\tau_{1/2}$ were observed for the G-Quadruplexes formed in the presence of K^+ compared to Na^+, even when the guanine arrangement is the same, parallel for $(TG_4T)_4/M^+$ and antiparallel for OXY/M^+. Such difference was not observed for genomic DNA. Moreover, in the case of $(TG_4T)_4/M^+$. I found that upon diluting the buffer by a factor 10, the radical decays remained the same.

Therefore, it seems that the cation in the central cavity of the quadruplex is responsible for this effect. Finally, we observed that the radical decays are not affected by the presence of oxygen. They are the same for aerated and argon saturated solutions, which means that their disappearance occurs via reactions that do not involve oxygen.

4.3 Radicals in duplexes

4.3.1 Radical spectra

The transient absorption spectrum determined for CT-DNA at 50 s, shown in Figure 4, strongly resembles that of $(G\text{-}H1)^{\bullet}$ radical reported for dGMP,[1,2] even reproducing the ε values. However, there is a small intensity increase between 600 and 700 nm. We also found such an increase in the case of S1•S2; the same increase was reported for the spectra of alternating GC duplexes.[12] As explained in Chapter 1 (Figure 7) in duplexes the H1 proton of the radical cation may be transfer to either the cytosine or the aqueous solvent.[13,14] The spectra of these two deprotonated guanine radicals for a short duplex composed of two guanine-cytosine pairs in alternating GC sequence were computed by quantum chemistry methods.[12] The study concluded that the transfer of the H1 proton to the aqueous solvent induces a long red tail in the radical absorption spectrum. The same conclusion was reached from a subsequent theoretical study.[13] In view of these studies and considering that we did not detect any variation in the decays between 500 and 700 nm, the spectra of both S1•S2 [10] and CT-DNA (Figure 4) should correspond to transfer of H1 proton to the bulk water.

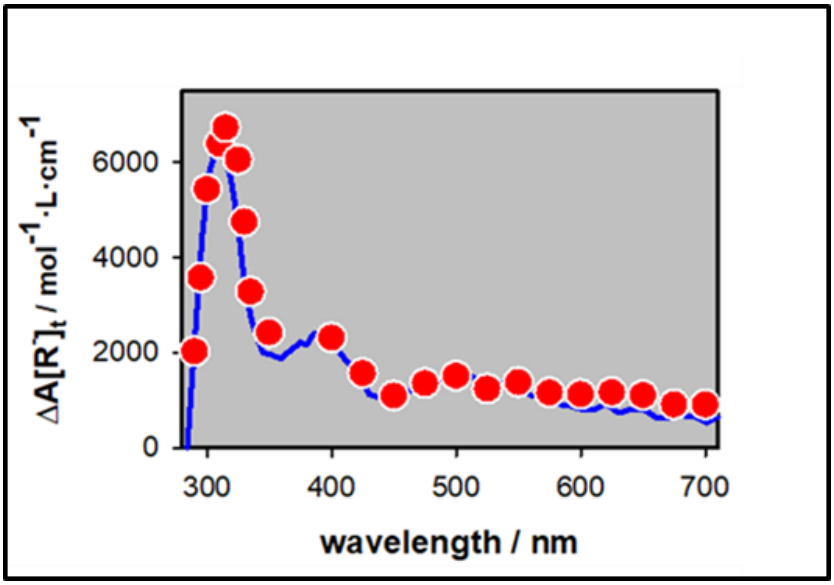

Figure 4. *Transient absorption spectrum determined for CT-DNA at 50 μs (red circles); ΔA was divided by* $[R^{\bullet}]_t$. *The blue line corresponds to the deprotonated radical of dGMP attributed to* ***(G-H1)•****,*[2] *represented with ε values .*

4.3.2 Radical reaction dynamics

I determined the deprotonation dynamics for the first time in CT-DNA by monitoring the transient absorption at 700 nm. To this end, I eliminated the much stronger absorption of e_{hyd}^- using efficient electron scavengers (N_2O and NO_3^-).[14] Under these conditions, I observed a rise which is completed within ~2 μs (Figure 5a); it can be approximated with a mono-exponential function with a time constant of 0.3 μs, in line with the fast deprotonation rate obtained for short duplexes using pulse radiolysis.[15] Subsequently, I found that the signal starts decaying slowly on the μs time-scale (Figure 5b).

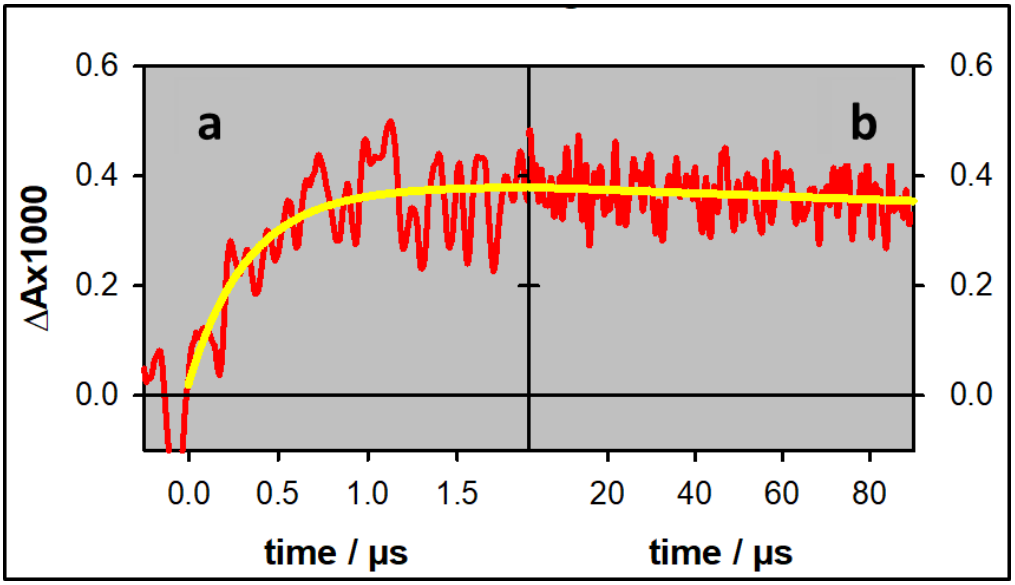

***Figure 5**. Transient absorption signals recorded for N_2O saturated solutions of CT-DNA at 700 nm; yellow lines are derived from fits with mono-exponential functions; incident excitation intensity: 2.0×10^6 Wcm^{-2}.*

In the case of S1•S2, the relative intensity of the UV band on the ms time-scale, in respect to the absorption in the visible spectral domain increases, suggesting contribution of photoproducts appearing on this time-scale (Figure 6a). For example, thymine 64PPs are formed within 4 ms.[7] The coexistence of radicals and photo-products is also reflected in the dependence of the decays recorded on the ms time scale as a function of the laser intensity (Figures 6b and c). Those at 500 nm remain unchanged (Figure 6b), showing that the dynamics of radicals formed by one- or two-photon ionization is the same (see Chapter 3 the ionization curve in Figure 7b). On the other hand, dimers, whose absorptions is in the 300 to 400 nm range, are generated by one-photon ionization processes, and, therefore, their relative concentration is higher at low excitation intensities. Similar results were found for the **S1** and **S2** single strands but, as single strands are more prone to dimerization reactions compared to duplexes,[6] thus the effect on the 305 nm is much stronger (Figure 6c).

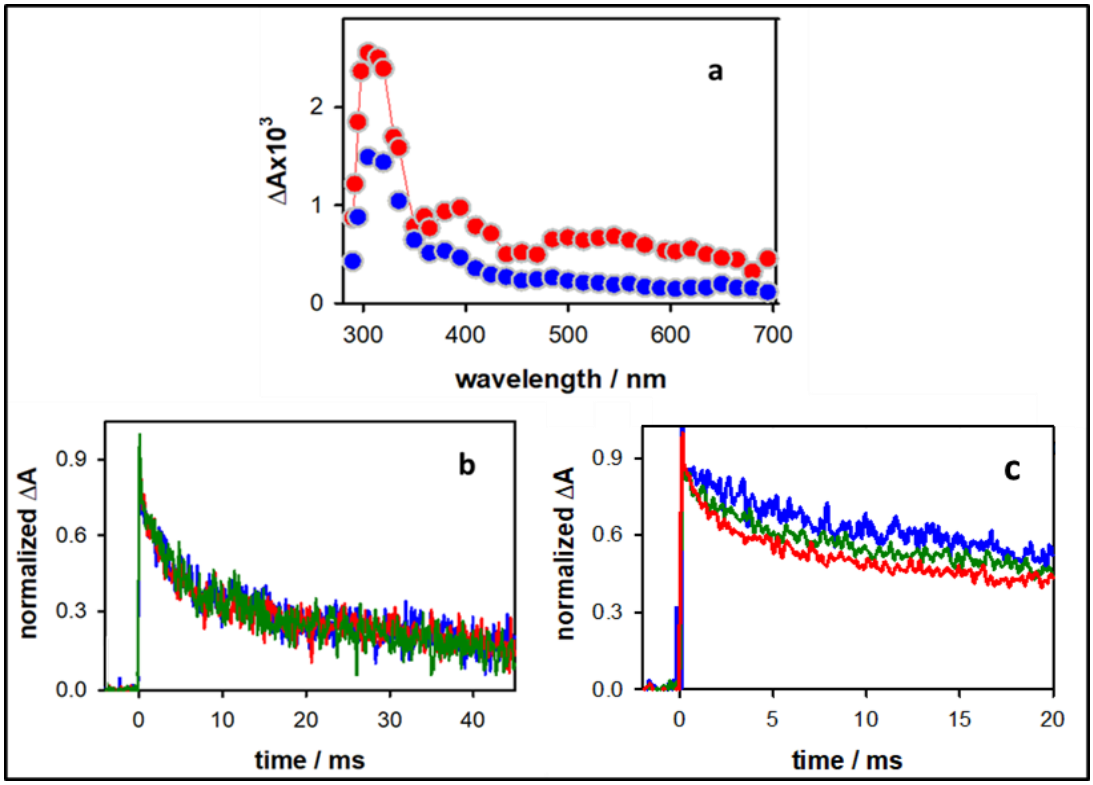

***Figure 6. a**) Transient absorption spectra determined for the duplex S1•S2 at 5 µs (red circles) and 10 ms (blue circles). Normalized transient absorption signals recorded for the duplex S1•S2 at 500 nm **b**) and for the single strand S1 at 305 nm **c**) for excitation energies of 4 mJ (blue), 6 mJ (green) and 7 mJ (red).*

4.4 Radicals in G-Quadruplexes

4.4.1 Spectra of radical cations at pH 3

The spectrum of the radical cation in a given system can be determined experimentally by its photoionization in pH 3 solution, provided that protonation does not occur in the ground state. Under this condition, deprotonation of $(G^{+})^{\bullet}$ is hindered[1]. We performed this experiment for four tetramolecular G-Quadruplexes $(TG_4T)_4/Na^+$,[16] the $(AG_4A)_4/K^+$, the $(AG_4)_4/K^+$ and the $(G_4A)_4/K^+$. The spectra of their radical cations $(G^{+})^{\bullet}$ are compared with that of the monomeric analog in Figures 7

and 8. We note that below 400 nm, it is impossible to determine reliable spectra due to strong photo-degradation occurring in acidic solutions during the measurements.

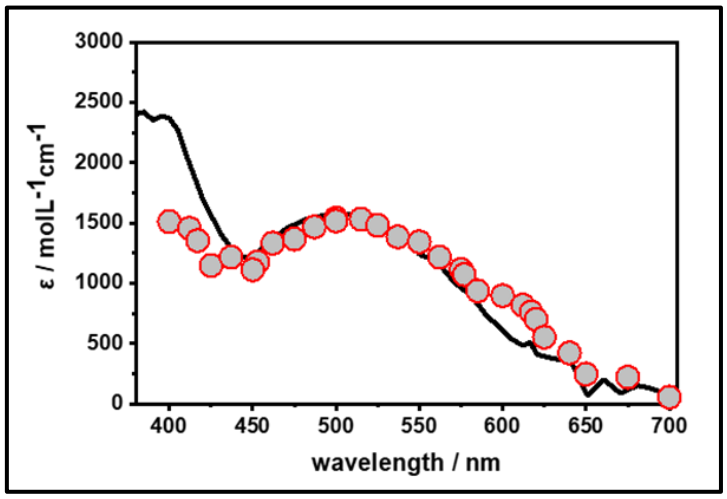

Figure 7. *Transient absorption spectrum obtained for $(TG_4T)_4/Na^+$ at pH 3 at 2.5 µs (circles); ΔA is divided by $[e_{hyd}^-]_0$, determined in the same experiment; the spectrum of the dGMP radical cation (red) is represented with ε values.*[2]

In Figure 7, we observe that the spectrum obtained for $(TG_4T)_4/Na^+$ resembles the spectrum of the monomeric radical cation in the 450-700 nm domain. This similarity concerns not only the spectral shape but also the molar extinction coefficients ε determined by dividing the observed transient absorption ΔA at 2.5 µs by $[e_{hyd}^-]_0$, which corresponds to that of generated electron holes. More precisely, the ε of the $(TG_4T)_4/Na^+$ radical cation coincides with that of the monomeric analog at 500 nm. At 400 nm, the ε is ca. 40% lower. Such lower intensity of the latter band with respect to the dGMP cation[1], was also predicted by quantum chemistry calculations in the case of $(TG_4T)_4/Na^+$ as well as the TEL21/Na^+,[5,16] and was experimentally observed for TEL21/Na^+.[5] The small but clearly distinguishable feature around 600 nm in Figure 7a could be correlated with delocalization of the electron hole over two guanines occurring for a small part of the population.[17] Quantum chemical calculations also suggested that charge delocalization is possible only for G-Quadruplex structures with parallel

arrangement (such as $(TG_4T)_4/Na^+$) but not for antiparallel structures (such as TEL21/Na^+)[17,18] whose spectra do not show such a feature.[5]

As in the case of $(TG_4T)_4/Na^+$, the spectra recorded for $(AG_4A)_4/K^+$, $(AG_4)_4/K^+$ and $(G_4A)_4/K^+$ in pH 3 condition (Figure 8) exhibit the same maximum ε value (1500±100 mol $L^{-1}cm^{-1}$) with that of the monomeric radical cation. By observing these spectra we can derive the following conclusions. The first is that all three spectra are peaking at wavelengths longer than the dGMP analog. The second finding here is that the $(AG_4A)_4/K^+$ is located between those of the asymmetric analogs (Figure 8b). This means that there is an interaction between guanines and adenines and this interaction is more important when the adenines are located at the 3' position instead of 5'. We recall that a similar symmetry effect was observed for the photoionization of these three systems (Chapter 3).

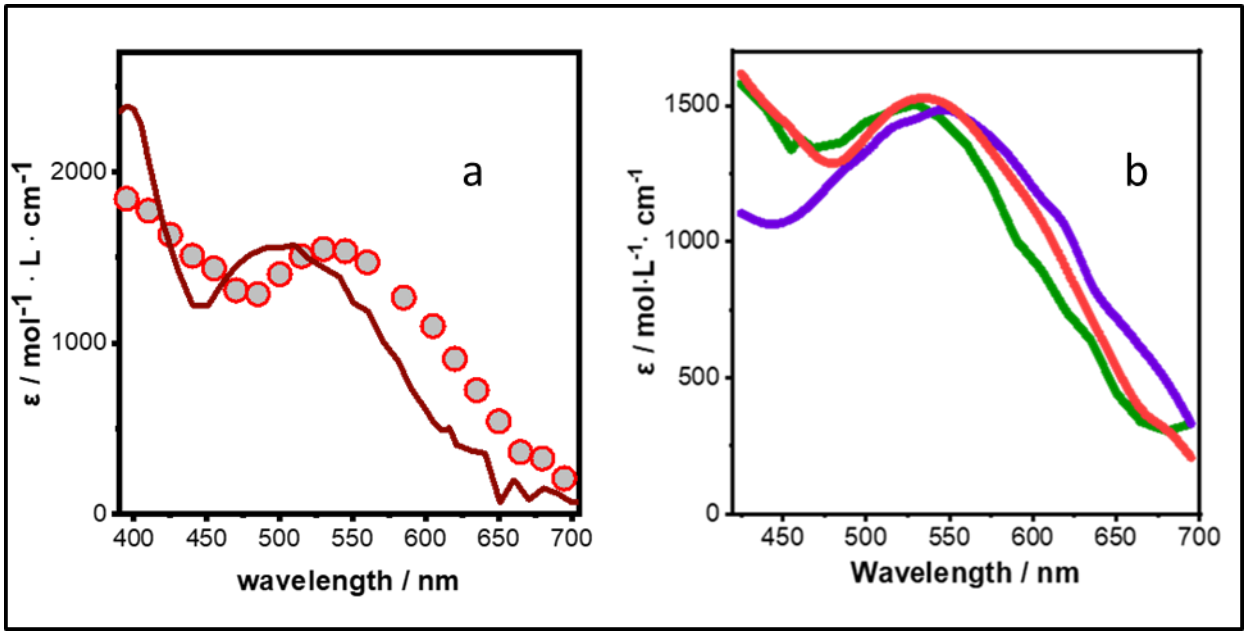

***Figure 8. a**) Transient absorption spectrum obtained at 3 µs for $(AG_4A)_4/K^+$ in pH 3 (red); the ΔA is divided by $[e_{hyd}^-]_0$, determined in the same experiment, and the spectrum of the dGMP radical cation (brown)[2] is represented with ε values. **b**) Comparison of the $(AG_4A)_4/K^+$ (red), $(AG_4)_4/K^+$ (green) and $(\mathbf{G}_4A)_4/K^+$ (purple).*

4.4.2 Spectral evolution at pH 7

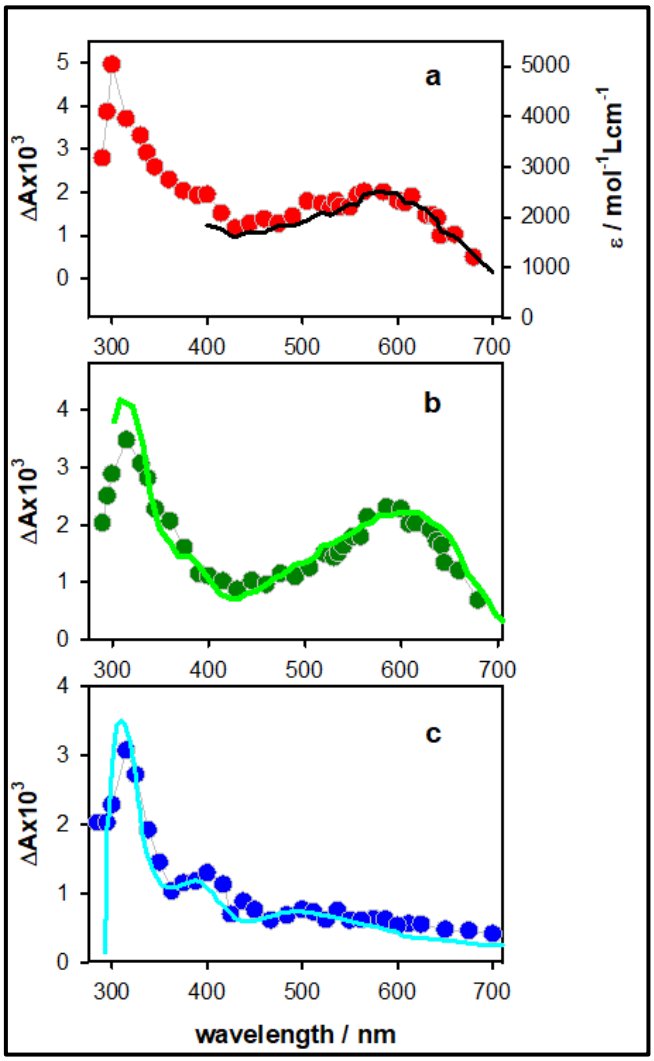

***Figure 9**. Transient absorption spectra recorded for aerated solutions of $(TG4T)_4/Na^+$ in pH 7 (circles) at 2.5 µs **a**), 50 µs **b**) and 6 ms **c**). Excitation intensity: 2 $MWcm^{-2}$. The black line in **a**) is a linear combination of the $(TG4T)_4/Na^+$ spectra corresponding to its radical cation (Figure 2) and the **(G-H2)•** deprotonated radical (Figure 9b) at a ratio 25:75. The green **b**) and cyan **c**) lines correspond, respectively, to the spectra of **(G-H2)•** [3] and **(G-H1)•** [2] radicals of monomeric guanosine, their intensity being arbitrarily normalized in respect to that of the **G**-quadruplex spectra.*

Figure 9, shows the time evolution of the transient absorption spectra obtained for $(TG_4T)_4/Na^+$ in pH 7 condition. At the earliest probed time (2.5 µs),

the spectrum exhibits a broad band in the visible spectral domain and a more intense one around 300 nm. As time passes by, the relative intensity of the UV band in respect to that in the visible decreases significantly, dropping from 2.5 to 1.5 at 50 μs. In parallel, the band in the visible becomes narrower and shifts slightly toward the red. The spectrum at 50 μs strongly resembles that reported in the literature for **(G-H2)•** radicals of monomeric guanosine derivatives.[2,3] Thus, we assign it to the **(G-H2)•** radical. Further transformations take place in the ms time-scale. At 6 ms, the spectral profile has completely changed. We now distinguish three bands of decreasing intensity, peaking at 315, 400 and 515 nm, as reported for the **(G-H1)•** radical of dGMP.[2,19]

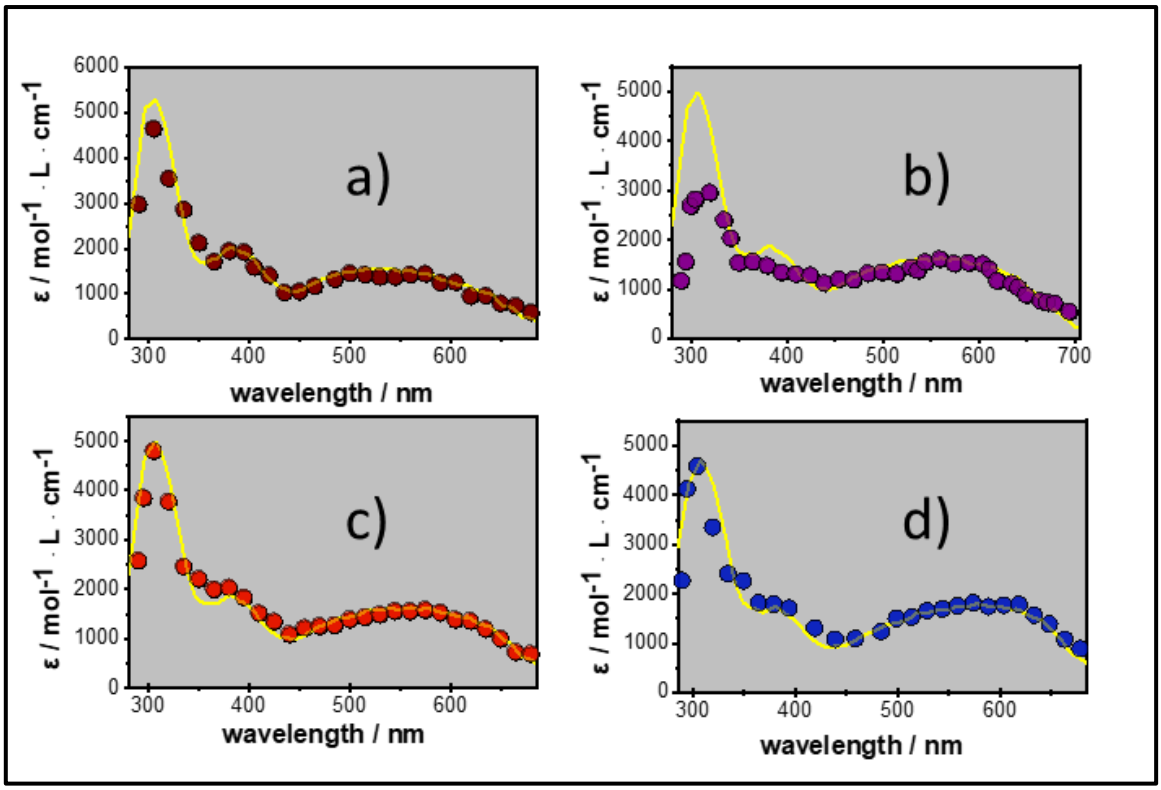

Figure 10. *Transient absorption spectra (circles) recorded for aerated solutions of* ***a)*** *TEL21/K+ and* ***b)*** *TEL25/Na+* ***c)*** *OXY/K+,* ***d)*** *OXY/Na+ at 3 μs; ΔA was divided by the initial concentration of ejected electrons. Yellow lines corresponds to linear combinations of* ***(G+)•1*** *and* ***(G-H2)•3*** *radicals reported for the monomeric guanosine derivatives represented with their molar absorption coefficient; the ratios of the linear combinations are given in Table 2.*

From the above observations, we can already draw a rough picture of the successive events taking place on the probed time-scale. First, we have a mixture of the radical cation and the deprotonated radical **(G-H2)•**. After completion of the deprotonation process, only **(G-H2)•** radicals are present. Finally, at least part of the latter radicals undergoes tautomerization, giving rise to **(G-H1)•** radicals. For all the studied G-quadruplexes, the coexistence of radical cations and **(G-H2)•** radicals was also observed. This is shown in Figure 10 for bimolecular (OXY/Na^+ and OXY/K^+) and monomolecular (TEL21/K^+ and TEL25/Na^+).

(G-H2)• → **(G-H1)•** tautomerization was previously reported for TEL21/Na^+. We observed the same effect for TEL21/K^+, OXY/Na^+ and OXY/K^+. In the case of TEL21/K^+, we observed this formation on the microsecond time-scale (Figure 11). This appears as a rise at 720 nm where only the **(G-H1)•** radical absorbs (see Figure 2).

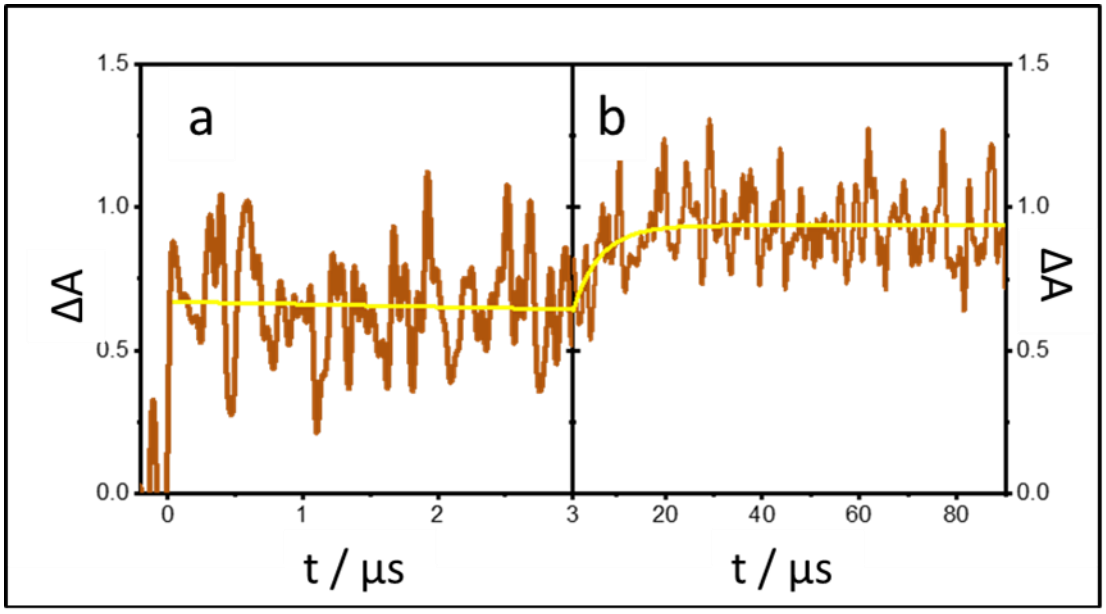

Figure 11. a) *Transient absorption signal of TEL21/K^+ recorded for the first few microseconds at 720 nm and* ***b)*** *Formation of the* ***(G-H1)•*** *radical in TEL21/K^+, estimated by the transient absorption signal recorded at 100 µs at 720 nm. The yellow line is the fit with a mono-exponential model function. Solutions were saturated with N_2O.*

(G-H2)• → **(G-H1)•** tautomerization was not clear in TEL25/Na^+ and totally absent in the case of tetramolecular **G**-Quadruplexes formed in the presence of K^+ ions, $(TG_4T)_4/K^+$, $(AG_4A)_4/K^+$ and $(TAG_4AT)_4/K^+$. An example is illustrated in Figure 12 in the case of $(AG_4A)_4/K^+$. The characteristic bands at 380 and 515 nm of **(G-H1)•** do not appear at long times. In addition, the normalized decays recorded at 500 nm, 605 nm and 685 nm practically overlap suggesting that we deal with only one transient species in this spectral area. The absence of tautomerization could be due to competition with reaction of **(G-H2)•** toward an unknown photoproduct, which is accelerated in these systems for a reason we have not yet clarified.

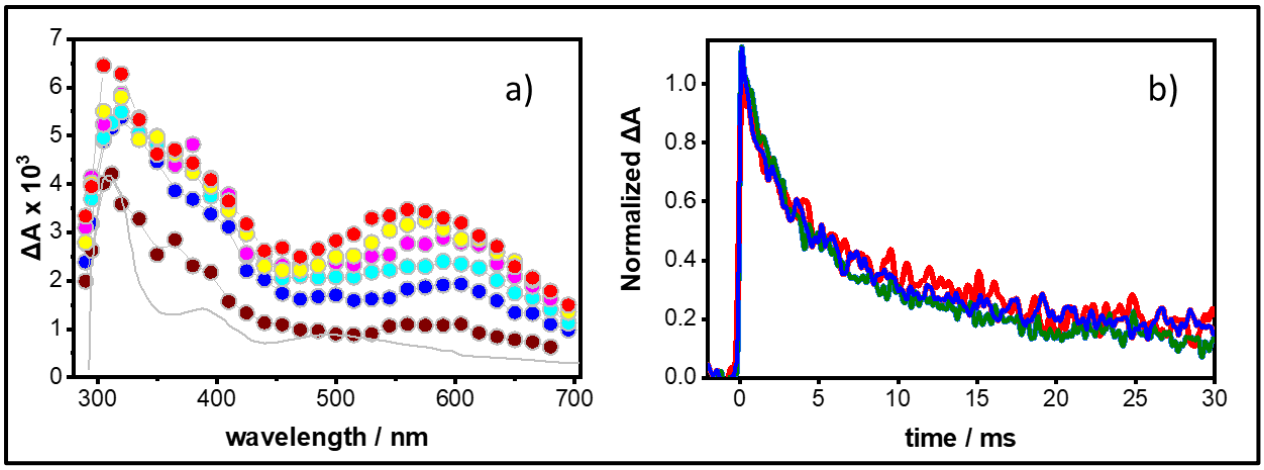

***Figure 12**. Tetramolecular $(AG_4A)_4/K^+$ **G**-quadruplexes. **a**) transient absorption spectra (circles) at 3 µs (red), 50 µs (yellow), 165 µs (pink), 0.5 ms (cyan), 2 ms (blue) and 6 ms (brown). The grey line corresponds to the **(G-H1)•** radical of dGMP,[2] whose intensity was arbitrarily scaled; **b**) normalized decays recorded at 500 nm (blue), 605 nm (green) and 685 nm (red) for aerated solutions of $(AG_4A)_4/K^+$.*

4.4.3 Deprotonation dynamics

We mentioned above that the spectra recorded at 3 µs indicate the coexistence of radical cations and **(G-H2)•** radicals. We determined the percentage

of the initial radical cation surviving at this time. To this end, we reconstructed the transient absorption spectra with linear combinations of the corresponding monomeric radicals taking into account both their shape and their molar absorption coefficients (Figures 9a and 10). These percentages, ranging from 25 to 60 (error ±5%) are gathered in Table 2. Their variation cannot be correlated to some structural parameter. For the $(TG_4T)_4/M^+$ pair, characterized by a parallel arrangement of guanines, a higher value is found for the K^+ analog. In contrast, for the OXY/M^+ the opposite trend is observed.

Table 2. Populations of ***(G$^+$)$^\bullet$*** *and* ***(G-H2)$^\bullet$*** *radicals in* ***G****-Quadruplexes (in percentage) at 3 µs, as % of* $[e_{hyd}^-]_0$*; In blue are the data collected prior to this thesis*

Sequence	Cation	Population of (G)$^\bullet$	Population of (G-H2)$^\bullet$
$(TG_4T)_4$	Na^+	25	75
	K^+	40	60
TEL21	K^+	60	40
	Na^+	50	45
TEL25	Na^+	45	55
OXY	Na^+	45	55
	K^+	30	70

In the case of TEL21/K^+, OXY/K^+, OXY/Na^+ and $(AG_4A)_4/K^+$, we determined the dynamics of the fast deprotonation process occurring before 3 µs (Figure 13) and corresponding to **(G-H2)$^\bullet$** populations indicated in Table 2. We achieved that by recording the rise of the **(G-H2)$^\bullet$** signal at wavelengths where its absorption is higher than that of the radical cation (see Figure 2). In the case of TEL21/K^+, we found that the rise of the **(G-H2)$^\bullet$** signal at 620 nm is concomitant with the decay of the **(G$^+$)$^\bullet$** signal at 400 nm. We remark that this deprotonation step is completed

within 0.5 µs for TEL21/K^+, while it is twice as slow for both OXY/M^+ systems and $(AG_4A)_4/K^+$, for which a plateau is reached at ca. 1 µs.

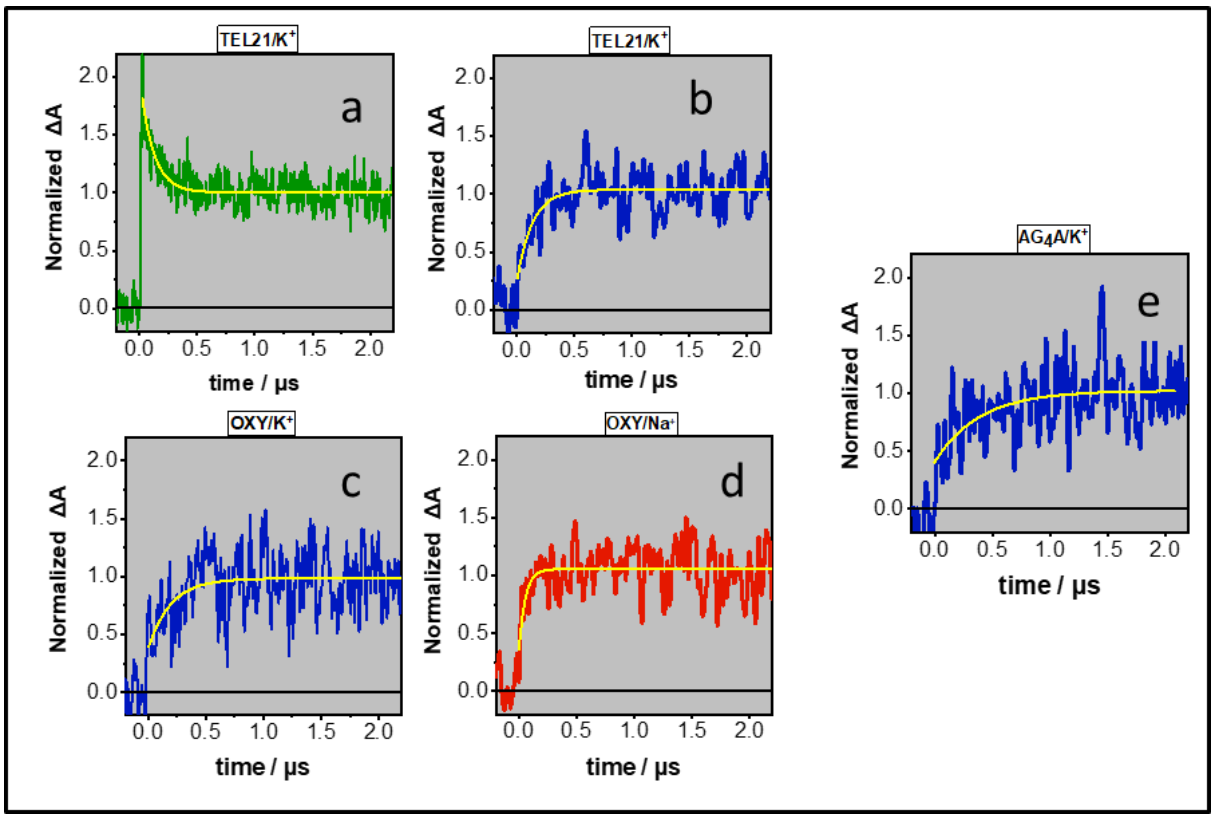

Figure 13. *Transient absorption signals recorded for the TEL21/K^+ at 400 nm* ***a****), TEL21/K^+ at 620 nm* ***b****), OXY/K^+ at 620 nm* ***c****), OXY/Na^+ at 620 nm* ***d****) and $(AG_4A)_4/K^+$ at 605 nm (****e****); ΔA was normalized to 1 at 2 µs. The yellow lines correspond to fits with mono-exponential functions.*

Coming to the slow deprotonation process, it could be determined directly by transient absorption signal only in the case of tetramolecular G-quadruplexes. For these systems, the **(G-H2)•** population at 50 µs is equal to that of the total radical population at 3 µs (Figure 9b). Thus, the decay of the differential absorbance at 500 nm and the rise at 600 nm correspond to the deprotonation process. This is shown for $(TG_4T)_4/Na^+$ in Figure 14a, where both the decay and the rise can be approximated by single exponential functions, $B_1 \exp(-t/\tau)+B_0$ and $B_1 \exp(t/\tau)+B_0$, respectively, with the same time constant of 6 ± 1 µs. The

deprotonation is practically completed at 20 μs. A shorter deprotonation time (ca. 10 μs) is found for $(TG_4T)_4/K^+$ (Figure 14b). For $(AG_4A)_4/K^+$ deprotonation is completed within 1.5 μs; however, in this case the variation of the signal intensity is lower compared to the other systems because the absorption spectra of $(G^+)^\bullet$ (Figure 8a) is located closer to that of $(G\text{-}H2)^\bullet$.

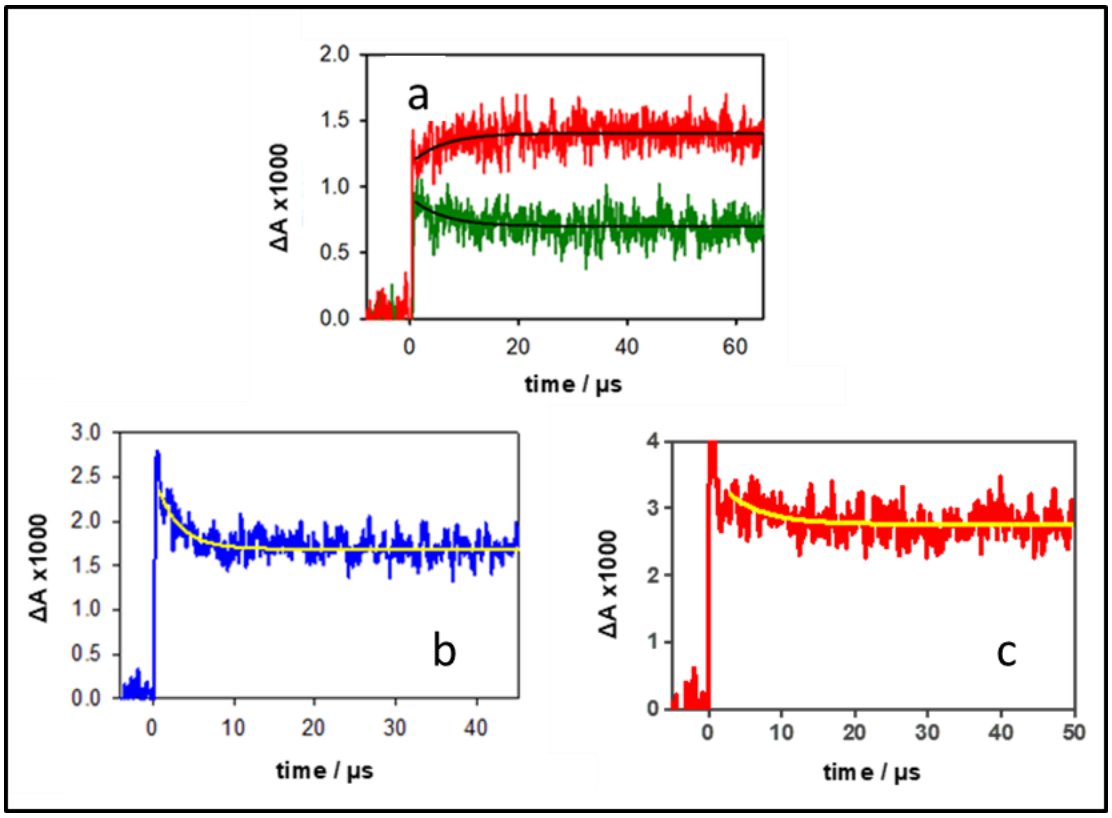

***Figure 14**. Transient absorption signals recorded for $(TG_4T)_4/Na^+$ **a**) at 500 nm (green) and 600 nm (red) $(TG_4T)_4/Na^+$ **b**) at 500nm and $(AG_4A)_4/K^+$ **c**) at 605 nm. Black and yellow lines correspond to fits with mono-exponential functions.*

For the other systems, the total radical population starts decreasing before completion of the deprotonation process (see for example the decay in Figure 14c). For this reason, I adopted a different approach in order to determine the dynamics of $(G^+)^\bullet$. I recorded several time-resolved spectra on the microsecond timescale.

Subsequently, I reconstructed them using linear combinations of the $(G^+)^\bullet$ and $(G\text{-}H2)^\bullet$ radical spectra corresponding to monomers, exactly in the same way followed for the 3 µs spectra. Finally, I plotted the $(G^+)^\bullet$ concentration (as a percentage of the initially generated electron holes) as a function of time. Figure 15 shows the results derived from this analysis for the OXY/M^+ and TEL21/M^+ pairs. For TEL21/Na^+ we used the data obtained in the laboratory prior to my thesis. For three of the analyzed systems, the $(G^+)^\bullet$ radical population is followed down to at least 15%. Below this limit the error becomes too important. In the case of TEL21/K^+, I stopped the plots much earlier because the coexistence in this systems of the three types of radicals made the analysis too difficult.

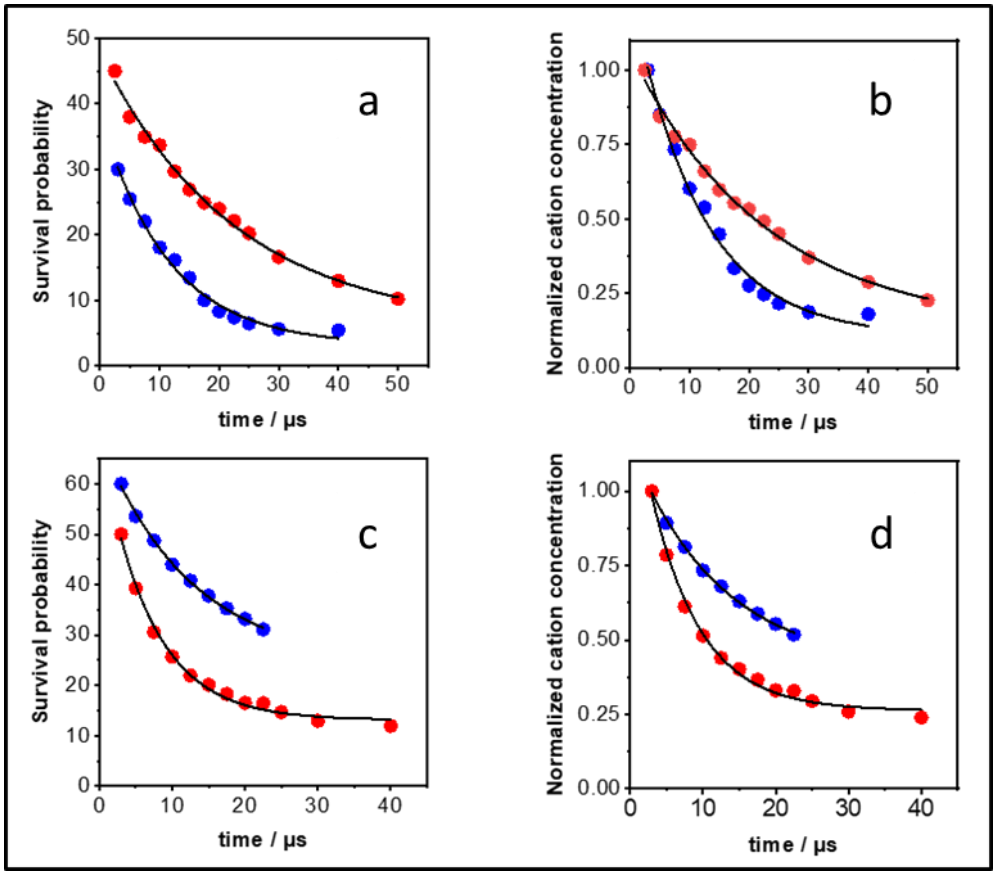

Figure 15. *Survival probabilities of the radical cation populations in OXY/M^+ (**a** and b) and TEL21/M^+ (**c** and **d**) in the presence of K^+ (blue) and Na^+ (red); they were determined from reconstruction of the time-resolved spectra with linear combinations of the $(G^+)^\bullet$ and **(G-H2)•** spectra of monomeric guanosine. In **a**) and **c**) the survival probabilties are given as % of $[e_{hyd}^-]_0$ while in **b**) and **d**) they have been normalized to 1 at 3 µs. Black lines correspond to fits with mono-exponential functions;*

We observe in Figures 15a and 15b that $(G^+)^\bullet$ decay in OXY/K^+ is much faster compared to OXY/Na^+. This is particularly interesting because the only difference between these two structures is the type of metal ion in the central cavity. The same effect was found for the tetramolecular quadruplexes (Figure 14). Thus it appears that K^+ is a factor favoring the $(G^+)^\bullet$ reactivity. The decrease of $(G^+)^\bullet$ population may be due to deprotonation and/or other reactions, such as hydration.[20] In order to estimate an upper limit for reactions other than deprotonation, we determined the survival probability of the total radical population at 40 μs: it is 80% for OXY/K^+ and 82% for OXY/Na^+. The missing 20% and 18%, respectively, correspond to reactions taking place either via $(G^+)^\bullet$ or via $(G\text{-}H2)^\bullet$. This means that the major path of the $(G^+)^\bullet$ decays is indeed due to deprotonation.

In Figures 15c and 15d, the $(G^+)^\bullet$ decay appears to be slower in TEL21/K^+ than in TEL21/Na^+, at least in the restricted time domain in which the comparison is made. Unlike the OXY/M^+ and $(TG_4T)_4/M^+$, whose structure does not change when Na^+ ions are replaced by K^+ ions, those formed by the human telomeric sequences undergo drastic geometrical rearrangements. NMR experiments on G-quadruplexes formed by sequences containing four telomer repeats TTAGGG in the presence of K^+ ions evidenced the coexistence of two hybrid forms in equilibrium.[21,22] The two forms differed in the successive order of the loop arrangement and the strand orientation.

According to our analysis the $(G^+)^\bullet$ in TEL21/Na^+ is less than 15% at 50 μs. In reference [5] was reported that the radical cations in this system survive till the ms time-scale. This conclusion was drawn from fitting the decays with exponential functions. But the $(G^+)^\bullet$ decay is not a first order reaction because it involves water molecules and the system is highly anisotropic (see next section). In order to further test this approach, I also analyzed the transient absorption spectra on longer times between 100 and 1200 μs (Figure 16). These spectra could be reconstructed with linear combinations of $(G\text{-}H2)^\bullet$ and $(G\text{-}H1)^\bullet$ monomeric

radicals. If instead of **(G-H1)•** spectrum that of **(G+)•** one is used, the red part of the transient spectrum around 700 nm cannot be reproduced.

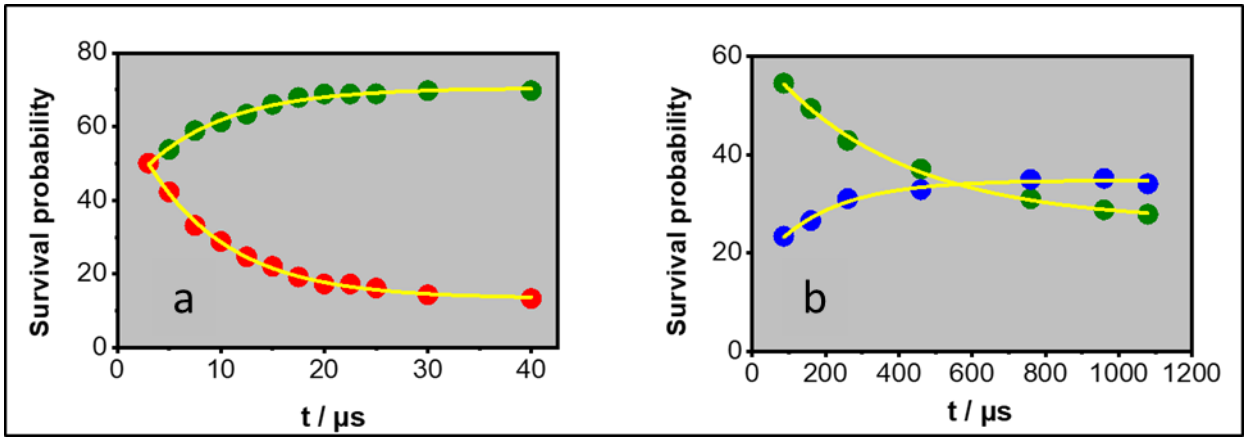

Figure 16. *Evolution of* ***(G+)•*** *(red),* ***(G-H2)•*** *(green) and* ***(G-H1)•*** *(blue) populations (expressed as % of* $[e_{hyd}^-]_0$*) in TEL21/*Na^+ *derived from reconstruction of the time-resolved spectra with linear combination of the spectra reported for monomeric radicals*[3]

4.4.4 Detection of unknown reaction products

It is already mentioned that the transient absorption spectra in the UVA spectral domain spectra may contain fingerprints of reaction products. Nevertheless, so far, UVA absorbing reaction products have not been detected by transient absorption spectroscopy for G-quadruplexes. I present below two such cases observed for TEL21/K^+ and $(AG_4A)_4/K^+$.

The transient absorption spectrum recorded for TEL21/K^+ at 30 ms, when the major part of radicals have disappeared, exhibits a peak at 320 nm and a shoulder at the 350-400 nm area (Figure 17a). The latter spectral features are correlated with reaction intermediates and/or final reaction products. The spectral signature of final reaction products can be identified in the steady-state differential absorption spectrum, determined by subtracting the spectrum recorded prior irradiation from that recorded after irradiation. This differential spectrum is also shown in Figure 17a, where ΔA was normalized by the

concentration of photons absorbed in the probed volume. The two spectra are clearly different, not only in their profile, but also in their intensity, the one at 30 ms being 7 times more intense. The transient signal at 365 nm (Figure 17b) shows a slow decay, lasting for more than 180 ms, which is the longest time that we can determine. Accordingly, we could deal with a reaction intermediate.

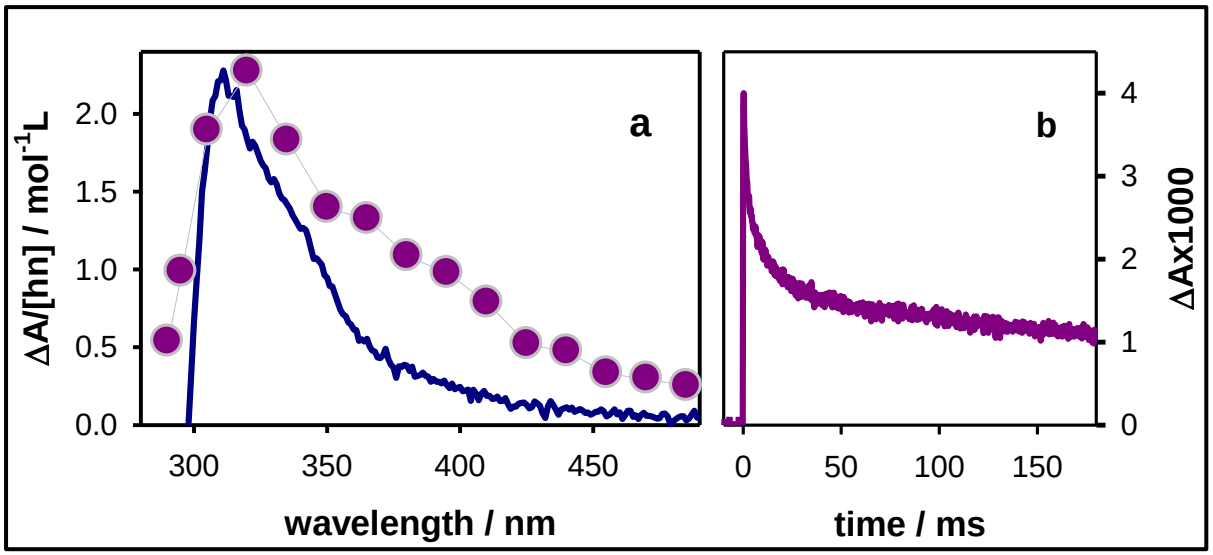

***Figure 17. a**) Steady-state (blue line) and time-resolved (violet circles; 30 ms; intensity divided by 7) differential absorption spectra determined for TEL21/K^+; the steady-state spectrum was determined by subtracting the absorption spectrum recorded after irradiation with 266 nm pulses from that recorded before irradiation. [hv] is the total concentration of absorbed photons in the probed volume. **b**) Transient absorption trace at 365 nm obtained with incident excitation intensity of 2×10^6 Wcm^{-2}.*

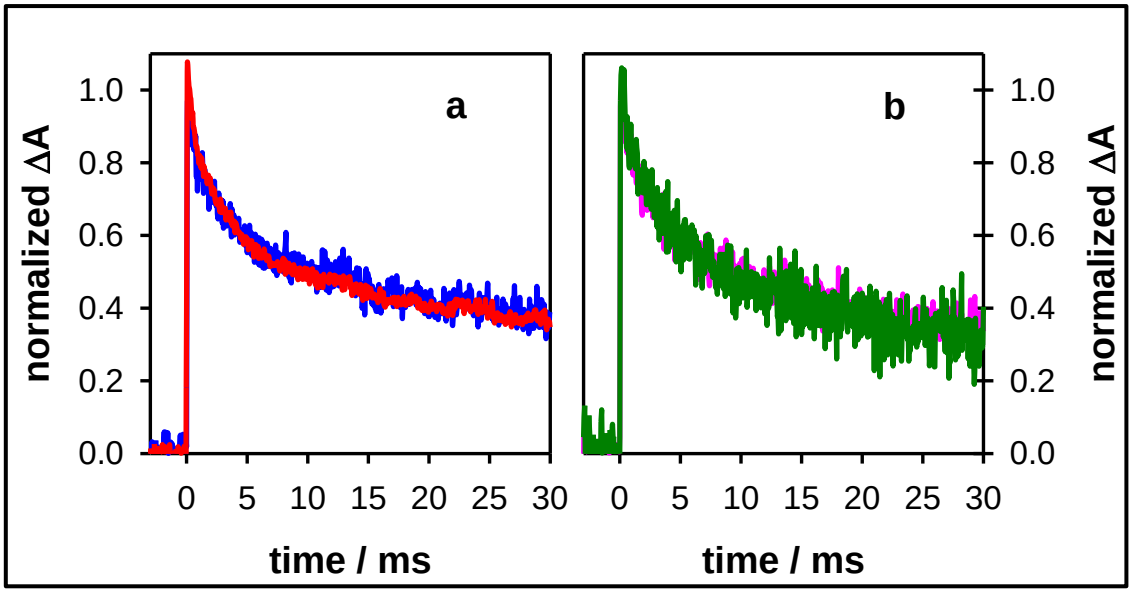

***Figure 18**. Transient absorption signals recorded for TEL21/K^+ at 365 nm **a**) and 395 nm **b**). Aerated solutions; incident laser pulses: 3 mJ (blue) and 6 mJ (red) **a**) and argon-saturated solutions (pink) and in aerated solutions (green) with incident laser pulses: 6 mJ **b**).*

In transient absorption experiments, reaction intermediates may originate either from guanine radicals or from photochemical reactions, being formed at the potential energy surface of an excited state. This is the case, for example, of an adenine dimer, determined on the millisecond time scale in the case of adenine tracts, in parallel with that of adenine radicals.[11] The concentration of the chemical species issued from radicals is proportional to ejected electrons, while that related to photoreactions is proportional to the number of absorbed photons. I found that the transient absorption signals at 365 nm, bearing fingerprints of both radicals and the unknown reaction intermediate, are not altered when the ratio $[e_{hyd}^-]_0/[hv]$ increases by 50%, from 0.017 to 0.026. Not only the excitation intensity but also the presence of oxygen has no effect on the decays (Figure 18b); this observation concerns both the radical decays and those of the reaction intermediate and final photoproduct. Regarding the latter, we remark that the steady-state differential absorption spectrum determined for TEL21/K^+ is similar to that reported for TEL21/Na^+ (Figure 19), which was tentatively attributed to guanine dimers.[23] However, in the case of TEL21/K^+, the spectral intensity,

normalized by the number of absorbed photons, was three times lower compared to that of TEL21/Na^+, suggesting a lower quantum yield of the associated photoreaction. However, the reaction intermediate detected for TEL21/K^+, is absent from the transient absorption spectra of TEL21/Na^+.

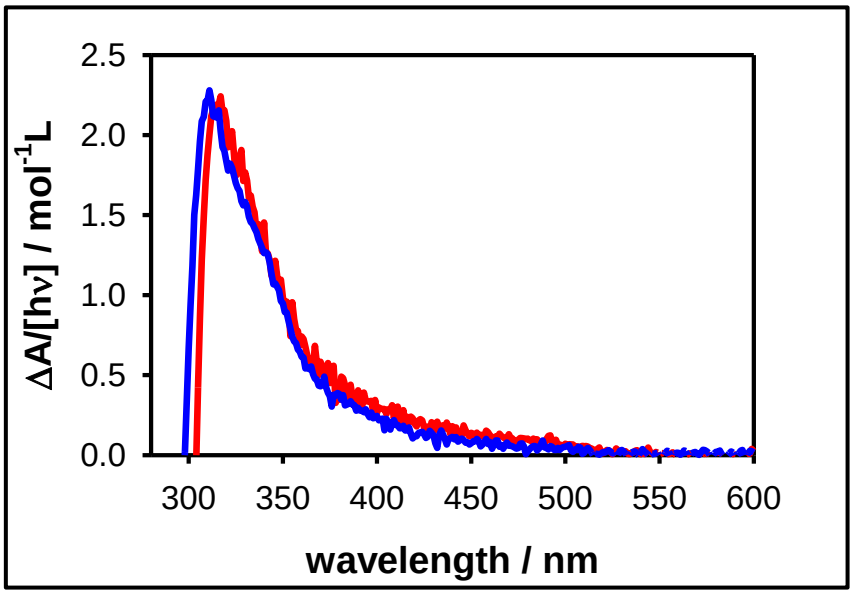

***Figure 19**. Comparison of the steady-state differential absorption spectra obtained for TEL21/K^+ (blue) and TEL21/Na^+ (red; intensity divided by 2.3);[5] [hv] is the total concentration of photons absorbed by the solution.*

In the case of $(AG_4A)_4/K^+$, the spectrum at 3 μs presents a peak around 360 nm which is absent from the corresponding spectrum of $(TG_4T)_4/K^+$ (Figure 20a), suggesting that this band is connected with the presence of adenines. We remark that the spectra of the radical cation obtained in pH 3 for $(AG_4A)_4/K^+$ and $(AG_4)_4/K^+$ exhibit an increased intensity at this spectral region, but not the spectrum of $(G_4A)_4/K^+$. Therefore we conclude that this spectral feature is correlated with the adenines located in position 5'. Such a species could result from radical cations or from a photoreaction occurring on the singlet excited state. This band is still present at 2 ms but it disappears at 6 ms: at this time

the transient absorption spectra of $(AG_4A)_4/K^+$ and $(TG_4T)_4/K^+$ practically overlap in the 300-450 nm region (Figure 20 b and c). Therefore, it seems that, also in this system, we are dealing with a reaction intermediate. One possibility would be that this intermediate results from hydration of $(\mathbf{G}^+)\bullet$; the resulting hydrate is a precursor of the 8-oxo-7,8-dihydro-2'-deoxyguanosine (8-oxodG). According to quantum chemical calculations this hydration product is expected to absorb between the UV and the visible absorption band guanine radicals.[9] However, transient absorption experiments alone cannot provide correct characterization of this reaction intermediate.

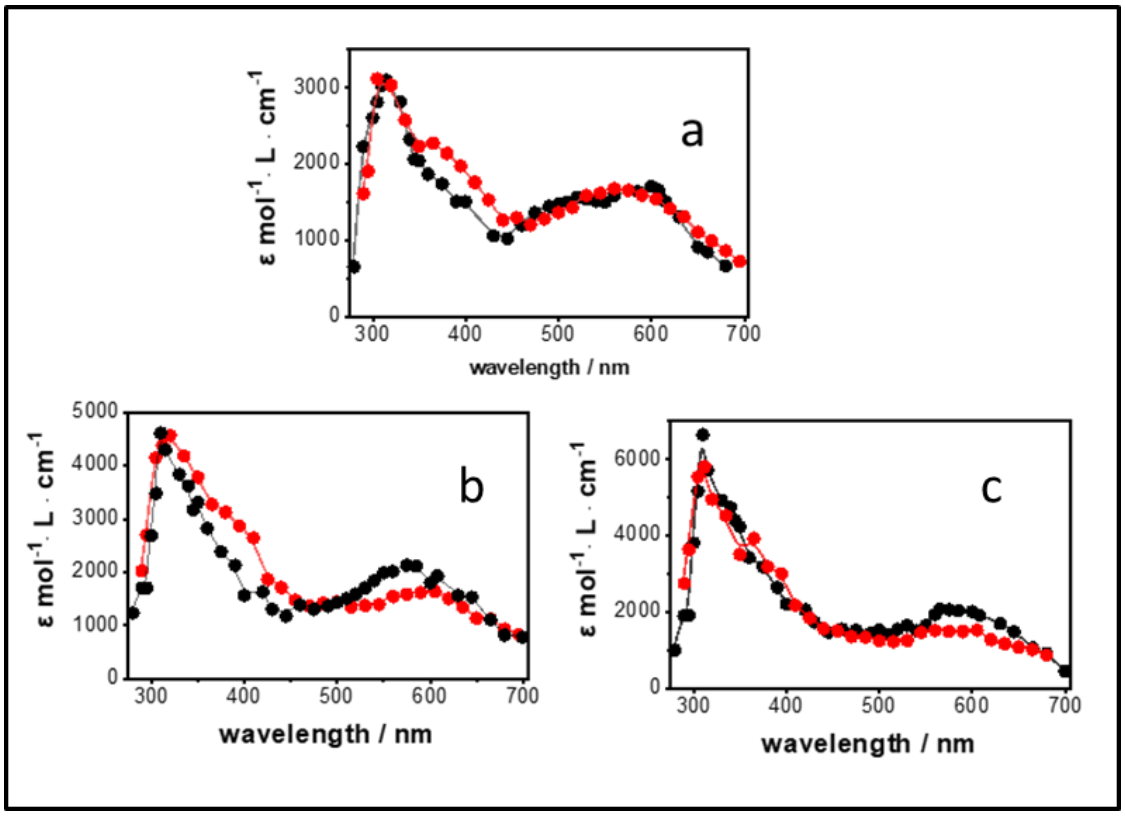

Figure 20. *Transient absorption spectra of $(TG_4T)_4/K^+$ (black circles) and the $(AG_4A)_4/K^+$ (red circles) recorded at 3 µs a) 2 ms b) and 6 ms c). The buffer concentration (PBK) is 0.15M and the pH was adjusted at 7; each of the spectra are normalized by their initial concentration of hydrated electrons $[e_{hyd}^-]_0$.*

4.5. Reaction schemes in DNA multimers

In general, reactions involving radicals of nucleobases are likely to be bi-molecular. For example, the formation of 8-oxodG involves a hydration step requiring addition of a water molecule to $(G^{+})^{\bullet}$, while that of guanine-thymine adducts requires the attack of thymine to the $(G^{+})^{\bullet}$.[24,25] The probability that the reactants come close to each other is not homogeneous over the three-dimensional space but it is determined by the conformation of the nucleic acid, which, in turn, structures the local environment, including the water network.[26] Thus, conformational motions, occurring on the same timescale as the reaction, may have two effects. On the one hand, it may differentiate the behavior of various reaction sites and, on the other, it may modify the behavior of a given site in the course of the observation. As a result, important deviations appear from the classical models widely used to describe kinetics of chemical reactions in homogenous solutions. The underlying assumption in such models is that of a well-stirred chemical reactor, which means that at the time scale of the observation, there is an internal averaging of all the reaction sites, randomly distributed in three dimensions. The lack of these conditions leads to multiscale decay patterns and renders the notion of rate constant inappropriate, with the reaction rate being time dependent. A good illustration of such multiscale dynamics in DNA is provided by the relaxation of the electronic excited states in helical structures, involving interactions among nucleobases, which spans over, at least, six decades of time.[27] The description of inhomogeneous dynamical processes necessitates specific theoretical treatments and/or simulations, developed in various fields such as photocatalysis, charge and energy transport in restricted geometries, polymerization reactions, reactions in biological cells, etc. (see for example references [28-32]).

Given the above considerations, the fits of the decays with exponential functions presented in this Chapter are devoid of physical meaning. The fitted

functions are simply used for a quantitative description of the decays, allowing easier comparison among the dynamics of the various systems.

This anisotropic behavior is reflected in the deprotonation dynamics in G-Quadruplexes, presented in 4.4.3. This process spans at least over four magnitude of time. Probably, the faster part is related with outer tetrads, which are most exposed to water. The decays of deprotonated radicals in duplex DNA are also multiscale (Figure 3).

Non classical reaction kinetics was suspected to be the reason for the important discrepancies between the radical lifetimes determined for single and double strands (Chapter 1.4) by photosensitized oxidation[19] and photoionization. [10] In order to check that the base sequences, which were different in the two types of studies, I studied here exactly the same systems (S1, S2 and S1•S2) as those reported by photosensitization. The half-lives observed by the two methods are compared in Table 3. including those of TEL25/Na^+, reported in the meantime by the same group.[33] The largest difference is encountered for the single strands, for which the $\tau_{1/2}$ values obtained by photosensitization are more than one order of magnitude larger than those found by photoionization.

Table 3. *Half-lives (in ms) determined by photoionization and photosensitized oxidation.*

Method	S1	S2	S1•S2	TEL25/Na^+
Photoionization	1.8[1]	2.2[1]	4[1]	2.4[1] / 3.1[2]
Photosensitized	120[3, 19]	40[3, 19]	7.5[3, 19]	8[3, 33]

[1] 500 nm; [2] 605nm; [3] 510nm.

In photoionization, radicals are formed at time-zero, considering our time resolution and after 3 μs their concentration equals that of the observed ejected electrons. Thus, it is possible to follow the fate of the entire radical population, even if parts of the deprotonation process were missed for some

systems. In the indirect approach, the laser induced reaction occurring at time-zero is the production of an oxidant (Chapter 1.4), while the charge transfer reaction with DNA is a diffusion controlled bi-molecular process.[34] As the nucleobase undergoing the oxidation is not necessarily a guanine,[34] the occurrence of many spatially correlated electron donors, renders the reaction scheme highly inhomogeneous. In addition, nucleic acids are negatively charged electrolytes making the approach of a negatively charged donor, such a sulfate anions, particularly selective. Thus, it would not be surprising that the formation of radicals is also a multiscale reaction.

An additional reason for the observed discrepancies is that in photosensitization, studies used analytical grade chemicals. Based on their results, we estimated that the impurity concentration in the studied solutions could be two orders of magnitude higher than that of G radicals[10] and could react with them.

4.6 Final DNA damage after low energy photoionization

Although the studies presented in this Chapter concern the primary species issued from photoionization, they provide indirect information regarding the associated final DNA damage. An important outcome of these studies is the interplay between dynamics and populations. In other terms, if there is competition between two reactions, the most important part of the reactant population evolves along the faster path. This is illustrated in Figure 21 for two reactions involving $(G^{+})^{\bullet}$: on the one hand deprotonation and, on the other, hydration which ultimately leads to formation of 8-oxodG. For example in the case of calf thymus DNA deprotonation is a fast reaction, being completed within 2μs; at this time the quasi-entire $(G^{+})^{\bullet}$ population (>95%) has been transformed to deprotonated $(G\text{-}H1)^{\bullet}$ radicals. Thus, it is not surprising that the quantum yield

determined for the formation of 8-oxodG by analytical methods corresponds only 2% of the ϕ_1.[35] In contrast, as part of $(G^{+})^{\bullet}$ survives in TEL21/Na^{+} for longer times, a higher level of 8-oxodG (corresponding to 7% of the ϕ_1) has been detected for this G-quadruplex.[5] The corollary is that 8-oxodG, widely used as marker of oxidative damage, is not representative of the extent of this damage when it is initiated by the formation of radical cations, as happens, not only in direct photoionization, but also in photosensitized electron abstraction.

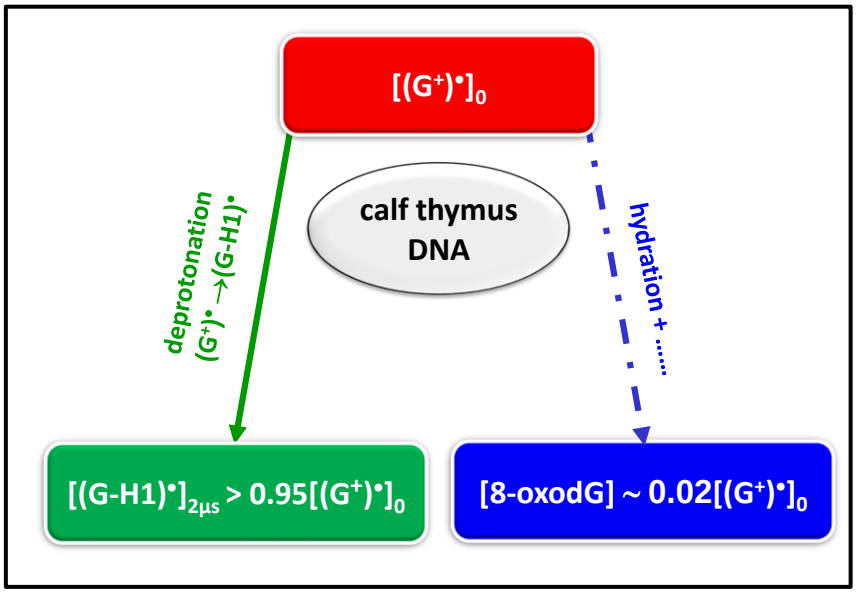

***Figure 21**. Competition between two reactions involving guanine radical cations: deprotonation and hydration, ultimately leading the formation of 8-oxodG.*

According to the above reasoning, the great majority of oxidative lesions are expected to stem from deprotonated radicals. The fact that radical decays are not sensitive versus oxygen shows that neither imidazolone nor oxazolone are expected to constitute major lesions since their formation requires aerated conditions.[36] In contrast, oxygen does not affect strand breakage, which was detected following both 193 nm irradiation[37,38] and UVA irradiation.[39]

Finally, the reactions involving $(G\text{-}H2)^{\bullet}$, which constitute the only deprotonated radical in some G-quadruplexes, have never been explored. Yet, the

fingerprint of a reaction intermediate has been observed in the transient absorption spectra of TEL21/K^+ around 350-450 nm.[40] And also the role of metal cations in the central cavity of G-quadruplexes, which affect the radical reaction rate, remains very intriguing.

4.7 *References* Chapter 4

(1) Candeias, L. P.; Steenken, S. Ionization of purine nucleosides and nucleotides and their components by 193-nm laser photolysis in aqueous solution: model studies for oxidative damage of DNA. *J. Am. Chem. Soc.* **1992**, *114*, 699-704.

(2) Candeias, L. P.; Steenken, S. Stucture and acid-base properties of one-electron-oxidized deoxyguanosine, guanosine, and 1-methylguanosine. *J. Am. Chem. Soc.* **1989**, *111*, 1094-1099.

(3) Chatgilialoglu, C.; Caminal, C.; Altieri, A.; Vougioukalakis, G. C.; Mulazzani, Q. G.; Gimisis, T.; Guerra, M. Tautomerism in the guanyl radical. *J. Am. Chem. Soc.* **2006**, *128*, 13796-13805.

(4) Balanikas, E.; Banyasz, A.; Baldacchino, G.; Markovitsi, D. Guanine Radicals Generated in Telomeric G-quadruplexes by direct absorption of low-energy UV photons: Effect of Potassium Ions. *Molecules* **2020**, *accepted*.

(5) Banyasz, A.; Martinez-Fernandez, L.; Balty, C.; Perron, M.; Douki, T.; Improta, R.; Markovitsi, D. Absorption of Low-Energy UV radiation by human telomere G-Quadruplexes generates long-lived guanine radical cations. *J. Am. Chem. Soc.* **2017**, *139*, 10561-10568.

(6) Douki, T. Effect of denaturation on the photochemistry of pyrimidine bases in isolated DNA. *J. Photochem. Photobiol B* **2006**, *82*, 45-52.

(7) Marguet, S.; Markovitsi, D. Time-resolved study of thymine dimer formation. *J. Am. Chem. Soc.* **2005**, *127*, 5780-5781.

(8) Banyasz, A.; Ketola, T.; Martinez-Fernandez, L.; Improta, R.; Markovitsi, D. Adenine radicals generated in alternating AT duplexes by direct absorption of low-energy UV radiation. *Faraday Disc.* **2018**, *207*, 181-197.

(9) Banyasz, A.; Martínez-Fernández, L.; Improta, R.; Ketola, T.-M.; Balty, C.; Markovitsi, D. Radicals generated in alternating guanine–cytosine duplexes by direct absorption of low-energy UV radiation. *Phys. Chem. Chem. Phys.* **2018**, *20*, 21381-21389.

(10) Balanikas, E.; Banyasz, A.; Baldacchino, G.; Markovitsi, D. Populations and dynamics of guanine radicals in dna strands: direct versus indirect generation. *Molecules* **2019**, *24*, 2347.

(11) Banyasz, A.; Ketola, T.; Muñoz-Losa, A.; Rishi, S.; Adhikary, A.; Sevilla, M. D.; Martinez-Fernandez, L.; Improrta, R.; Markovitsi, D. UV-induced

adenine radicals induced in DNA A-tracts: spectral and dynamical characterization *J. Phys. Chem. Lett.* **2016**, *7*, 3949-3953.

(12) Banyasz, A.; Martinez-Fernandez, L.; Improta, R.; Ketola, T. M.; Balty, C.; Markovitsi, D. Radicals generated in alternating guanine-cytosine duplexes by direct absorption of low-energy UV radiation. *Phys. Chem. Chem. Phys.* **2018**, *20*, 21381-21389.

(13) Kumar, A.; Sevilla, M. D. excited states of one-electron oxidized Guanine-Cytosine base pair radicals: a time dependent density functional theory study. *J. Phys. Chem. A* **2019**, *123*, 3098-3108.

(14) von Sonntag, C.: *Free-Radical-Induced DNA damage and its Repair* Springer-Verlag: Berlin-Heildelberg, 2006.

(15) Kobayashi, K.; Tagawa, S. Direct observation of guanine radical cation deprotonation in duplex DNA using pulse radiolysis. *J. Am. Chem. Soc.* **2003**, *125*, 10213-10218.

(16) Banyasz, A.; Balanikas, E.; Martinez-Fernandez, L.; Baldacchino, G.; Douki, T.; Improta, R.; Markovitsi, D. Radicals generated in tetramolecular guanine quadruplexes by photo-ionization: spectral and dynamical features. *J. Phys. Chem. B* **2019**, *123*, 4950-4957.

(17) Martinez-Fernandez, L.; Banyasz, A.; Markovitsi, D.; Improta, I. Topology controls the electronic absorption delocalization of electron hole in guanine quadruplexes. *Chem. Europ. J.* **2018**, *24*, 15185-15189.

(18) Sun, W. M.; Varsano, D.; Di Felice, R. Effects of G-Quadruplex Topology on Electronic Transfer Integrals. *Nanomaterials* **2016**, *6*.

(19) Rokhlenko, Y.; Cadet, J.; Geacintov, N. E.; Shafirovich, V. Mechanistic aspects of hydration of guanine radical cations in DNA. *J. Am. Chem. Soc.* **2014**, *136*, 5956-5962.

(20) Ravanat, J. L.; Saint-Pierre, C.; Cadet, J. One-electron oxidation of the guanine moiety of 2'-deoxyguanosine: influence of 8-oxo-7,8-dihydro-2'deoxyguanosine. *J. Am. Chem. Soc.* **2003**, *125*, 2030-2031.

(21) Phan, A. T.; Kuryavyi, V.; Luu, K. N.; Patel, D. J. Structure of two intramolecular G-quadruplexes formed by natural human telomere sequences in K+ solution. *Nucl. Ac. Res.* **2007**, *35*, 6517-6525.

(22) Dai, J. X.; Carver, M.; Punchihewa, C.; Jones, R. A.; Yang, D. Z. Structure of the Hybrid-2 type intramolecular human telomeric G-quadruplex in K+ solution: insights into structure polymorphism of the human telomeric sequence. *Nucl. Ac. Res.* **2007**, *35*, 4927-4940.

(23) Martinez-Fernandez, L.; Changenet, P.; Banyasz, A.; Gustavsson, T.; Markovitsi, D.; Improta, I. A Comprehensive study of guanine excited state relaxation and photoreactivity in G-Quadruplexes. *J. Phys. Chem. Lett.* **2019**, *10*, 6873-6877.

(24) Cadet, J.; Douki, T.; Ravanat, J. L. Oxidatively generated damage to the guanine moiety of DNA: Mechanistic aspects and formation in cells. *Acc. Chem. Res.* **2008**, *41*, 1075-1083.

(25) Di Mascio, P.; Martinez, G. R.; Miyamoto, S.; Ronsein, G. E.; Medeiros, M. H. G.; Cadet, J. Singlet molecular oxygen reactions with nucleic acids, lipids, and proteins. *Chem. Rev.* **2019**, *119*, 2043-2086.

(26) Laage, D.; Elsaesser, T.; Hynes, J. T. Water Dynamics in the Hydration Shells of Biomolecules. *Chem. Rev.* **2017**, *117*, 10694-10725.

(27) Gustavsson, T.; Markovitsi, D. Fundamentals of the Intrinsuc DNA Fluorescencee. *Acc.Chem. Res.* **2021**.

(28) Blumen, A.; Klafter, J.; Zumofen, G.: Models for reaction dynamics in glasses. In *Optical spectroscopy of glasses*; Zschokke, I., Ed.; Springer: Dordecht, the Netherlands, 1986; pp 199-265.

(29) Markovitsi, D.; Germain, A.; Millie, P.; Lécuyer, I.; Gallos, L.; Argyrakis, P.; Bengs, H.; Ringsdorf, H. Triphenylene columnar liquid crystals: excited states and energy transfer. *J. Phys. Chem.* **1995**, *99*, 1005-1017.

(30) Emelianova, E. V.; Athanasopoulos, S.; Silbey, R. J.; Beljonne, D. 2D Excitons as primary energy carriers in organic crystals: the case of oligoacenes. *Phys. Rev. Lett.* **2010**, *104*.

(31) Benichou, O.; Chevalier, C.; Klafter, J.; Meyer, B.; Voituriez, R. Geometry-controlled kinetics. *Nature Chem.* **2010**, *2*, 472-477.

(32) Dolgushev, M.; Guerin, T.; Blumen, A.; Benichou, O.; Voituriez, R. Contact kinetics in fractal macromolecules. *Phys. Rev. Lett.* **2015**, *115*.

(33) Merta, T. J.; Geacintov, N. E.; Shafirovich, V. Generation of 8-oxo-7,8-dihydroguanine in G-Quadruplexes models of human telomere sequences by one-electron oxidation. *Photochem. Photobiol.* **2019**, *95*, 244-251.

(34) Candeias, L. P.; Steenken, S. Electron transfer in di(deoxy)nucleoside phosphates in aqueous solution: rapid migration of oxidative damage (via adenine) to guanine. *J. Am. Chem. Soc.* **1993**, *115*, 2437-2440.

(35) Gomez-Mendoza, M.; Banyasz, A.; Douki, T.; Markovitsi, D.; Ravanat, J. L. Direct oxidative damage of naked DNA generated upon absorption of UV radiation by nucleobases. *J. Phys. Chem. Lett.* **2016**, *7*, 3945-3948.

(36) Ravanat, J. L.; Douki, T.; Cadet, J. Direct and indirect effects of UV radiation on DNA and its components. *J. Photochem. Photobiol., B: Biology* **2001**, *63*, 88-102.

(37) Melvin, T.; Plumb, M. A.; Botchway, S. W.; Oneill, P.; Parker, A. W. 193 nm Light induces single-strand breakage of DNA predominantly at guanine. *Photochem. Photobiol.* **1995**, *61*, 584-591.

(38) Melvin, T.; Plumb, M. A.; Botchway, S. W.; Oneill, P.; Parker, A. W.: *The distribution of single strand breakage at guanine initiated by 193nm light is different for single and double stranded DNA*, 1995.

(39) Teychene, J.; Didacus-Prins, D.; Chouini-Lalanne, N.; Sartor, V.; Dejugnat, C. Formulation induces direct DNA UVA photooxidation. Part I. Role of the formulating cationic surfactant. *Journal of Molecular Liquids* **2019**, *295*.

(40) Balanikas, E.; Banyasz, A.; Baldacchino, G.; Markovitsi, D. Guanine radicals generated in telomeric g-quadruplexes by direct absorption of low-energy UV photons: effect of potassium ions. *Molecules* **2020**, *25*, 2094.

Conclusions

As mentioned in the Prologue, at the beginning of my work, the host laboratory had reported the intriguing effect of low-energy photoionization of DNA. It had been detected for four oligomeric single and double strands and one G-Quadruplex. The photoionization quantum yield of the G-Quadruplex at 266 nm (4.5×10^{-3}) was found to be at least 4 times higher compared to the other systems. It was also reported that guanine radical cations in the examined G-Quadruplex survive on the ms time-scale and that $(G^{+})^{\bullet} \rightarrow (G\text{-}H2)^{\bullet}$ deprotonation is followed by $(G\text{-}H2)^{\bullet} \rightarrow (G\text{-}H1)^{\bullet}$ tautomerization.

The results obtained during my thesis for 13 G-Quadruplexes and 7 single and double strands, including genomic DNA, confirmed part of these results. They also brought more detailed insights on both the photoionization process and the evolution of guanine radicals, revealing the importance of various structural parameters.

Although I followed in my experiments the methodology established previously in the host laboratory, I also made some methodological developments. Firstly, the protocol for the study of radical cations of G-Quadruplexes was improved. Secondly, by using electron scavengers, I managed to follow the deprotonation of $(G^{+})^{\bullet}$ on much shorter times (30 ns - 2.0 μs). Finally, I could determine the $(G^{+})^{\bullet}$ deprotonation dynamics between 2 and 50 μs in a more precise way, by analyzing the transient absorption spectra.

In agreement with the previous studies, I found that low-energy photoionization depends on the secondary DNA structure and requires efficient stacking of nucleobases. The ϕ_1 values of duplexes and single strands are in the range of 1×10^{-3} to 2×10^{-3} while those of G-quadruplexes are all higher and exhibit larger variation, from 3.5×10^{-3} to 15×10^{-3}, which was correlated with specific structural elements. The number of DNA strands, the number of G tetrads or the topology (parallel/antiparallel) do not play an important role. In contrast, ϕ_1 is greatly affected by the metal cations (Na^{+}/K^{+}) in their central cavity, as well as by the nature (adenine/thymine) and the position (3' of 5') of the ending groups. In

the case of duplexes, the occurrence of **GG** and **GGG** steps leads to somewhat higher values.

In view of the above findings, a complex indirect mechanism was proposed to explain low-energy photoionization of DNA: a small population of charge transfer states formed during the excited state relaxation undergoes charge separation. Subsequently, the positive charge is trapped by guanine stack due to their low oxidation potential while electron ejection occurs from the negatively charged base. *Direct information about the proposed mechanism can in principle be obtained by femtosecond transient absorption experiments. However, due to the very small of the excited state population leading to photoionization, such measurements are very difficult.*

Going now to the guanine radicals in the examined systems, as previously were identified and quantified by comparing their absorption spectra with those reported in the literature for three types of monomeric radicals. Moreover, the spectra of $(G^{+})^{\bullet}$ in four G-Quadruplexes were also determined, the most important finding being that they may be affected by adenines in the ending groups. *Theoretical calculations should bring information on the exact origin of these spectral modifications.*

I confirmed previous reports that $(G^{+})^{\bullet}$ deprotonation in single strands and duplexes leads to $(G\text{-}H1)^{\bullet}$ radicals and in G-Quadruplexes to $(G\text{-}H2)^{\bullet}$ radicals. I managed to determine for the first time the deprotonation dynamics in genomic DNA, which is completed within 2 μs. The deprotonation process in **G**-Quadruplexes was found to be highly anisotropic. A first, very fast step, possibly correlated with outer tetrads more exposed to water, takes place within 1.0-1.5 μs. Deprotonation is nearly completed (~90% of the population) within ~50μs. In contrast to the first step, the second one is clearly accelerated in the presence of K^{+} cations in the central cavity compared to the Na^{+}. *The reason for this different behavior is not clear; theoretical calculations could help for its understanding.*

(G-H2)• →**(G-H1)•** tautomerization appeared not to be a general rule for **G**-Quadruplexes. More precisely, tautomerization is not observed for tetramolecular quadruplexes formed with K^+ ions. It is possibly hindered because of the competition with a reaction of **(G-H2)•** toward an unknown photoproduct, which is accelerated in these systems. *The reason for this effect is not yet clear.*

Guanine radicals in the examined systems decay within tens of ms, their half-lives been of a few ms. Base-pairing slows down this decay. These general findings results were in contradiction with those obtained by the photosensitized method. In order to clarify such a discrepancy, I studied by low-energy photoionization exactly the same systems. Two reasons were determined for the observed differences. First, the photosensitized study used analytical grade chemicals. Thus impurities in higher concentration than the radical, may react with them altering the transient absorption signals. Secondly, generation of radicals, requiring the approach between a negatively charged oxidant and the anionic DNA macromolecules, may be not instantaneous but take place on longer times, artificially slowing down the radical decays. Therefore, low-energy/low-intensity photoionization provides a more accurate description of the radical reaction dynamics in absence of other molecules.

It was also shown that 8-oxod**G**, a widely used oxidation marker, is not representative of the extent of oxidative damage, when this is triggered by photoionization. In this case, the major oxidative lesions, in particular in duplex genomic DNA, should stem from deprotonated radicals and be context dependent. Photoionization quantum yields provide an estimation for the expected total amount of oxidative lesions. In association with analytical methods, they could contribute to quantify the various types of final reaction products and, possibly, lead to the characterization of new ones. *For example, the lesions resulting from (G-H2)• radicals, detected in all G-Quadruplex structures, remain to be identified.*

Finally, beyond the biological issues discussed above, the largest propensity of **G**-Quadruplexes to undergo low-energy photo-ionization, compared to duplex DNA, deserves attention. These structures are currently studied for applications

in the field of nanotechnology. Their behavior as molecular wires, connected to external electric circuits, was reported. *But so far, their properties as photoconductors have not been explored. Electron photodetachment is closely related to photoconductivity and photoelectromistry, used, among others, in biosensors. Such devices could be optimized by controlling the structural parameter affecting* $\boldsymbol{\phi}_1$ *(metal cations, peripheral groups).*

Publications

Published articles

Balanikas, E.; Banyasz, A.; Baldacchino, G.; Markovitsi.D, **Deprotonation dynamics of guanine radical cations,** *manuscript under revision 2021*

Balanikas, E.; Martinez-Fernandez, L.; Improta, R.; Podbevšek, P.; Baldacchino, G.; Markovitsi, D. *The Structural Duality of Nucleobases in Guanine Quadruplexes Controls Their Low-Energy Photoionization*. **J. Phy. Chem. Lett. 2021,** 12, 8309-8313 DOI: 10.1021/acs.jpclett.1c01846.

Hal version: https://hal-cea.archives-ouvertes.fr/cea-03346313v1

Balanikas, E.; Banyasz, A.; Douki, T.; Baldacchino, G.; Markovitsi, D. *Guanine radicals induced in DNA by low-energy photoionization*. **Acc. Chem. Res. 2020**, 53, 1511-1519 DOI: 10.1021/acs.accounts.0c00245

Hal version: https://hal-cea.archives-ouvertes.fr/cea-03053797v1

Balanikas, E.; Banyasz, A.; Baldacchino, G.; Markovitsi, D. *Guanine radicals generated in telomeric G-Quadruplexes by direct absorption of low-energy UV photons: effect of potassium ions*. **Molecules 2020**, 25, 2094 DOI: 10.3390/molecules25092094.

Hal version: https://hal-cea.archives-ouvertes.fr/cea-02571985v1

Behmand, B.; **Balanikas, E.;** Martinez-Fernandez, L.; Improta, R.; Banyasz, A.; Baldacchino, G.; Markovitsi, D. *Potassium Ions Enhance Guanine Radical Generation upon Absorption of Low-Energy Photons by G-quadruplexes and Modify Their Reactivity*. **J. Phys. Chem. Lett. 2020**, 11, 1305−1309 DOI: https://pubs.acs.org/doi/10.1021/acs.jpclett.

Hal version: https://hal-cea.archives-ouvertes.fr/cea-03053797v1

Balanikas, E.; Banyasz, A.; Baldacchino, G.; Markovitsi, D. *Populations and Dynamics of Guanine Radicals in DNA strands: Direct versus Indirect Generation.* ***Molecules*** **2019**, *24*, 2347 DOI: 10.3390/molecules24132347.

Hal version: https://hal-cea.archives-ouvertes.fr/cea-02370029v1

Banyasz, A.; **Balanikas, E.**; Martinez-Fernandez, L.; Baldacchino, G.; Douki, T.; Improta, R.; Markovitsi, D. *Radicals generated in tetramolecular guanine quadruplexes by photo-ionization: spectral and dynamical features*. **J. Phys. Chem. B 2019**, 123, 4950-4957, DOI: 10.1021/acs.jpcb.9b02637.

Hal version: https://hal-cea.archives-ouvertes.fr/cea-02160879v2

Book chapter

Balanikas, **E.**; Markovitsi, D. DNA photoionization: from high to low energies . In "DNA photodamage: from light absorption to cellular responses and skin cancer, Eds. Douki, T. Improta, R. Publisher: **Royal Society of Chemistry 2021**. *In press*

université PARIS-SACLAY
ÉCOLE DOCTORALE
Sciences Chimiques : Molécules, Matériaux, Instrumentation et Biosystèmes (2MIB)

Titre : Photoïonisation à basse énergie de quadruplexes de guanine

Mots clés : quadruplexes de guanine, photoïonisation, radicaux, spectroscopie résolue en temps, ADN, dommages oxydatifs

Résumé : La thèse décrit la photoïonisation à basse énergie des quadruplexes de guanine (G-Quadruplexes) en solution aqueuse. Ces structures ADN à quatre brins sont impliquées dans d'importantes fonctions biologiques et étudiées dans le domaine de la nanotechnologie. Leur photoïonisation génère des électrons et des radicaux de guanine, qui conduisent à des lésions d'ADN et sont essentiels pour le développement des biocapteurs basés sur la photoconductivité.
16 structures modèles, ainsi que de l'ADN génomique, ont été étudiées par spectroscopie d'absorption nanoseconde avec excitation à 266 nm. Les rendements quantiques de photoïonisation ϕ dépendent fortement de la structure secondaire. Les ϕ des G-Quadruplexes atteignent 10^{-2}, alors que ceux des duplexes ne dépassent pas $2x10^{-3}$. Ces résultats ont permis de formuler un mécanisme complexe, incluant la formation des états excités à transfert de charge et une séparation de charges, pour expliquer la photoïonisation de l'ADN à des énergies bien plus faibles que les potentiels d'ionisation verticale de ses composants.
Les radicaux de guanines dans des systèmes examinés ont été identifiés et quantifiés en comparant leur spectres d'absorption avec ceux décrits dans la littérature pour les espèces monomériques: le radical cation $(G^+)•$ et deux radicaux déprotonés (G-H1)• and (G-H2)•. Dans l'ADN génomique, la déprotonation $(G^+)• \rightarrow$ (G-H1)• se termine en 2 µs. Seule une déprotonation $(G^+)• \rightarrow$ (G-H2)• est observée dans des G-Quadruplexes; ce processus est hautement anisotrope, ayant lieu de 30 ns à au moins 50 µs. Pour certains G-quadruplexes une tautomerisation (G-H2)• → (G-H1)• a été détectée à des temps longs. Dans tous les cas, la demi-vie de la population totale de radicaux est de quelques ms.

Title : Low-energy photoionization of guanine quadruplexes

Keywords : guanine quadruplexes, photoionization, radicals, time-resolved spectroscopy, DNA oxidative damage

Abstract : The thesis describes the low-energy photoionization of DNA guanine quadruplexes (G-Quadruplexes) in aqueous solution. G-quadruplexes are four-stranded structures involved in important biological functions and studied for applications in nanotechnology. Their photoionization generates electrons and guanine radicals, which are precursors to DNA damage and essential for the development of photoconductivity-based biosensors.
16 different model structures, as well as genomic DNA were studied by is nanosecond transient absorption spectroscopy with 266 nm excitation. It was shown that the photoionization quantum yields ϕ strongly depend on the secondary structure. The ϕ values of G-Quadruplexes reach 10^{-2}, while those of duplexes does not exceed $2x10^{-3}$. On the basis of the obtained results, a complex mechanism, involving formation of excited. charge transfer states and charge separation, was proposed to explain DNA photoionization at energies significantly lower than the vertical ionization potentials of its components.
Guanine radicals in the examined systems were identified and quantified by comparing their absorption spectra with those reported for monomeric species: radical cations $(G^+)•$ and two deprotonated radicals (G-H1)• and (G-H2)•. In genomic DNA, $(G^+)• \rightarrow$ (G-H1)• deprotonation is completed within 2 µs. In contrast, only $(G^+)• \rightarrow$ (G-H2)• deprotonation is observed in G-Quadruplexes; this process is highly anisotropic, spanning from 30 ns to at least 50 µs. For some G-quadruplexes, (G-H2)• → (G-H1)• tautomerization was also detected on longer times. The half-lives of the total radical population in all the studied systems amounts to a few ms.